Construction and Characterization of a Targeting M13-Based Phagemid Carrying an Anti-Angiogenic DNA-Encoded Virus-Like Particle

by

Jiayang Li

A thesis
presented to the University of Waterloo
in fulfilment of the
thesis requirement for the degree of
Master of Science
in
Pharmacy

Waterloo, Ontario, Canada, 2024

AUTHOR'S DECLARATION

I hereby declare that I am the sole author of this thesis. This is a true copy of this thesis, including any required final revisions, as accepted by my examiners. I understand that my thesis may be made electronically available to the public.

Abstract

Over the past several years, molecular targeted therapy has emerged as a promising strategy for cancer treatment. Unlike broad-spectrum cytotoxic drugs used in conventional chemotherapy, targeted therapy aims to address specific molecular alterations unique to cancer cells. To develop effective targeted therapies, numerous delivery platforms have been investigated to optimize safety, specificity, and efficiency. The work presented here investigates the construction and characterization of a miniphagemid-mediated cancer therapy delivering anti-angiogenetic DNA-encoded virus-like particles (VLPs). VLPs have shown a robust ability to stimulate potent immune responses and overcome the immunosuppressive state of the tumour microenvironment (TME). Additionally, the filamentous bacteriophage (phage) M13 has been explored as a safe and efficient vehicle for delivering therapeutic genes and drugs. Phage-based vectors (phagemids) can be engineered to transfer exogenous genetic material to mammalian cells safely, as they possess no natural tropism. The present study aims to combine the advantages of both VLPs and phagemids to construct a hybrid biological platform for the specific delivery of DNA encoding VLP-displaying anti-tumour peptides, specifically VGB4, to tumour cells via M13 – a filamentous phage capable of phagemid production as well as phage display. The VGB4 peptide has demonstrated potent ability to inhibit angiogenesis in the tumour vasculature by blocking the downstream signalling pathways of vascular endothelial growth factor receptor (VEGFR). The human papillomavirus (HPV) type 16 L1 capsid gene with an inserted VGB4 peptide sequence was cloned into a miniaturized phagemid (miniphagemid) engineered by our lab. This genetically engineered miniphagemid was produced in *Escherichia coli* using a novel non-packaging M13 helper plasmid. The helper plasmid not only complements phagemid packaging but also enables the display of a cell-specific targeting ligand, the epidermal growth factor

(EGF), which promotes receptor-mediated endocytosis for specific phage uptake by tumour cells overexpressing epidermal growth factor receptors (EGFRs). This thesis project investigated the formation of VGB4-displaying HPV VLPs within HEK 293T and HeLa cells. Our results demonstrated that the EGF-displaying miniphagemid improves gene delivery to cells compared to non-displaying miniphagemids. Furthermore, the VGB4-displaying HPV VLPs do not form in cells treated with miniphagemids, but these VLPs are successfully formed in cells treated with the precursor phagemids encoding the same gene cassette. Overall, this study highlights the necessity for further investigation and optimization to enhance miniphagemid-mediated gene transfer by overcoming cellular barriers, paving the way for its application as a novel targeted gene therapy for cancer.

ACKNOWLEDGEMENTS

I wish to express my deep gratitude to my supervisors, Dr. Roderick Slavcev and Dr. Marc Aucoin, for their unwavering support and patience. I consider myself extremely fortunate to have received guidance from two mentors who believed in me and provided numerous opportunities for my growth as a researcher.

I would also like to express my gratitude to my advisory committee members, Dr. Michael Beazely, Dr. Christian Euler and Dr. Nafiseh Nafissi for providing me with valuable insights and guidance throughout the duration of my thesis project. The work presented in this thesis would not have been possible without the assistance of numerous individuals to whom I am deeply grateful. I would like to extend my heartfelt thanks to Rohini Prakash and Jesse St. Jean for training me in all aspects of molecular and microbiology work throughout my graduate studies; Deborah Pushparajah for her guidance in cell culture techniques; Madhuja Chakraborty, Scott Boegel, and Jacqueline Powichrowski for their invaluable help during my experiments in the Department of Chemical Engineering, particularly with flow cytometry; and Andrea Monjo for her expertise in training me on ELISA experiments. I also wish to express my sincere appreciation to our research project manager, Julia Lumini, for her unwavering support in the lab and ensuring the smooth operation of all activities.

I am incredibly fortunate to have had wonderful lab mates from both the Slavcev lab and Aucoin lab: Jesse St. Jean, Deborah Pushparajah, Rohini Prakasah, Heba Alattas, Nicholas Cheng, Mehraveh Hosseinali, Shirley Cheung, Merium Fernando, Jacqueline Powichrowski, Madhuja Chakraborty, Lisa Nielsen, Christopher Sung, and Scott Boegel. They provided me with endless

laughter, shoulders to cry on, and much-needed coffee and pastries—my graduate studies would not have been possible without them. Lastly, I want to express my deepest gratitude to my parents, brother, and friends for their unconditional love and support. You are truly my world, and I thank you for everything you do.

TABLE OF CONTENTS

LIST OF TABLES

LIST OF FIGURES

TABLE OF ABBREVIATIONS

AA	Amino acid
AAV	Adeno-associated virus
Ab	Antibody
Amp	Ampicillin
APC	Antigen presenting cell
ATP	Adenosine triphosphate
ATCC	American Type Culture Collection
ADCC	Antibody-dependent cellular cytotoxicity
bp	Base pair
CAR-T	Chimeric Antigen Receptor T-Cell
CDC	Complement dependent cytotoxicity
CFU	Colony forming units
CpG	Unmethylated cytosine–guanine dinucleotide
cmv	Cytomegalovirus
DMEM	Dulbecco's Modified Eagle's Medium
DC	Dendritic cell
MADLS	Multi-angle dynamic light scattering
DNA	Deoxyribonucleic acid
dsDNA	Double-stranded DNA
EGF	Epidermal growth factor
EGFR	Epidermal growth factor receptor
ELISA	Enzyme-linked immunosorbent assay
FBS	Fetal bovine serum
GFR	Growth factor receptor
GFP	Green fluorescent protein
Grb2/Sos	Growth factor receptor-binding protein 2
HCV	Hepatitis C virus
HER2	Human epidermal growth factor receptor 2
HIV	Human immunodeficiency virus

HPV	Human papillomavirus
HRP	Horseradish peroxidase
IL	Interleukin
Kan	Kanamycin
kb	Kilobases
kDa	Kilodaltons
LB	Luria broth
MAC	Membrane attack complex
MHC	Major histocompatibility complex
MCS	Multiple cloning site
MVB	Multivesicular bodies
mAb	Monoclonal antibody
NEB	New England Biolabs
NLS	Nuclear localization signal
NK	Natural killer
OD	Optical density
ori	Origin of replication
PAMP	Pathogen-associated molecular patterns
PBS	Phosphate-buffered saline
PEG	Polyethylene glycol
PRR	Pattern recognition receptors
PS	Packaging signal
PCR	Polymerase chain reaction
PI3K	Phosphoinositide 3-kinase
PLCγ1	phospholipase C- γ1
PTB	Phosphotyrosine binding
RE	Restriction enzyme
RF	Replicative factor
rpm	Revolutions per minute
RTK	Receptor tyrosine kinase
SEM	Standard error mean

SS	Super sequence
ssDNA	Single-stranded DNA
SH2	Src homology 2
SOS	Son of Sevenless
SV	Simian virus
TBS	Tris-buffered saline
Th	T helper
Treg	T regulatory
TK	Tyrosine kinase
TME	Tumour microenvironment
TLR	Toll-like receptor
TRAIL	Tumour necrosis factor-related apoptosis-inducing ligand
V	Volts
VEGF	Vascular endothelial growth factor
VEGFR	Vascular endothelial growth factor receptor
VLP	Virus-like particle
X-SCID	X-linked severe combined immunodeficiency
MVB	Multivesicular bodies
NSCLC	Non-small cell lung cancers

Chapter 1: Perspective

Gene therapy is a revolutionary medical technique that introduces exogenous DNA to human cells to treat genetic diseases (Dunbar et al., 2018). The theoretical advantage of this strategy is that a durable and possible curative benefit would be achieved in a single treatment. The primary goals of gene therapy include correcting defective genes responsible for disease development, providing new or modified genes that help fight disease, and improving the body's natural ability to combat or repair genetic disorders. Specifically in the field of cancer research, the concept is best illustrated by genetic editing of T cells for cancer immunotherapy, known as Chimeric Antigen Receptor T-Cell (CAR-T) therapy (Dunbar et al., 2018). In this therapy, T cells are genetically modified to express chimeric antigen receptors (CARs) on their surface (Dunbar et al., 2018; Sadelain et al., 2017). This is commonly engineered using viral vectors, such as lentiviruses or retroviruses, to introduce the CAR gene into the T cells (Esensten et al., 2017). The genetically engineered T cells are cultured in the laboratory and infused back into the patient. The component of the CAR on the T cell surface recognizes and binds to a specific antigen on the surface of tumour cells (Sadelain et al., 2017). The binding of the CAR to the antigen is highly specific, allowing the CAR-T cell to target and engage tumour cells precisely. The successful binding and activation of CAR-T cells triggers a cascade of immune responses, leading to the release of cytotoxic granules and cytokines that kill tumour cells. In recent years, CAR-T cell therapy have achieved remarkable clinical outcomes, particularly in treating hematologic malignancies (Sadelain et al., 2017). This underscores the benefits of designing a targeted immunotherapy in the context of treating cancer with gene therapy.

Gene delivery technology has significantly progressed. An optimal gene therapy should exhibit the following characteristics: (1) the capacity to carry relatively large genetic inserts with a high transfection rate; (2) a non-invasive administration method; (3) the ability to sustain gene expression at therapeutic levels or to titrate to therapeutic index via a redosable profile; (4) a high target-specific selectivity for the tumour type; (5) a high safety profile; and (6) high bioavailability (T. Li et al., 2018). Among the prevalent methods for delivering genetic material to targeted cells are nanoparticles. However, these nanoparticles present challenges, including manufacturing complexity, potential toxicity, and delivery efficiency (Gavas et al., 2021). Once administered, nanoparticles must overcome various intracellular barriers to deliver their genetic material effectively. Achieving efficient delivery to specific cell types while avoiding non-target tissues remains a significant challenge (Gavas et al., 2021).

M13 bacteriophage (phage), a filamentous virus that infects bacteria, has gained attention as a promising vehicle for targeted gene delivery in therapeutic applications (Chongchai et al., 2024). M13 phage can be genetically modified to display ligands on its capsid proteins, allowing for precise targeting of specific cell types (Larocca et al., 2001). Additionally, their lack of tropism for mammalian cells and their natural residence in the human gut makes them a potentially a safe gene delivery vehicle for therapeutic use in humans (Huh et al., 2019; Kim et al., 2012). Lastly, M13 phages can also be produced in large quantities using bacterial cultures, facilitating scalable production for clinical applications. These unique properties make it an attractive candidate for gene therapy, offering several advantages over traditional delivery methods. By engineering M13 phage to display peptides or antibodies that bind to specific receptors on the targeted cells, high specificity in gene delivery can be achieved. In this project, an epidermal growth factor (EGF)

peptide is fused to the coat protein III of M13 phage to promote targeted entry to tumour cells with epidermal growth factor receptor (EGFR) overexpression. EGFR is overexpressed or mutated in many types of cancers, including non-small cell lung cancer, colorectal cancer, and breast cancer (Raymond et al., 2000). EGFR is a transmembrane receptor that triggers a cascade of downstream signalling pathways such as the mitogen-activated protein kinase (MAPK) pathway, the phosphoinositide 3-kinase (PI3K)/AKT pathway, and phospholipase C gamma (PLCγ) pathway upon binding with its natural ligand EGF (Wee & Wang, 2017). These pathways promote cell proliferation and survival making EGFR a critical target for cancer therapy. Targeting EGFR with EGF-displaying phages may potentially interfere with the receptor's natural function (Huh et al., 2022) and may also enhance the specificity of the therapy reducing off-target effects and increasing the therapeutic index.

Human papillomavirus (HPV) virus-like particle (VLP) is a non-infectious particle, composed of HPVs structural proteins but lacking its harmful genetic material (Uddin et al., 2019). The major capsid protein of HPV, L1, can self-assemble into functional VLPs and trigger potent immune responses after administration (Van den Bergh et al., 2014). HPV VLP-based vaccines including Gardasil® and Cervarix® have proven to be highly effective in preventing HPV infections, and consequently HPV-related cancers (Nicoli et al., 2020). By genetically engineering the L1 protein, specific peptides can be displayed on the surfaces to direct VLPs towards specific receptors (Huber et al., 2017). Due to their ease of production and characterization, strong immunogenicity, and peptide fusion tolerance, HPV VLPs have emerged as promising tools in cancer immunotherapy (Huber et al., 2017). In a previous project, the Slavcev and Aucoin's research group successfully constructed an HPV VLP displaying a known anti-tumour peptide,

VGB4 (Pushparajah, 2022). This peptide simultaneously targets two vascular endothelial growth factor receptors (VEGFRs), VEGFR-1 and VEGFR-2, and has been shown to limit tumour formation, which has been attributed to its robust anti-angiogenic effect (Farzaneh Behelgardi et al., 2018, 2020). We chose to insert this peptide within the DE loop of the L1 protein as it has consistently demonstrated the formation of VLPs (Huber et al., 2017; Pushparajah, 2022). To further advance the delivery of the previously constructed HPV VLPs, this project aims to encapsulate a DNA sequence expressing VGB4-displaying HPV VLPs in M13 phage engineered with a EGF surface display, and subsequently assess the presence of these VLPs in EGFR-overexpressing tumour cells. The successful formation of the HPV VLPs will support the potential of this hybrid gene delivery system as a novel cancer immunotherapy.

Chapter 2: Introduction

2.1 Cancer and growth factor receptors

Cancer arises from uncontrolled cell proliferation, leading to the formation of tumours that can potentially spread to other parts of the body (Yahya & Alqadhi, 2021). Unlike normal cells, tumour cells often overexpress growth factor receptors, which play an essential role in promoting uncontrolled cell proliferation (Lee et al., 2018). Receptor tyrosine kinases (RTKs) are a family of cell surface receptors that play pivotal roles in the regulation of cell growth, differentiation, metabolism, and survival. The dysregulation of RTKs in particular contributes to the development and progression of cancer (Du & Lovly, 2018; Lemmon et al., 2014). There are currently 58 known RTKs identified in humans which are categorized into 20 subfamilies (Lemmon & Schlessinger, 2010). These receptors all share similar structures, including an extracellular domain for ligand binding, a single transmembrane helix, and a cytoplasmic tail that contains the protein tyrosine kinase (TK) domain with an additional carboxyl terminus (Lemmon & Schlessinger, 2010). RTKs are generally activated by receptor-specific ligands, binding to the extracellular region of the receptor. Once a RTK is bound to its corresponding growth factor ligand, the phosphorylation of the TK domain triggers a conformational change in the receptor and initiates a downstream signalling cascade. This autophosphorylation activity recruits and activates a wide range of molecules in the cytoplasm to perform different biological processes for growth (Du & Lovly, 2018). This project focuses on two key RTKs involved in cancer – epidermal growth factor receptor (EGFR) and vascular endothelial growth factor receptor (VEGFR). The roles and functions of these two receptors will be discussed in the following subsections.

2.1.1 EGFR and other ErbB family proteins

EGFR, also known as ErbB1 or HER1 is by far the most studied protein in the ErbB family, and plays a critical role in regulating cell proliferation, survival, differentiation, and migration (Normanno et al., 2006). These receptors are often overexpressed in epithelial tumour cells, which contribute to tumour progression. On average, 50-70% of lung, colon, and breast cancer have been found to express a high number of EGFRs (Raymond et al., 2000). In normal cells, the expression of EGFR is estimated to be from 40,000 – 100,000 receptors per cell, however, expression of more than 10^6 receptors per cell is observed in cancer cells (Wee & Wang, 2017). EGFR is a 170 kDa transmembrane glycoprotein that has ligand-dependent tyrosine kinase activity. It consists of three major domains, including an extracellular N-terminus ligand-binding region (622 AA), a hydrophobic transmembrane region (23 AA) and a cytoplasmic C-terminus region with tyrosine kinase activity (542 AA) (Wang et al., 2015). Other ErbB family proteins including ErbB2/HER2, ErbB3/HER3, and ErbB4/HER4 all share similar structures (Halder et al., 2023). EGFR and HER4 are activated through ligand binding to form homodimers or heterodimers with other ErbB receptors, and subsequently triggers phosphorylation (Halder et al., 2023). HER2 has no direct ligand and acts as a preferred dimerization partner for other ErbB receptors (Brennan et al., 2000). HER3 requires heterodimerization with other ErbB receptors (primarily HER2) for activation, as it has impaired kinase activity in the kinase domain (Shi et al., 2010). Various ligands can bind to the extracellular domains of the ErbB receptors to induce dimerization. More specifically, EGF, TGF-α, amphiregulin, epiregulin and betacellulin are ligands for EGFR (Frey & Brent Polk, 2014). Neuregulins, such as NRG1 and NRG2, act as ligands for ErbB3 and ErbB4 (Frey & Brent Polk, 2014). In this project, EGF is displayed on the surface of our M13 phage-derived gene vector to enable specific gene transfer to EGFR

overexpressed tumour cells. To understand the interactions between EGF and EGFR it is important to understand the key steps involved in EGFR activation and endocytosis upon EGF ligand binding, explained in the next subsection.

2.1.2 EGFR dimerization, phosphorylation and endocytosis

Dimerization and phosphorylation are the key steps in EGFR activation, enabling downstream signalling pathways that mediate various cellular activities, including growth, survival, proliferation and differentiation (Oda et al., 2005). Data have demonstrated the significant overexpression of EGFR in the development of malignancy in cancer, and EGFR has been extensively investigated as a promising molecular target for cancer therapy (Olayioye et al., 2000). The 721st lysine residue within the cytoplasmic region is necessary for ATP binding to generate a phosphate for tyrosine phosphorylation reaction (Sorkin & Goh, 2008). Most EGFRs exist as transmembrane glycoprotein monomers before ligand-binding. Characterized ligands that bind to EGFR include EGF, transforming growth factor-α (TGFα), amphiregulin, heparin-binding EGF-like growth factor, betacellulin, and epiregulin (Sasaki et al., 2013). EGF is the most common ligand that binds to EGFR. The binding of EGF leads to dimerization of two EGFRs and subsequently induces phosphorylation of specific tyrosine residues within the cytoplasmic tail (Normanno et al., 2006). The phosphorylated residues in the C-terminus serve as docking sites for several Src homology 2 molecules (SH2) and phosphotyrosine binding (PTB) domains, resulting in the activation of downstream signalling pathways for cell proliferation, adhesion, migration and differentiation (Wang et al., 2015). These molecules contain signal transducers such as p85, growth factor receptor-binding protein 2 (Grb2/Sos), and phospholipase C-γ1 (PLCγ1). While most RTKs can be activated upon ligand binding, the activating ligands

have no direct contribution to the dimerization of EGFRs. Instead, the binding of ligand induces substantial conformational change in the extracellular region of EGFR, which exposes the dimerization arm in its domain II (Lemmon et al., 2014; Lemmon & Schlessinger, 2010). Without the bound ligand, the dimerization arm is completely buried in a tethered conformation and dimerization is inhibited. Ligand binding breaks the tether which allows the dimerization arm to protrude and interact with another ligand-bound EGFR (Lemmon & Schlessinger, 2010).

Studies showed that the dimerization of EGFRs upon ligand binding initiates endocytosis, which occurs independently of tyrosine phosphorylation (Wang et al., 2015). Activated EGFRs can be internalized through clathrin-dependent and clathrin-independent pathways (Pinilla-Macua & Sorkin, 2015; Sorkin & Goh, 2008). In the clathrin-dependent pathway, EGFRs are internalized in clathrin-coated vesicles and fused with endosomes for recycling. Clathrin-dependent endocytosis is a fast and highly regulated process. This process is mediated by transferrin receptors and is the major pathway of EGFR internalization (Normanno et al., 2006). There are several molecular determinants that dictate this rapid internalization including the Lys721 residue on EGFR which is known to be a critical site for phosphorylation to initiate the process. Additionally, the C-terminal domain of EGFR serves as a docking site which interacts with multiple signalling molecules upon on dimerization. Mutation in the major binding sites of the Grb2 (growth factor receptor-bound protein 2) adaptor protein is able to significantly inhibit EGFR internalization (Sorkin & Goh, 2008). In both porcine aortic endothelial (PAE) and HeLa cell lines expressing high level of endogenous EGFRs, Grb2-EGFR binding complex was found in the coated pits, suggesting Grb2 is essential for recruiting EGFR into the clathrin-coated pits (Sorkin & von Zastrow, 2009). After internalization into the early endosome, the EGF:EGFR

complex can be either recycled back to the cell membrane or retained in the endosome and transported to lysosomes for degradation (Raymond et al., 2000). Accumulation of EGF and EGFR in the early endosome is observed after 2 – 5 min at 37°C after being endocytosed (Sorkin & Goh, 2008). During the endosomal maturation process, some EGFRs are recycled back to the cell membrane along with EGF. These EGF:EGFR complexes are brought back together because EGFs do not significantly dissociate from the receptor. Simultaneously, some EGF:EGFR complexes remain in the endosome, and those that are attached with the multivesicular bodies (MVB) are subjected to degradation (Sorkin & von Zastrow, 2009). MVB are unique membrane-enclosed structures surrounding the intraluminal vesicles. EGF:EGFR complexes in the MVB are ubiquitinated, which is essential for lysosomal targeting and degradation (Sorkin & von Zastrow, 2009). Notably, the clathrin-dependent pathway has limited capacity and is primarily observed when the physiological concentration of EGF is low (Sorkin & Goh, 2008). In addition to this, increasing EGF concentration in A431 cell lines decreased the rate of EGF uptake (Sorkin & Goh, 2008). Further studies using small interference RNA (siRNA) to knock down the clathrin heavy chain showed that EGFR internalization is not significantly affected when EGF concentration is high (Sigismund et al., 2005). This suggests that the EGF:EGFR complexes can be internalized through clathrin-independent endocytosis. At high EGF concentrations, dimerized EGFRs are internalized through extensive plasma membrane ruffling and formation of micro- and macro-pinocytic vesicles containing labeled EGF and lacking the clathrin coat (Sorkin & Goh, 2008). There is evidence suggesting multiple receptors are involved in mediating clathrin-independent endocytosis, such as GPCRs, RTKs, TGFβ, Wnt, and Notch receptors (Sorkin & von Zastrow, 2009). However, the precise mechanisms of these pathways *in vivo* remain unclear. In general, all the clathrin-independent pathways demonstrated a much slower

rate of endocytosis than the clathrin-dependent pathway (Sorkin & Goh, 2008). The intricate processes of EGFR-mediated phosphorylation and endocytosis underscores the complexity of cellular communication and regulation.

The following subsection will delve into some key EGFR signalling pathways, explaining the significant roles of EGFR in cellular activities and cancer development. Understanding these processes not only provides insight into cellular regulation, but also opens avenues for therapeutic interventions targeting EGFR-mediated pathways.

2.1.3 Key EGFR signalling pathways in HeLa cells

HeLa cells, derived from cervical cancer cells of Henrietta Lacks, are one of the most widely used cell lines in biomedical research (Masters, 2002). These cells exhibit high levels of expression of the EGFRs, making them an important model for studying EGFR-related signalling pathways and testing EGFR-targeted therapies (Capuani et al., 2015). The key signalling pathways activated by EGFR include the mitogen-activated protein kinase (MAPK) pathway, the PI3K/AKT pathway, and the PLCγ pathway (Wee & Wang, 2017). All these pathways are critical for the growth and survival of tumour cells, including HeLa. HeLa cells exhibit EGFR at approximately 300,000 molecules per cell (Capuani et al., 2015). Some colorectal carcinoma cell lines such as Caco2, HCT116, HT29, and SW948 also show EGFR overexpression, ranging from 20,000 to 40,000 molecules per cell, but not to the same level as HeLa cells (Gruijs et al., 2022). Therefore, HeLa cells were chosen as the primary cell model in this study.

The MAPK pathway, activated by EGFR phosphorylation recruits adaptor proteins such as Grb2 and SOS (Son of Sevenless), which facilitate the activation of RAS, a small GTPase (Guo et al., 2020). Activated RAS then recruits and activates RAF, a serine/threonine kinase. RAF phosphorylates and activates MEK (mitogen-activated protein kinase kinase), which in turn phosphorylates and activates ERK (extracellular signal-regulated kinase). ERK, a type of serine/threonine protein kinase, is a signal transduction protein that transmits mitogen signals (Zhang & Liu, 2002). It promotes cell proliferation by translocating to the nucleus and activating transcription factors that drive the expression of genes involved in cell cycle progression and division (Zhang & Liu, 2002). In tumour cells, the MAPK signalling pathway is crucial for sustaining their rapid proliferation and growth (Guo et al., 2020).

In tumour cells, the PI3K/AKT/mTOR (PAM) pathway is often hyper-activated due to activating mutations to EGFRs (Wee & Wang, 2017). Upon phosphorylation, EGFR initiates the PAM pathway by recruiting and activating phosphoinositide 3-kinase (PI3K) through its SH2 domain-containing regulatory subunit (Glaviano et al., 2023). The activated PI3K catalyzes the conversion of phosphatidylinositol 4,5-bisphosphate (PIP2) to phosphatidylinositol 3,4,5-trisphosphate (PIP3), which serves as a docking site for protein kinase B (AKT). Subsequent phosphorylation and activation of AKT are mediated by phosphoinositide-dependent kinase-1 (PDK1) and the mammalian target of rapamycin complex 2 (mTORC2). Once activated, AKT phosphorylates a variety of downstream targets, including the mammalian target of rapamycin (mTOR), a key regulator of protein synthesis and cellular growth. Consequently, the hyperactivation of the PAM pathway augments tumour cell survival, metabolic reprogramming,

and resistance to apoptotic signals, thereby promoting the malignant phenotype (Peng et al., 2022).

The PLCγ/PKC pathway activates phospholipase C gamma (PLCγ), which is an essential mediator of cellular signalling. PLCγ1 is frequently enriched and mutated in various cancers and is involved in the processes of tumourigenesis (Jang et al., 2018; Mandal et al., 2021). Upon activation, PLCγ1 hydrolyzes phosphatidylinositol 4,5-bisphosphate (PIP2) to generate diacylglycerol (DAG) and inositol trisphosphate (IP3). DAG subsequently activates protein kinase C (PKC), while IP3 facilitates the release of calcium ions from intracellular stores (Jang et al., 2018). This pathway is pivotal in regulating cell motility and cytoskeletal reorganization. Notably, PLCγ1 has been implicated in the regulation of tumour cell migration, thereby contributing to metastasis (Mandal et al., 2021). However, the role of PLCγ1 in cellular proliferation remains to be fully elucidated (Jang et al., 2018).

In summary, the HeLa cell line serves as a pivotal model for dissecting the complexities of EGFR-related signalling pathways, given its significant expression of EGFRs. Understanding the activation mechanisms and downstream effects of EGFR in these cells is essential for developing targeted therapies. The next subsection outlines the signalling pathways and functions of VEGFR, which is be targeted by the HPV VLPs constructed in this study.

2.1.4 VEGFR signalling in angiogenesis

Another frequently overexpressed RTK in tumour cells are VEGFRs. These receptors are predominantly expressed by vascular endothelial cells and are activated through ligand-induced

conformational changes in the intracellular domain of VEGFRs. This promotes receptor dimerization, leading to the phosphorylation of specific tyrosine residues and the activation of several downstream signalling pathways, including MAPK, RAS/RAF/MEK/ERK, and PAM (Y. Liu et al., 2022). The ligand of this receptor, vascular endothelial growth factor (VEGF) is a well-known angiogenesis modulating ligand that plays a dominant role in promoting endothelial cell proliferation, migration, invasion, and capillary tube formation (Costache et al., 2015; Shibuya, 2011). The VEGF family includes VEGF-A, VEGF-B, VEGF-D, and placental growth factor (PIGF). VEGF-A, commonly referred to as VEGF, is one of the most extensively studied signalling ligands, and acts as a rate-limiting factor in blood vessel formation (Shibuya, 2011). It acts to promote vascular endothelial cell proliferation and increases vascular permeability. VEGF interacts with both VEGFR-1 and VEGFR-2 (Goel & Mercurio, 2013). Studies have suggested that VEGFR1 binds to VEGF with a higher affinity than VEGFR2, but the tyrosine phosphorylation of VEGFR1 in response to VEGF is weaker (Goel & Mercurio, 2013), thus, VEGFR-2 is considered the major mediator of angiogenesis in tumour vasculature.

Angiogenesis is a biological process in which new blood vessels are formed from pre-existing vasculature, supplying tissues with a sufficient amount of oxygen and nutrients to maintain homeostasis and grow (Liu et al., 2023). This process is a hallmark for the development and growth of solid tumours exceeding 1-2 mm^3 (Liu et al., 2023). The primary trigger for angiogenesis in cancer is hypoxia, a key feature of the tumour microenvironment (TME), characterized by insufficient oxygen supply to maintain tissue homeostasis (Goel & Mercurio, 2013). Hypoxia significantly drives the overexpression of VEGF in tumour cells, making anti-angiogenic therapy an effective approach to suppress tumour growth.

In summary, understanding the roles of EGFR and VEGFR in tumour growth highlights the complexity of cancer biology, and underscores the importance of targeted therapies that can simultaneously address multiple pathways involved in cancer progression. The next section will provide an overview of the current cancer therapy developed to target these two receptors.

2.2 Cancer therapy

Cancer has consistently been the first or second leading cause of premature death worldwide since 2000 (Harding et al., 2018). Higher rates of cancer incidence and mortality are more frequently reported in developed countries, largely reflecting increased risk factors such as aging, higher average socioeconomic status, obesity, and smoking (Sung et al., 2021). Recent statistics indicate that the global cancer burden is projected to reach 28.4 million by 2040, representing a 47% increase from 2020 (Sung et al., 2021). In the United States alone, the estimated number of cancer cases in 2022 was approximately 1,918,030, equating to about 5,250 new cases each day (Siegel et al., 2022). Despite these rising numbers, the overall mortality rate has been declining since 2000, primarily due to significant advancements in cancer diagnosis and treatment over the past two decades (Siegel et al., 2022).

Traditional chemotherapies employ broad-spectrum cytotoxic drugs to induce cell apoptosis by interfering with mitosis and disrupting DNA replication processes (Amjad et al., 2022). Unfortunately, this cytotoxicity also affects normal cells, particularly those that frequently divide, such as cells in the bone marrow, gastrointestinal tract, and hair follicles (Amjad et al., 2022). This results in various adverse effects, including pain, loss of appetite, and hair loss.

Additionally, the nonspecific distribution of conventional chemotherapeutic agents is associated with poor bioavailability, rapid blood clearance, and low solubility in the body (Yahya & Alqadhi, 2021). Therefore, many research efforts have been dedicated to minimizing these adverse complications associated with chemotherapy. Over the past few decades, targeted cancer therapy has emerged as a major therapeutic advancement. The ultimate goal of targeted cancer therapy is to selectively eliminate tumour tissues without harming surrounding healthy tissues (Zhong et al., 2021). By inhibiting specific molecules from activating tumour signalling pathways, the idea is to formulate a drug that is specifically toxic to the targeted tumour cells with no adverse effects on normal cells (Lee et al., 2018). These molecular targets often play crucial roles in tumour cell survival, growth, and proliferation, including extracellular ligands, membrane receptors, and various types of protein kinases (Min & Lee, 2022). The following two subsections will highlight some of the promising therapies developed to target EGFR and VEGFR.

2.2.1 EGFR targeted therapy

Due to the critical role of EGFR signalling pathways in tumour progression, EGFR-targeted therapies, such as monoclonal antibodies and tyrosine kinase inhibitors (TKIs) are effective in inhibiting tumour growth and survival. Cetuximab (Erbitux®) is an approved mAb therapy for the treatment of colorectal cancer that acts by targeting EGFR (Berger et al., 2012). Cetuximab binds to the extracellular ligand-binding domain on EGFR, thereby inhibiting the activation of the receptors to prevent downstream signalling. Furthermore, cetuximab can trigger Fcγ-receptor-dependent phagocytosis or cytolysis by immune-effector cells such as neutrophils, macrophages and natural killer (NK) cells by complement dependent cytotoxicity (CDC) or

antibody-dependent cellular cytotoxicity (ADCC) (Berger et al., 2012). CDC is a mechanism of cell lysis where antibodies bound to target cells trigger the complement system to form a membrane attack complex (MAC). The MAC forms pores in the cell membrane, causing an influx of water and ions, leading to the osmotic lysis of the target cell (Adams & Weiner, 2005). ADCC is a mechanism of immune defense where antibodies bound to a target cell recruit immune effector cells that mediate the destruction of the target cell (Adams & Weiner, 2005). The Fc region of the bound antibodies is recognized by Fc receptors on immune effector cells such as natural killer cells, macrophages, and neutrophils. The interaction between the Fc region to the Fc receptors activate effector cells to release cytotoxic substances, such as perforin and granzymes (from NK cells), or induce phagocytosis (by macrophages), leading to the destruction of the target cell (Adams & Weiner, 2005; Chen et al., 2020). While mAbs can stimulate a relatively strong cell-mediated immune response to target tumour cells, this could be a double-edged sword. Clinical evidence showed that a significant number of patients treated with mAb therapies also suffered from immune-related adverse events, especially with antibodies targeting essential immune checkpoints (Marhelava et al., 2019). Gefitinib (Iressa®) is a clinically-approved small molecule inhibitor for EGFR (Berger et al., 2012). In comparison to cetuximab, gefitinib solely acts as an ATP analogue that competes for the ATP binding site on the catalytic kinase domain on EGFR. As a result, the downstream activation of various molecules through EGFR is blocked (Huang et al., 2004). One study used xenograft model mice with a human non-small cell lung cancer (NSCLC) cell line and treated the mice with a combination of cetuximab and gefitinib; the results showed significant reduction in tumour volume by 75% compared to monotherapy which only showed 50% to 20% reduction (Huang et al., 2004).

2.2.2 VEGFR targeted therapy

Bevacizumab (Avastin®) was approved as a first-line immunotherapy by the FDA for treating metastatic colorectal cancer in 2004 (Ferrara et al., 2004). It is a recombinant humanized monoclonal IgG1 that inhibits the binding of VEFG-A to its receptors, thus blocking the downstream signalling necessary for angiogenesis. A more recently FDA approved mAb drug, known as ramucirumab (Cyramza®) blocks the binding site on VEGFR-2 preventing ligand binding and thus reduces tumour cell density (Oholendt & Zadlo, 2015). Since 2014, ramucirumab has been a promising option to treat advanced gastric cancer in combination with other therapeutic options (Refolo et al., 2020). The use of peptides to inhibit angiogenesis has emerged as a promising targeted treatment for cancer. The interaction between VEGFR and VEGF is one of the most important modulators in tumour angiogenesis, thereby inhibiting the activation of this signalling pathway could present an effective therapeutic approach for cancer (Rosca et al., 2011). A promising candidate known as VGB4 has demonstrated the ability to block the extracellular ligand-binding domain on VEGFR-1 and VEGFR-2 (Farzaneh Behelgardi et al., 2018), thereby preventing VEGF from binding to both receptors. This peptide is only 23 amino acids (AA) in length and acts as an antagonist to VEGF as it was derived from two binding regions of VEGF-B and a receptor binding region of VEGF-A (Farzaneh Behelgardi et al., 2018). VGB4 contains three major segments that were designed based on α2-β3 loop (loop1) and β5-β6 loop (loop3) of VEGF-B as well as β5-β6 loop (loop3) of VEGF-A (Farzaneh Behelgardi et al., 2018). All of these regions contain essential binding residues in forming the interfaces for ligand-binding on the receptors. VEGFR-1 and VEGFR-2 are primarily responsible for activating PI3K/AKT and MAPK/ERK signalling pathways, respectively (Shibuya, 2011). While the PI3K/AKT signalling cascade is not fully understood, it is critical in facilitating cell

migration and proliferation in mice models (Shibuya, 2011). On the other hand, VEGFR-2 has a much stronger autophosphorylation activity than VEGFR-1. The activation of MAPK/ERK signalling via VEGFR-2 is essential for directing pro-angiogenic activity. Based on cell model studies, VGB4 markedly induced apoptosis by simultaneously preventing VEGFR-1 and VEGFR-2 mediated angiogenesis (Farzaneh Behelgardi et al., 2018, 2022). As a result, this therapeutic peptide has demonstrated a strong potential to either reduce or completely block the signalling of PI3K/AKT and MAPK/ERK pathways (Farzaneh Behelgardi et al., 2018). A recent cell model study showed that VGB4 induces apoptosis in human lung adenocarcinoma cells (A549) and human colorectal adenocarcinoma cells (HT-29) (Farzaneh Behelgardi et al., 2022). The inhibitory effect of VGB4 peptides act in a dose-dependent manner. In HT-29 cell lines, the apoptosis portion was 34.6% at a VGB4 concentration of 0.74 μM. As the concentration increased to 0.93 μM, there was a profound impact on inducing apoptosis in HT-29 cells leading to 87.3% cell death (Farzaneh Behelgardi et al., 2022). VGB4 disrupts the interaction between VEGF and VEGFR leading to the activation of p53/BAX/caspase 9/caspase 3 pathway directing apoptosis and inactivation of PI3K/AKT/XIAP pathway, which is responsible for tumour cell proliferation and migration.

2.2.3 Gene therapy for cancer

Nearly five decades ago, scientists hypothesized that introducing exogeneous DNA to the human genome might be an effective way to treat genetic and inherited human diseases (Dunbar et al., 2018). Gene therapy relies heavily on constructing an efficient, safe, and specific delivery system. The choice of delivery vector is a critical determinant of the successful expression of the gene of interest. The gene-delivery vehicle must facilitate entry into the cell and transfer the gene

to the nucleus, where it can be transcribed into mRNA. Gene transfer vectors are broadly classified as either viral or non-viral (T. Li et al., 2018; Nayerossadat et al., 2012).

Viral gene delivery systems are the first and most widely applied delivery platform. These viral vectors can transfer exogenous genetic material into target cells via the natural infection mechanisms of viruses. Various viruses have been extensively studied for gene therapy, including adeno-associated virus (AAV), lentivirus, adenovirus, retrovirus, and herpes simplex virus (HSV) (Nayerossadat et al., 2012). Viral-based systems offer high transduction efficiency and sustained gene expression (Nayerossadat et al., 2012). Nevertheless, they are associated with several drawbacks such as immunogenicity, toxicity, mutagenicity, high production costs, and limited cargo capacity (Sinclair et al., 2016). One of the most successful gene therapy trials to date involved using retroviral vectors to treat X-linked severe combined immunodeficiency (X-SCID) (Dunbar et al., 2018). Patients with X-SCID lack the ability to mount cell-mediated immune responses and produce antibodies, primarily due to mutations in the gene encoding the γ_c-encoding gene, a crucial component of several hematopoietic cytokine receptors (Cavazzana et al., 2016). A clinical trial conducted in 2002 demonstrated four of five patients with X-SCID treated with a gene therapy aiming to restore the function of γ_c had successfully restored a functional immune system (Hacein-Bey-Abina et al., 2002).

Non-viral gene therapy utilizes vectors not originally derived from viruses. These vectors are typically composed of either DNA or RNA, encapsulated by a protective vehicle to bypass biological barriers and reach targeted sites (Nayerossadat et al., 2012). The spontaneous uptake of DNA by cells is generally low, necessitating additional methods to effectively deliver non-

viral vectors, which can be physical or chemical (Nayerossadat et al., 2012; Sinclair et al., 2016). Physical methods of non-viral gene delivery are based on assisting with the transient penetration of cell membrane by mechanical, electrical, ultrasonic, hydrodynamic, or laser-based energy so that DNA can enter into the cells (Nayerossadat et al., 2012; Sinclair et al., 2016). The most common chemical method of non-viral gene delivery is using cationic polymers that encapsulate the negatively charged DNA. Non-viral gene vectors tend to be less immunogenic than viral vectors, indicating a relatively safer profile. However, while non-viral vectors offer a safety advantage, their transfection efficiency is lower compared to viral vectors since non-viral vectors must be formulated to escape the endosomes and enter the nucleus effectively.
(Sinclair et al., 2016).

Gene therapy has been extensively explored as a treatment option for cancer. The goal is to deliver foreign genes to cancer cells with the ability to inhibit tumourigenesis by promoting the expression of tumour suppressor genes or decreasing the expression of oncogenes (Cross & Burmester, 2006). Alternatively, certain genes can enhance the immunogenicity of TME to promote immune cell recognition and ultimately lead to tumour destruction as a cancer immunotherapy (Cross & Burmester, 2006). Figure 1 illustrates a schematic of gene therapy-based cancer immunotherapy application. The administration of gene therapy can be either *in vivo* or *ex vivo*. *In vivo* gene therapy involves direct injection of the therapeutic agent into the body, which can be administered intravenously, injected into muscles, infused or injected into an organ or bodily structure, or injected directly into a tumour (Sinclair et al., 2016). With an *ex vivo* delivery system, cells are first harvested from the patient or a healthy donor, gene modifications are performed on these cells, and then transferred into the patients (Sinclair et al.,

2016). The modified cells should theoretically replicate and spread through the body. Unlike *in vivo* therapy, *ex vivo* therapy transfers or modifies genes in a specific cell type without affecting other cells. This avoids undesirable immune responses which is an apparent advantage of *ex vivo* therapy (Sinclair et al., 2016).

Both viral and non-viral vectors present certain drawbacks in terms of safety and efficacy with each existing gene delivery vector having its advantages and limitations. Consequently, substantial research efforts have been dedicated to developing innovative vectors with enhanced gene delivery capacities. In this study, we develop a novel M13 phage-based gene delivery vector. The following section will provide an overview of M13 phage and how it can be used as a promising candidate for gene transfer applications.

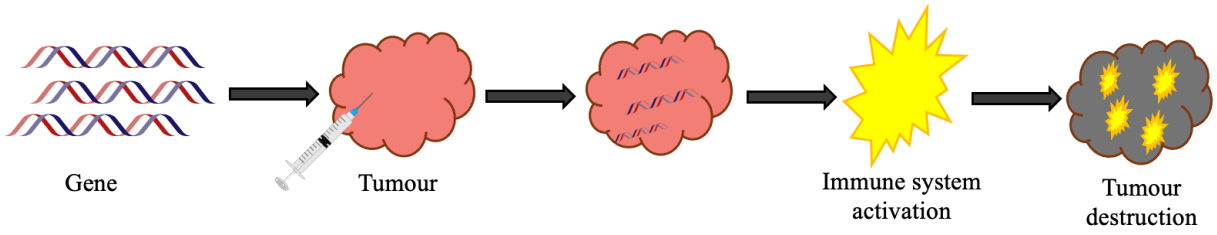

Figure 1: Schematic diagram of cancer immunotherapy with gene therapy. Once the genes are delivered to the tumour, their expression enhances the immunogenicity of the tumour, promoting immune cell recognition, and ultimately leading to the destruction of tumour cells (Image adapted from Cross & Burmester, 2006). This is the fundamental basis of the cancer immunotherapy platform approach investigated in this project.

2.3 Bacteriophage-based therapy

The number of phages on Earth is approximately 10^{31}, making them the most abundant entities in the biosphere (Aloisio et al., 2021; Wu et al., 2016). Phages are defined as viruses that specifically infect bacteria; the human microbiome is extensively colonized by a diverse range of phages (Zuppi et al., 2022). Numerous studies have demonstrated the importance of phage in

modulating and maintaining a healthy human gut microbiota (Aloisio et al., 2021; Zuppi et al., 2022). Initially, phage therapy was developed to treat bacterial infections by leveraging their unique ability to infect bacteria exclusively (Hatfull et al., 2022; Manivannan et al., 2022). Significant research has focused on creating effective phage cocktails to combat antibiotic-resistant bacterial infections (Hatfull et al., 2022). With advancements in gene therapy, phages have attracted attention as potential vectors (Petrov et al., 2022). A variety of phages have been investigated as non-viral gene delivery vectors for cancer therapy, such as M13, lambda, and T4 (Petrov et al., 2022). Phages are considered non-viral vectors because they already exist symbiotically with humans and do not replicate within eukaryotic cells, offering a safer alternative to viral vectors for therapeutic purposes (Huh et al., 2019; Petrov et al., 2022). Phages such as M13 have shown remarkable ability to penetrate various physiological barriers in the human body, including the blood-brain barrier (Huh et al., 2019). The capsid coding genes of various phages can fuse with different epitope coding genes. Upon a phage infection into host cells, the epitope coding genes are translated and then displayed on the phage surface. This phage display technology involves constructing a biopanning library to screen for therapeutic molecules (Aloisio et al., 2021; Wu et al., 2016). This technology has enabled the rapid selection of high-affinity mAbs. In targeted cancer therapy, the use of M13, T4, and lambda phages have all been engineered to display various RTK inhibitors (Aloisio et al., 2021). In our previous research projects, we have constructed M13 and lambda phages displaying EGF. We found that the internalization of both EGF-targeted M13 and lambda phages was more efficient and persistent than wild-type phages in EGFR+ cell lines (Huh et al., 2022; Wong, 2022). Additionally, our lab examined the internalization and accumulation of EGF-displaying lambda phages on tumour spheroids and assessed their impacts on spheroid formation and growth.

Tumour spheroids mimic the pathophysiological environment and morphology of *in vivo* solid tumours, providing an effective model for evaluating the early-stage effects of cancer therapy. Our EGF-targeted lambda phages demonstrated the ability to penetrate colorectal carcinoma spheroids and interfere with their formation and growth, suggesting that targeted phage technology is a promising and feasible delivery platform for targeted cancer therapy (Huh et al., 2022).

2.3.1 M13 phage display and life cycle

Phages are generally categorized as lytic or filamentous (Clokie et al., 2011). Lytic phages burst out of the host bacteria and kill the host at the end of their infection cycles. By contrast, filamentous phages are non-lytic, which means they do not lyse the host, rather their progenies are expelled out of the host during the infection cycle with a decreased growth rate (Loh et al., 2019). Filamentous phages such as M13 are the typical choice for phage display because they can carry relatively large foreign gene inserts at their coat protein genes (Sidhu et al., 2007). M13 is a F+ *Escherichia coli (E. coli)*-specific phage with a single-stranded (ss) DNA (ssDNA) core surrounded by 5 different coat proteins. Its coat proteins pIII and pVIII are the two most common sites for displaying peptides (Ledsgaard et al., 2018). As shown in Figure 2, there are 5 copies of pIII located at the tail end of the phage and pVIII is the major coat protein wrapping around the ssDNA core with approximately 2700 copies (Smeal et al., 2017). The life cycle of M13 phage begins with attaching to the extended pilus on the bacteria via its pIII protein. The bacterial pilus retracts and brings the phage in contact with Tol proteins, which mediate the entry into the cell (Karlsson et al., 2003). M13 phages are capable of binding to specific Tol proteins on the surface of mammalian cells and are then subsequently endocytosed into the cytoplasm

(Karlsson et al., 2003). The penetration of bacterial membrane and transfer of foreign DNA is dependent on the presence of bacterial membrane protein TolQRA (Click & Webster, 1998). The Tol proteins of *E. coli* maintain outer membrane stability and are required for the uptake of group A colicins (Click & Webster, 1998). Colicins are proteins produced by some *E. coli* strains that are toxic to other *E. coli* strains (Cascales et al., 2007). Group A colicins can be translocated by Tol proteins because they are encoded by relatively small plasmids (Cascales et al., 2007). Tol proteins are found within the adhesion zones which are the contact site between inner and outer membranes. They are essential for bridging the inner and outer membranes across the periplasmic space and peptidoglycan. The initial uptake of M13 phage is similar to that of group A colicins, in which it starts with the interaction between the N1 domain of pIII and TolA (Click & Webster, 1998; Karlsson et al., 2003). TolA protein consists of three domains: its N-terminal domain is anchored in the inner membrane of the bacteria which interacts with TolQ and TolR, its central domain spans through the periplasmic space with an α-helical conformation (Click & Webster, 1998), and finally, its C-terminal domain extends to the outer membrane of the bacteria and acts as a coreceptor for pIII during M13 phage infection. Upon a M13 phage infection, the N2 domain of pIII interacts with the F-pilus on the outside of the bacteria, it also interacts with other membrane proteins including OmpF and Pal lipoprotein that help to retract the pilus (Karlsson et al., 2003). After F-pilus retraction, the N1 domain of pIII binds to the C-terminal domain of TolA. Since TolA proteins are attached to both the inner and outer bacterial membrane, the interaction with the phage brings the two membranes in close contact (Karlsson et al., 2003). The membrane-spanning central domain of TolA can interact with the N2 domain of pIII. Finally, pIII is inserted into the inner membrane and the cap of M13 phage opens to allow phage DNA to enter into the bacteria. As the phage moves past the inner membrane, coat

proteins are deposited (Karlsson et al., 2003). pIII plays a crucial role in the initial attachment to the host cell's F pilus and the subsequent introduction of phage DNA into the host. Therefore, it is a common and suitable site for display short peptide sequence such as EGF.

Once in the cytoplasm, the single-stranded viral genome must be converted to a dsDNA replicative form (RF) by the host DNA replication machinery (Smeal et al., 2017). After the initial expression of phage genes in the host cell, M13 replication proceeds through a rolling circle mechanism of amplification to produce more RFs. The binding of phage coat protein pII initiates this process (Smeal et al., 2017). As the replication proceeds and more RF dsDNA copies are produced, the accumulation of coat protein pV binds to free ssDNA copies and prevents the host replication proteins from producing more RFs (Mazur & Model, 1973). Multiple pV proteins bind and collapse the phage ssDNA into a rod-like shape. Along with the phage DNA replication process, other necessary coat proteins are produced and assembled around the packaged ssDNA. Once the assembly is complete, a new M13 phage particle is extruded at the cell membrane (Smeal et al., 2017). The initial assembly of new phage particles also relies on a functional packing signal (PS) which is recognized by pI proteins. The binding of pI mediates the interactions between ssDNA and other coat proteins to produce the final phage progenies at the host cell membrane (Haigh & Webster, 1999). The phage progenies are extruded by passing through the host cell membrane, and the process is mediated by the phage-encoded proteins.

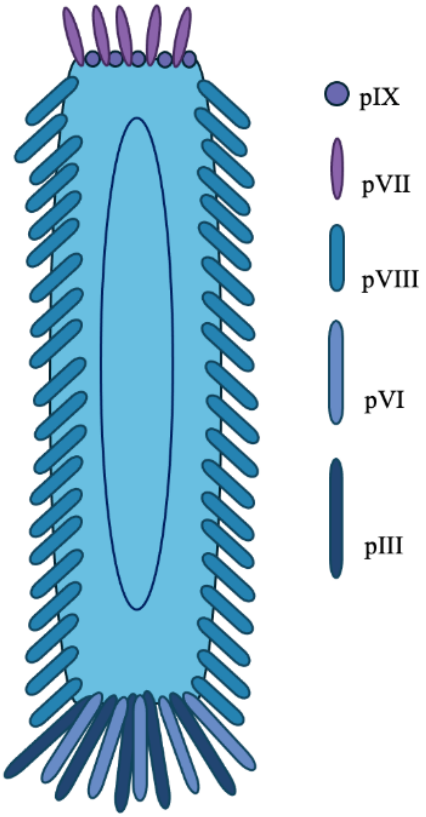

Figure 2: A schematic diagram of M13 phage. A circular closed ssDNA core is surrounded by approximately 2700 copies of pVIII. At the top, approximately 5 copies of pIX and 5 copies of pVII form a blunt cap. At the bottom, approximately 5 copies of pIII and 5 copies of pVI form a protruding tail. In this project, the M13 phage is engineered to display EGF at the N-terminus of pIII, oriented outwards to facilitate the internalization of phage into targeted cells. The details of how M13 phage can be engineered as a promising gene vector will be explained in the next two subsections.

2.3.2 M13 phage-based gene delivery

Both viral and non-viral vectors have their advantages and limitations, prompting significant research efforts to develop innovative vectors with enhanced gene delivery capacities. Among these, M13 phages have emerged as a promising non-viral vector for delivering therapeutic genes to tumour cells (Petrov et al., 2022). M13 phages offer a stronger safety profile than viral vectors because they specifically infect bacteria, show no intrinsic tropism, and do not replicate in mammalian cells.

When a non-viral vector such as a liposome is endocytosed by a cell, it becomes trapped in the endosome and must escape the endosomal pathway to avoid being degraded by enzymes in the lysosome, therefore, endosomal escape is a known bottleneck for non-viral gene delivery (Degors et al., 2019). In the case of phage entry, the harsh environment of the endosome, such as low pH, may aid in digesting the phage coat protein and exposing its encapsulated DNA (Wong, 2022), therefore, endosomal entry may be necessary for phage-mediated gene delivery. Our studies also showed that the addition of a cationic polymer, TurboFect helps phage to escape the endosomal compartment and increase gene transfer efficiency (Wong, 2022). However, the use of TurboFect *in vivo* is not recommended because it can be toxic and expensive to scale up, thus, further research is needed to enhance the gene transfer efficiency of an M13-mediated gene delivery system.

Utilizing the advantages of M13 phage, a recent study has developed a novel therapeutic approach for chondrosarcoma, a type of bone cancer (Chongchai et al., 2024). The M13 phage-derived particle (PDP) displays a double cyclic RGD4C ligand on its capsid, which binds specifically to avb3 and avb5 integrin receptors, which are overexpressed in tumour cells but not in normal chondrocytes. The PDP was designed to carry a transgene cassette encoding a secreted form of the tumour necrosis factor-related apoptosis-inducing ligand (sTRAIL), and was shown to selectively deliver genes to chondrosarcoma cells, inducing high expression of TRAIL receptors and subsequent tumour cell apoptosis without harming normal chondrocytes. In both cell culture and mice models, a significant decrease in tumour cell viability and tumour size was observed (Chongchai et al., 2024). These findings highlighted the potential of M13 phage-based

vectors in delivering therapeutic genes specifically to tumour cells, opening new avenues for cancer gene therapy.

2.3.3 Production of a miniaturized M13 phage-based gene delivery vector

The f1 origin of replication (*ori*) on the M13 phage genome is a necessary element needed for replication and extrusion of new phage particles (Cleary & Ray, 1980). In the presence of a M13 helper phage expressing the necessary coat proteins for phage assembly and extrusion, the f1 *ori* can be cloned into any plasmids to initiate phage-mediated replication of the target vectors in the bacterial host infected by M13 phage and then encapsulated by phage progenies (Levinson et al., 1984). Vectors being delivered through this process are known as phagemids, containing a phage *ori*, a targeted gene, and an antibiotic resistant marker (Bazan et al., 2012). Compared to the use of viral vectors for gene delivery, phagemids offer a much safer option due to a lack of intrinsic pathogenicity in addition to economical production (Larocca et al., 2001). Nevertheless, one of the major bottlenecks of the f1 *ori* on the helper phage genome naturally competes with the f1 *ori* on the phagemid for replication and assembly. Therefore, the final phage lysate obtained from bacterial cell culture infected by phages would contain phage progenies carrying a mix of either helper phage or phagemid DNA (Levinson et al., 1984). This represented a major limitation encountered during phagemid production because the presence of helper phage in the phage lysate significantly interfered the yield and purity of phagemid. The goal of this project is to modify the plasmid encoding the helper phage genome to eliminate the presence of helper phage in the lysate. One of the most successful approaches is to replace the f1 *ori* on the helper phage plasmid with a different plasmid origin of replication and simultaneously disrupt the structure of f1 *ori* to completely abolish its function. M13KO7 is a common, widely used helper

phage derived from M13 with a p15a *ori* that disrupts the structure of f1 ori and it also carries a kanamycin (Kan) resistance gene from Tn903 (Chasteen et al., 2006). The use of M13KO7 for the production of phage progeny carrying phagemid DNA shows significant reduction in helper phage plasmid self-packing (Chasteen et al., 2006).

Similar to conventional bacterial plasmids, the backbone elements of the phagemid such as bacterial *ori* and antibiotic-resistant markers are potential risk factors for horizontal gene transfer (Sum et al., 2014). Additionally, the presence of unmethylated cytosine–guanine dinucleotide (CpG) motifs on conventional plasmids stimulates immune responses that may ultimately trigger gene silencing (Krieg, 2002). CpG motifs are unique to prokaryotes and recognized as pathogen PAMPs by TLR-9 in mammalian cells (Krieg, 2002). This can trigger inflammatory responses and ultimately lead to gene silencing (Krieg, 2002). Furthermore, the removal of antibiotic resistance gene can avoid the spread of antibiotic resistance to the environment. Therefore, an alternative to conventional plasmids without the prokaryotic backbone could be a promising solution. Recently, a minivector phagemid referred to as miniphagemid was constructed without any prokaryotic elements by splitting the f1 *ori* into a start and stop region. In the presence of a M13 helper phage, the progeny virions encapsulated a single-stranded miniphagemid containing only the inserted transgene expression cassette between the split f1 *ori* (Wong et al., 2023). As a result, the final miniphagemid completely lacks a prokaryotic backbone which might include CpG motifs and antibiotic resistance genes. Additionally, the reduced size of miniphagemid compared to phagemid or conventional plasmid improves vector mobility and can facilitate diffusion into the perinuclear space, increasing nuclear uptake to aid the efficiency of gene transfer (Wong, 2022). The diffusional mobility of

DNA fragments in the cytoplasm is an important determinant of the efficiency of a gene delivery system (Lukacs et al., 2000), and the nuclear diffusion rate is significantly reduced as the DNA fragments become larger (Lukacs et al., 2000). Furthermore, a helper phage derived from a commercially available helper phage M13KO7 was genetically modified to increase the yield of miniphagemid production. The plasmid encoding the genome of this helper phage, referred as the SW8 helper phage plasmid, has the *PS* removed downstream of *gIV* and replaced with a Rho-independent (*trp*) terminator (Wong et al., 2023). PS is primarily involved in the assembly of phage particles, the complete deletion of PS eliminates the self-packaging of helper phages to a frequency of $<10^{-6}$ packaging almost exclusively the miniphagemid. In the *E. coli* JM109 strain, the production of miniphagemid was significantly higher in yield with reduced helper plasmid self-packaging (Wong et al., 2023). This project will continue to investigate miniphagemid propagation and maintenance using the self-packaging deficient helper phage, SW8, to produce the targeted miniphagemid. Previous research has shown clathrin-mediated endocytosis can accommodate up to 900 nm filamentous phage particles in length (Kim et al., 2012). A phage particle encoding miniphagemid DNA is less than half the size of the wildtype M13 genome which should render it less than 400 nm in length. Therefore, this size is sufficiently small to be internalized through clathrin-mediated endocytosis, thus making miniphagemid an attractive gene delivery vehicle (Wong et al., 2023).

Accumulation of cytosolic DNA, including dsDNA, ssDNA and RNA are all capable of activating the STING (Stimulator of Interferon Genes) pathway (Luo et al., 2022). In brief, cyclic GMP-AMP synthase (cGAS) binds to dsDNA in the cytoplasm and is converted to synthesize cyclic GMP-AMP (cGAMP) (Luo et al., 2022). In the case of phagemid-mediated

gene delivery, ssDNA is recognized when it forms internal duplex structures or a Y-shaped structure that includes a duplex and single-stranded overhangs containing a stretch of guanine residues, which are then detected by cGAS (Chen et al., 2016). However, the structural basis of this activation remains undetermined. cGAMP then binds directly to STING protein located on the endoplasmic reticulum (ER) membrane, leading to its activation. Activated STING translocates from the ER to the Golgi apparatus and subsequently to the perinuclear region where it induces the expression of type I interferons (IFN) and other inflammatory cytokines (Chen et al., 2016). This pathway is a critical component of stimulating the innate and adaptive immune response to cytosolic DNA, playing a crucial role in antiviral defense and antitumour immune responses by triggering the production of proinflammatory cytokines. Primarily, type I IFN is produced to promote the maturation and production of immune cells such as T cells, DCs, and NK cells to trigger effective anti-tumour immune effects (Luo et al., 2022).

The genetic simplicity and flexibility of the M13 phage make it a promising platform for cell targeting and gene transfer. Cell-specific ligands can be displayed on the surface of phagemids to facilitate specific tissue targeting. Additionally, we further engineered the phagemid production system by generating miniphagemids and drastically reduced the presence of helper phage contamination by generating a packaging-deficient helper phage plasmid (Wong et al., 2022). Taking all these innovations together, this study focuses on assessing the application of this novel miniphagemid gene delivery system to produce VLPs as a cancer immunotherapy. This next section will explain how VLPs can be used as a cancer immunotherapy with a specific focus on HPV VLPs.

2.4 VLPs Immunotherapy for Cancer

Vaccines were initially developed to protect the public from infectious diseases. However, ongoing research has been focused on studying viral vector-based vaccines to treat chronic infectious diseases and cancer. Tumours are composed of tumours cells with stromal features such as vasculature, fibroblasts, and infiltrating immune cells, which collectively form the TME (Tormoen et al., 2018). It is characterized by a range of immunosuppressive cells that enable the tumour to evade immune surveillance and promote tumour progression (Tie et al., 2022). Cancer immunotherapy is designed to overcome the immunosuppressive nature of TME by enhancing the immune system's ability to recognize and eliminate tumour cells. The use of a natural biological system like viruses can be exploited to overcome the immunosuppressive state of TEM and effectively recruit cytotoxic lymphocytes to destroy tumour cells. In this regard, virus-like particles (VLPs) have been employed as a promising candidate for a cancer vaccine. VLPs are derived from the structural proteins of a viral pathogen with no infectivity, which greatly enhances their safety profile. VLPs are either enveloped or non-enveloped depending on the characteristics of the viruses from which they are derived. Enveloped VLPs contain a layer of lipid with viral surface antigens outside the capsid structure. The extra layer of lipids is derived from the host cell membrane (Müller et al., 2019). Common enveloped viruses used for VLP-based vaccine production include human immunodeficiency virus (HIV), hepatitis C virus (HCV), influenza A, and retroviruses (Tariq et al., 2022). In comparison, non-enveloped VLPs contain only the capsid structural proteins (Nooraei et al., 2021). Examples of non-enveloped viruses include human papillomavirus (HPV), adeno-associated viruses (AAV) and hepatitis B virus (HBV). In general, non-enveloped viruses are easy to characterize, manipulate, purify and produce (Buonaguro et al., 2011; Naskalska & Pyrć, 2015).

As therapeutic cancer vaccines, VLPs can be genetically or chemically modified to display a wide variety of therapeutic epitopes on their surfaces (Caldeira et al., 2020). Engineering VLPs as a cancer vaccine may add the benefit of simulating and enhancing immune responses in the patient by presenting their pathogen-associated molecular patterns (PAMPs) (Nooraei et al., 2021).

VLPs displaying tumour cell antigens can trigger the desired immune responses via three major routes. Firstly, most VLPs are small ranging from 25 to 100 nanometres (nm) which allows easy entry into lymphatic vessels and passive drainage to the subcapsular region of lymph nodes (Caldeira et al., 2020). Abnormal blood flow and low diffusion rates in the hypoxic core of the tumour largely prevent conventional cytotoxic drugs from penetrating through and eliciting their therapeutic effects (Baghban et al., 2020). The nanoscale size of VLPs facilitates penetration through the dense and irregular architecture of the TME. Secondly, followed by the initial intradermal injection, the presence of VLPs gradually reduces and degrades after a week, which provides sufficient time for immune system recognition. Within the lymph nodes, as the VLPs reach to the subcapsular sinus, a large population of naïve B cells in the germinal center are activated to undergo somatic hypermutation (Stebegg et al., 2018). Subsequently during somatic hypermutation, B cells differentiate into plasma cells and produce antigen-specific antibodies. The antibodies then bind to tumour cells and are targeted by NK cells and macrophages (Michel et al., 2013). Lastly, VLPs can be taken up by dendritic cells (DCs), which are the most effective antigen-presenting cells (APCs) and promote adaptive responses by interacting with CD8+ and CD4+ cells (Caldeira et al., 2020). The PAMPs on VLPs can be detected by pattern recognition receptors (PRRs) such as toll-like receptor (TLR)-2 and TLR-4 on dendritic cells (DCs)

(Kawasaki & Kawai, 2014). Activation of TLRs leads to the maturation of DCs, which enables the transition from innate to adaptive immune responses (Reis e Sousa, 2004). The antigen-presenting VLPs can be recognized by MHC class I to induce the shift from naïve CD8+ T cells to cytotoxic T cells. In addition, APCs can present antigens to the MHC class II on naïve CD4+ T helper (Th) cells. In addition to cytokine and B7– CD28 engagement, this leads to the activation of Th cells which in turn help activate B cells to secrete antibodies and activate cytotoxic T cells in order to kill target tumour cells (Alberts et al., 2002) .

The utilization of VLPs as therapeutic cancer vaccines is a highly promising strategy due to their ability to evoke robust immune responses without the risk of infectivity. The intricate mechanisms through which VLPs interact with the immune system, including the activation of B cells, the induction of antigen-specific antibodies, and the engagement of dendritic cells underscore their versatility and efficacy in cancer immunotherapy. Transitioning to the specific application of VLPs, the development of HPV VLPs has shown significant promise in both preventive and therapeutic contexts which will be expanded upon in the following subsections.

2.4.1 HPV VLPs vaccines

The human papillomavirus (HPV) is a non-enveloped virus with a circular, double-stranded DNA genome (Chen et al., 2000). The target of HPV infection is the stratified epithelium (Kajitani et al., 2012). It is one of the most common sexually transmitted infections worldwide, and can lead to warts, juvenile respiratory papillomatosis, epithelial lesions, and cervical cancer (Burd & Dean, 2016). Vaccination has proven to be one of the most effective ways to prevent

HPV infection. The HPV vaccines are based on the production of VLPs derived from major capsid protein L1 from high-risk strains including types 6, 11, 16, and 18 (Zhao et al., 2014).

Among the HPV family, HPV 16 is the most extensively studied strain and is associated with almost all cervical cancers (Buck et al., 2013; Slupetzky et al., 2007). The production of VLPs using the major capsid protein (L1) from HPV 16 has been extensively characterized for immunogenicity and safety in humans (Buonaguro et al., 2011). L1 proteins induce a robust tumour-specific CD4+ and CD8+ T-cell response, which leads to strong cytolytic activity against autologous tumour cells (Bellone et al., 2009). HPV VLPs also confer the ability to induce cytotoxic activity of IL5-DCs against HPV-positive cervical cancer (Van den Bergh et al., 2014). The activation of IL5-DCs also stimulates the production of pro-inflammatory cytokines such as TNF-α and IL-1β which further strengthens the immune responses against HPV-infected cells (Van den Bergh et al., 2014).

The production of HPV VLPs from L1 proteins is notably efficient, primarily due to the inherent properties of the L1 protein that facilitate spontaneous self-assembly (Zhao et al., 2014). By cloning the L1 gene into an expression vector and introducing it into suitable host cells such as yeast, insect, or mammalian systems, high yields of the L1 protein can be achieved (Fuenmayor et al., 2017; Lamprecht et al., 2016). The human codon optimized L1 gene of HPV16 has been successfully expressed in mammalian cells, resulting in significant increases in L1 protein production and the accumulation of VLPs in the nuclei of transfected cells (Leder et al., 2001). The codon-optimized L1 gene also showed increased immunogenicity *in vivo*, as evidenced by higher antibody titers in mice immunized with the optimized L1 gene compared to those

immunized with the original L1 gene. This suggests that the optimized genes are more effective for DNA vaccination purposes (Leder et al., 2001). The HPV16 L1 protein sequence used in this study (accession no. CAC51367.1) is human codon optimized using the codon usage database from Genebank (https://www.kazusa.or.jp/codon/). In our previous study, we successfully produced and characterized HPV VLPs using this codon-optimized L1 sequence (Pushparajah, 2022). Therefore, the same sequence was used in this study, and assessed for its ability to produce HPV VLPs in mammalian cells.

2.4.2 Characterization of HPV VLPs

In comparison to other common enveloped and non-enveloped VLPs for the development of novel therapeutics, HPV VLP is easy to characterize, manipulate, produce and purify, which offers great advantages for displaying foreign peptides (Buonaguro et al., 2011; Naskalska & Pyrć, 2015). The major capsid protein, L1, self-assembles into VLPs (Zhao et al., 2014). L1 proteins form pentamers, which are the basic building blocks of the VLPs. 72 L1 pentamers come together to form the complete VLP, which mimics the structure of the native HPV virion (Zhao et al., 2014). These pentamers are organized into a T=7 icosahedral symmetry, containing 360 copies of the L1 protein. This symmetrical arrangement provides the VLP with a robust and stable structure (Zhao et al., 2014). The diameter of the VLPs is approximately 50-60 nanometers (nm).

Previously, HPV16 L1 capsid protein was modified to contain an anti-angiogenic peptide, VGB4 that could be exposed when L1 assembled into a VLP (Pushparajah, 2022). The constructed VLP gene cassette was cloned into a mammalian expression vector. To further confirm the formation

of HPV VLPs, H16.U4 antibodies (Abs) were used, which are conformational-dependent Abs that bind specifically to pentamer-like structure of HPV VLPs (Carter et al., 2003). This Ab binds specifically to AA residues between 422 to 445 on the C-terminal arm of L1 protein, which is in between the formed capsomers (Carter et al., 2003). The DE loop and the H4 helix region have shown effective peptide display on the VLP (Chabeda et al., 2019; Varsani et al., 2003). We have previously inserted VGB4 either in the DE loop or H4 helix region and assessed for the difference in their binding affinity towards the surface of VLPs. Our experimental data indicated slightly higher H16.U4 Ab binding affinity towards VGB4 inserted in the DE loop (between AA 136 and 137) of the L1 capsid (Pushparajah, 2022). This is consistent with other studies which demonstrated more consistent VLP formation when inserting a foreign peptide in the DE loop region (Huber et al., 2017; Varsani et al., 2003). We hypothesized that our HPV VLPs would accumulate and lyse the host cell for their release into the extracellular environment to target VEGFR. However, we did not demonstrate a sufficient release of VLPs to the extracellular matrix in the human embryonic kidney cell line, HEK 293T. Although research has suggested that the primary mode of escape for non-enveloped viruses is cell lysis, our previous data showed insignificant cell lysis and minimal decrease of tumour cell viability through the transfection of VGB4-displaying HPV VLPs in HEK 293T cells. Studies have shown that HPV L1 capsid proteins are preassembled in the cytoplasm and then translocated to the nucleus (Florin et al., 2002; Kajitani et al., 2012). Since VGB4 preferentially binds to the extracellular domain of VEGFR-1 and VEGFR-2, it would be ideal to have VGB4-displaying VLPs being released in the extracellular matrix to elicit a stronger anti-angiogenetic effect in tumour cells (Farzaneh Behelgardi et al., 2018). Therefore, in this study we optimize the HPV VLP gene cassette with VGB4 insertion to promote the release of VLPs in the extracellular environment.

2.4.3 Optimization of HPV VLP gene expression cassette

The HPV L1 is known as a nuclear protein which contains a nuclear localization signal (NLS) to direct the accumulation in the host cell nucleus (Zhou et al., 1991). The nuclear import plays an important role in the HPV infection cycle (Yang et al., 2006). It was suggested that in HPV16 L1, the NLS exist in a bipartite fashion comprising tight clusters of basic residues (lysine and arginine) with a spacer of 10-14 AAs (Tao et al., 2003; Yang et al., 2006; Zhou et al., 1991). The presence of double NLS in the L1 may provide a protection role and may possibly be a result of gene duplication or exchange during evolution (Zhou et al., 1991). The study demonstrated that both identified NLS regions are functionally redundant, meaning that the L1 protein can localize to the nucleus as long as one of the NLS sequences is intact (Zhou et al., 1991). Therefore, simultaneously deleting both NLS sequences would be an effective approach to prevent nuclear localization of HPV VLPs.

Interestingly, the production of HPV vaccines has shown that the deletion of the NLS not only produced intact VLPs but also promoted high concentration of viral particles assembled in the cytoplasm (Gissmann et al., 2000; Hallek & Burger, 2009). With the last 34 AA deleted at the C-terminus from the 472^{nd} to 505^{th} AA in HPV16, capsomeres were preferentially packaged in the cytoplasm (Burger & Hallek, 2003; Gissmann et al., 2000). This modification could significantly benefit HPV vaccine production, as VLPs can be more easily purified from the cytoplasm minimizing host cell contamination (Burger & Hallek, 2003; Gissmann et al., 2000).

The understanding of NLS in HPV L1 protein and its role in nuclear import is crucial for comprehending the HPV infection cycle. The bipartite nature of the NLS in HPV16 L1, consisting of clusters of basic residues underscores its evolutionary significance and protective

role. Intriguingly, the deletion of the NLS has demonstrated practical benefits in HPV vaccine production, leading to the formation of VLPs predominantly in the cytoplasm, which simplifies purification and reduces host cell contamination. These findings highlight the potential for optimizing vaccine production through strategic modifications of the viral protein structure, offering a streamlined approach to generating high-purity VLPs for effective immunization. As an exploratory study, we will attempt to delete the NLS in the previously constructed L1 protein with VGB4 peptide insertion, and assess for the formation of HPV VLPs.

Chapter 3: Rationale, Objectives and Hypothesis

3.1 Rationale

Conventional chemotherapeutic drugs used in cancer treatment often exhibit multiple side effects and high toxicity due to their nonspecific action against all cells, including non-cancerous cells. In contrast, targeted therapeutics have demonstrated high specificity, increased effectiveness, and lower toxicity. Both VLPs and phages have shown potential as safe and effective platforms for targeted cancer therapy (Bortot et al., 2022; Caldeira et al., 2020; Huh et al., 2022). Previous research from this lab has demonstrated the use of engineered phages displaying cell-targeting ligands to enable specific entry into targeted tumour cells (Huh et al., 2022; Wong et al., 2023). The overexpression of epidermal growth factor receptor (EGFR) is a hallmark of various tumour cells. Phage-displayed EGF binding to EGFR has been shown to penetrate and prevent 3D carcinoma cell expansion, facilitating phage internalization into mammalian cells. This allows for specific phage-mediated gene transfer in EGFR-expressing tumour cells through endocytosis. Endocytosis via a tumour-specific antigen not only targets the cargo to the appropriate cancer cells but also facilitates transport across the plasma membrane. Although the shape of the M13 phage appears long and rigid, its rod-like structures are quite flexible allowing them to be compact and easily internalized by host cells compared to more globular proteins and other phages (Wong, 2022). Additionally, our lab has generated HPV VLPs displaying the anti-angiogenic peptide VGB4, which was successfully expressed in mammalian cells. The use of VLPs is regarded as an effective cancer immunotherapy, capable of overcoming the immunosuppressed TME, and reestablishing innate immune responses to the environment. VGB4 was chosen for peptide display because it targets both VEGFR-1 and VEGFR-2, significantly limits the activation of downstream signalling pathways required for angiogenesis.

Combining the specificity of phage-displaying targeted ligands for cell uptake and the immunogenicity of VLPs, this project aims to generate a targeted cancer immunotherapy based on an HPV VLP displaying VGB4. This construct can be delivered and produced in tumour cells using a novel M13 miniphagemid as a gene delivery vector.

3.2 Hypothesis

EGF-displaying miniphagemids will enable targeted gene transfer to EGFR overexpressing tumour cells. The DNA sequence encoding the VGB4-displaying HPV VLPs will be expressed in the targeted cells and produce HPV VLPs displaying VGB4 with the ability to bind to VEGFR.

3.3 Objectives

1. Modify a packaging-deficient M13 helper plasmid (SW8) by inserting *egf* gene to *gIII*

2.1 Construct a precursor phagemid encoding VGB4-displaying HPV VLP gene cassette

2.2 Modify the precursor phagemid by deleting the nuclear localization signal (*NLS*) sequence in the VGB4-displaying HPV VLP gene cassette

3. Produce and quantify miniphagemids

4. Assess transfection efficiency of miniphagemids in HEK 293T and HeLa cells

5.1 Characterize HPV16 L1 proteins to be produced, assemble into VLPs, and escape the targeted cells

5.2 Characterize the binding capacity of VGB4-displaying HPV VLPs to VEGFR-2

Chapter 4: Materials and Methods

4.0 Strains and vectors

Bacterial strain, M13 phages, and mammalian cell lines used for this work are shown in Table 1. The plasmids and precursor phagemids used and constructed in this study are shown in Table 2. *Escherichia coli* (*E. coli*) K-12 JM109 was used in the generation of all phage and plasmid constructs. Bacterial strains were cultured in Luria–Bertani (LB) liquid medium at 37°C. Media were supplemented with the relevant antibiotic as required. Mammalian cells were cultured at 37°C in a humidified atmosphere with 5% CO_2 in Dulbecco's Modified Eagle's Medium (DMEM) (Catalog # 11965118, Thermo Fisher Scientific, Waltham, USA) supplemented with 10% fetal bovine serum (FBS) (Catalog # 26140079, Gibco, Waltham, USA) and 1% penicillin/streptomycin (Catalog # 15140122, Gibco, Waltham, USA).

Table 1: Summary of bacteria, M13 phage and mammalian cells used in this study.

Bacterial Strain	Genotype	Source	Additional information
JM109	F' traD36 proAB+ lacIq lacZΔM15/ Δ(lac-proAB) endA1 glnV44 thi-1 e14− recA1 gyrA96 relA1 hsdR17	NEB (Ipswich, USA)	Used for plasmid extraction, long-term storage of plasmids, and phage production.
M13 Phage	**Genotype**	**Source**	**Additional information**
SW7-EGF	*egf* fused between KpnI and EagI in gIII	This study	Derived from M13KE and M13KO7. M13KE has endonuclease sites in *gIII*, allowing EGF to be fused to the N-terminus. M13KO7 provides a p15a *ori,* Kan^R marker, and the backbone of SW7-EGF.
SW8	Packaging signal (*PS*) removed, Kan^R	This study	Derived from M13KO7. *PS* downstream of *gIV* was removed.
SW8-EGF	*PS* removed, *egf* fused to *gIII*, Kan^R	This study	This phage contains *egf::gIII* gene fragment from SW7-EGF, and SW8 backbone excluding *gIII*
Mammalian cell line	**Cell type**	**Source**	**Additional information**
HEK 293T	Human embryonic kidney cells	ATCC (Manassas, USA)	Used for the expression of precursor phagemids, ssDNA, and miniphagemids
HeLa	Human cervical adenocarcinoma	Gift, Dr. Brian Dixon	Used for the expression of precursor phagemids, ssDNA, and miniphagemids

NEB: New England BioLabs; ATCC: American Type Cell Culture Collection

Table 2: Summary of plasmid and precursor phagemids used in this study.

Plasmid	Encodes for	Source	Additional information
pGL2-cmv-L1-de	HPV16 L1 capsid protein with VGB4 peptide inserted in the DE loop region of the L1 protein	This study	Amp^R
pUC19	N/A	NEB (Ipswich, USA)	Amp^R
Precursor phagemid	**Encodes for**	**Source**	**Additional information**
pOri2	N/A	This study	An empty vector with a split f1 *ori* inserted in pUC57 (Genbank Accession No. Y14837.1), Amp^R
pOri2-cmv-gfp	Green fluorescence protein (GFP)	This study	A *cmv-gfp* gene cassette inserted between the split f1 *ori*, Amp^R
pOri2-L1-VGB4	HPV16 L1 capsid protein with VGB4 peptide inserted in the DE loop region of the L1 protein.	This study	Gene expression cassette from pGL2-cmv-L1-de was inserted between the split f1 *ori*, Amp^R
pOri2-L1-VGB4-ΔNLS	HPV16 L1 capsid protein with NLS truncated at the C-terminus, VGB4 peptide inserted in the DE loop region of the L1 protein	This study	Derived from pOri2-L1-VGB4, Amp^R

NEB: New England BioLabs

4.1 Construction of the helper phage plasmid displaying EGF

A sequence encoding EGF peptide was amplified from SW7-EGF (Wong, 2022), gel purified and inserted into SW8 (Wong, 2022) using Gibson assembly resulting in SW8-EGF (Figure 3).

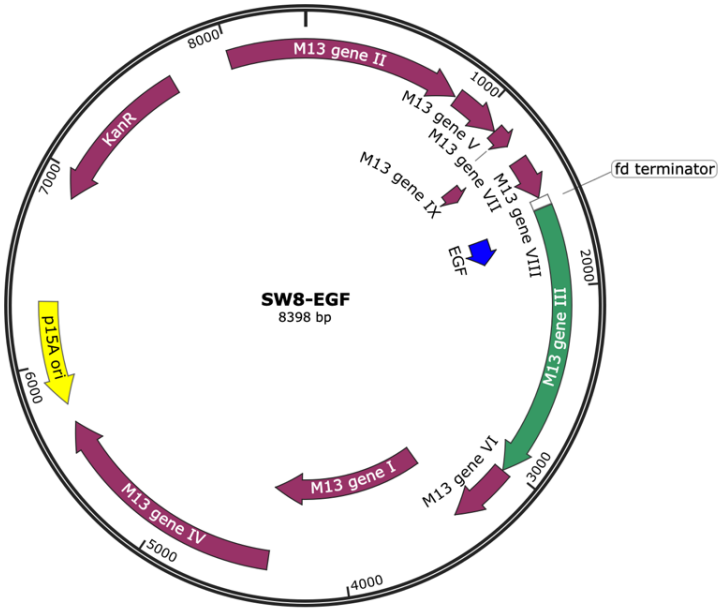

Figure 3: Map of modified SW8 displaying EGF helper plasmid. EGF is fused at the N-terminal of pIII. Packaging signal (*PS*) is removed downstream of *gIV* followed by a *trp* terminator.

4.1.1 SW7-EGF and SW8 PCR amplification and gel extraction

The helper phage plasmid SW7-EGF previously constructed in our lab was confirmed to produced EGF-displaying phagemids (Wong, 2022). Therefore, the same *egf* sequence in SW7-EGF will be cloned onto SW8 to produce SW8-EGF. Table 3 indicates the primers were designed to PCR amplify *gIII::egf* gene fragment on SW7-EGF plasmid (SW7-EGF-F and SW7-EGF-R), and the backbone of SW8 plasmid, excluding *gIII* was used for insertion of the *egf* sequence (SW8-F and SW8-R). For PCR amplification, the Bio-Rad (Hercules, USA) C1000 Thermal Cycler was used. The PCR reaction contained 25 µL of the 2X Phusion Flash High Fidelity PCR Master Mix (Thermo Fisher Scientific, Waltham, USA), 20 ng of plasmid DNA,

0.5 μM of forward and reverse primers, and remaining nuclease-free water to a final reaction volume of 50 uL. Table 4 outlines the conditions used for the PCR cycle. The amplified products were run on a 0.8% gel at 90 V for approximately 1 h and 30 min. The amplified fragments were gel-extracted using Monarch® DNA Gel Extraction Kit (NEB, Ipswich, USA). The concentration and purity of gel-extracted DNA was measured using the Thermo Fisher Scientific (Waltham, USA) Nanodrop 2000.

Table 3: Summary of primers used for this study

Primer	Amplicon	Sequence (5' – 3')
SW7-EGF-F	*gIII::egf*	TCGCAATTCCTTTAGTTGTTCCTTTCTATTCTCAC TCTAATAG
SW7-EGF-R	*gIII::egf*	CTGGCATGATTAAGACTCCTTAAGACTCCTTATT ACGCAG
SW8-F	SW8	CTGCGTAATAAGGAGTCTTAAGGAGTCTTAATCA TGC
SW8-R	SW8	TTAGAGTGAGAATAGAAAGGAACAACTAAAGGA ATTGC
L1-NLS-F	*L1*	TGAGTTTAAACGGCCGGCTG
L1-NLS-R	*L1*	CTGCAGCAGGAACTTTCTGC
L1-1-F	*L1*	GAACCGTCAGATCCGCTAG
L1-1-R	*L1*	GTGTTGATCAGCTCCAGG
L1-2-F	*L1*	CTACAAGCAGACCCAGCTG
L1-2-R	*L1*	GCTCATGTTGGTGCTTCTG
L1-3-F	*L1*	CAACCAGCTGTTCGTGAC
L1-3-R	*L1*	CCTCTACAAATGTGGTATGG
qPCR-gfp-F	*gfp*	CAAGATGAAGAGCACCAAAGG
qPCR-gfp-R	*gfp*	CGAAGTGGTAGAAGCCGTAG
qPCR-L1-F	*L1*	TACAGATTCGTGACCAGCCAGG
qPCR-L1-R	*L1*	CTCCTTCAGGTTCACCTCCCAG

Table 4: General PCR conditions used for amplification

Cycle Step	Temperature	Time	Number of Cycles
Initial Denaturation	98°C	10 s	1 cycle
Denaturation	98°C	1 s	30 - 35 cycles
Annealing	Determined using *Thermo Fisher Scientific Tm calculator*	5 s	
Extension	72°C	15 s/kb	
Final Extension	72°C	60 s	1 cycle
Incubation	4°C	Hold	N/A

4.1.2 Gibson Assembly of gel-extracted bands

The gel-extracted bands of SW8 backbone and *gIII::egf* gene fragment were ligated using the Gibson assembly cloning kit (NEB, Ipswich, USA). The reaction contained 1.4 µL of *gIII::egf* gene fragment, 7.0 µL of SW8 backbone, and 8.4 µL of Gibson assembly master mix. A positive control reaction was prepared containing 5 µL of positive control supplied by the kit and 5 µL of Gibson assembly master mix. The samples and positive control were incubated at 50°C for 1 h. 10 µL of the Gibson assembly reaction was added to competent JM109 *E. coli* cells.

4.1.3 Transformation of competent *E. coli* cells

Calcium competent JM109 *E. coli* cells were thawed on ice for 30 min before carrying out the heat shock transformation. DNA samples were as added to the competent cells and incubated on ice for 30 min. The cells were then transformed via heat shock at 42°C for 90 s, and immediately placed back on ice for 3 min. 900 µL LB broth was added, and then cells were incubated in a 37°C shaking incubator at 250 revolutions per min (rpm) for 1 h. The cells were plated on LB

agar plates containing kanamycin (Kan) and incubated overnight in a 37°C incubator. A negative control and positive control were also transformed into JM109 competent cells. The negative control was plated on LB + Kan plate using competent cells without the addition of DNA samples to detect any contamination. The positive control was plated on LB + ampicillin (Amp) plate using competent cells transformed with 100 ng of pUC19.

4.1.4 Plasmid extraction and sequence confirmation

A fresh colony of JM109 transformed with SW8-EGF helper phage plasmid was inoculated in 5 mL LB broth supplemented with Kan (70 μg/ml), and kept in a 37°C shaking incubator, at 250 rpm overnight. The next day, the culture was centrifuged at 10,000 x *g* for 10 min to separate bacterial pellet and supernatant. The pellet was obtained to extract SW8-EGF plasmid with Monarch Plasmid Miniprep Kit (NEB, Ipswich, USA). The purity of extracted SW8-EGF was measured using the Thermo Fisher Scientific (Waltham, USA) Nanodrop 2000.

To confirm the N-terminal fusion of *egf* to *gIII* as *egf::gIII*, SW7-EGF forward and reverse primers (Table 3) were used to PCR amplify SW8-EGF plasmid. The PCR conditions used to amplify *egf:gIII* on SW8-EGF are outlined in Table 4. The PCR amplified products were run on a 0.8% gel to visualize the band size. To further confirm that *egf* sequence was successfully inserted in-frame with *gIII*, the whole plasmid was sent to Plasmidsaurus (https://www.plasmidsaurus.com/) for sequencing.

4.2 Construction of a precursor phagemid encoding VGB4-displaying HPV VLPs

The VGB4-displaying HPV VLP gene cassette (*L1-VGB4*) was inserted into the precursor phagemid, pOri2 using restriction enzyme (RE) digestion, ligation, and transformed into competent JM109 cells. The constructed precursor phagemid pOri2-L1-VGB4 is shown in Figure 4.

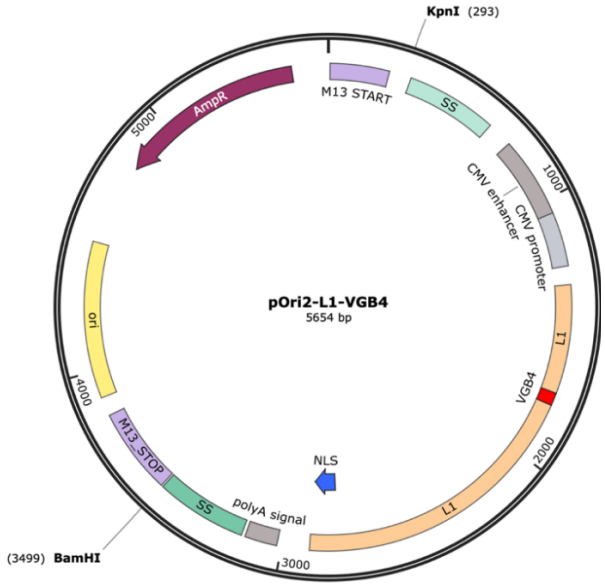

Figure 4: Map of pOri2-L1-VGB4. The *L1-VGB4* gene cassette is inserted between the split f1 *ori*, denoted as M13 start and M13 stop. The gene expression is controlled by a *cmv* promoter. The super sequence (*SS)* sequence at both ends promotes nuclear localization of the DNA sequence to be expressed. The ends of the *L1-VGB4* gene cassette have a unique KpnI and BamI restriction enzyme (RE) site, which is used for cloning. The location of *NLS* is coloured in blue. The sequence encoding for *VGB4* is fused to the *L1* sequence highlighted in red.

4.2.1 Restriction enzyme digestion of plasmids

The plasmid pGL2-cmv-L1-de previously constructed in our lab contains a *L1-VGB4* gene cassette encoding a VGB4-displaying HPV VLP. This gene cassette was inserted in the multiple cloning site (MCS) of a precursor phagemid pOri2 to generate pOri2-L1-VGB4. The plasmid pGL2-cmv-L1-de (Figure 5A) and the precursor phagemid pOri2 (Figure 5B) were both digested

with the same REs, KpnI and BamHI (NEB, Ipswich, USA). In each reaction, 1 µg of plasmid DNA was digested with 20 units of each enzyme, and 5 µL 10x rCutSmart Buffer in a total volume of 50 µL. The reactions were incubated at 37°C for 15 min, and run on a 0.8% gel. The band observed for the HPV VLP gene cassette (3.2 kb) and pOri2 backbone (2.4 kb) were gel-extracted using Monarch DNA Gel Extraction Kit (NEB, Ipswich, USA). The concentration and purity of gel-extracted DNA was measured using the Thermo Fisher Scientific (Waltham, USA) Nanodrop 2000.

A) B)

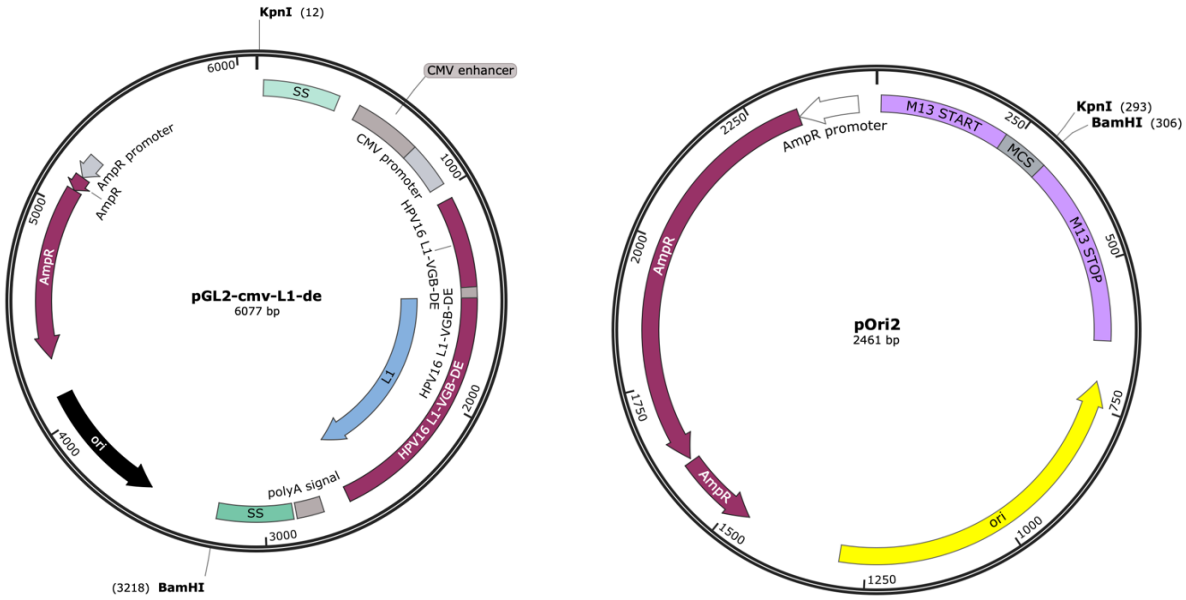

Figure 5. Maps of pGL2-cmv-L1-de and pOri2. A). Plasmid pGL2-cmv-L1-de contains the expression system for the *L1-VGB4* gene cassette. The expression will be controlled by a *cmv* promoter and flanked by two super sequence (*SS*) sequences at both ends. B) Plasmid pOri2 is the unmodified precursor phagemid which contains a split f1 *ori* (M13 start and stop) separated by a MCS region.

4.2.2 Ligation of vector: insert

The gel-extracted bands were ligated using T4 DNA ligase (NEB, Ipswich, USA). The amount of vector and insert DNA was calculated using the online *NEBioCalculator* tool. The reaction

contains 1 µL T4 DNA ligase, 2 µL T4 ligase buffer, vector DNA, insert DNA, and remaining nuclease-free water up to 20 µL in total. The reaction was incubated at 16°C overnight. Next day, the reaction was inactivated at 65°C for 15 min. The cells were then transformed with the ligation product in the same manner as outlined in Section 4.1.3.

4.2.3 Confirming the generation of pOri2-L1-VGB4

A colony PCR was performed to confirm the presence of the L1 sequence in the observed colonies. L1-3-F and L1-3-R primers used for the colony PCR are shown in Table 3. In brief, a single colony from an agar plate using a sterile pipette tip was steaked onto a master LB + Amp agar plate. Then, the tip with the colony was transferred to a PCR tube containing 10 µL of sterile water. The PCR tube with the colony suspension were incubated at 95°C for 10 min in a heating block to lyse the cells and release the DNA. The PCR reaction contained 5 µL of 2X Phusion Flash High Fidelity PCR Master Mix (Thermo Fisher Scientific, Waltham, USA), 0.1 µM of forward and reverse primer, 2 µL of the lysed colony suspension, and remaining nuclease-free water to a final reaction volume of 10 µL. The PCR run conditions are shown in Table 3.

A fresh colony verified by colony PCR was inoculated in 5 mL LB broth supplemented with Amp (100 µg/mL). The next day, a plasmid extraction was performed using the Monarch Plasmid Miniprep Kit (NEB, Ipswich, USA) and digested with the same REs used for cloning (KpnI and BamHI). The restriction digestion was then run an agarose gel to confirm the DNA fragment length corresponding to the pOri2 backbone (2.4 kb) and *L1-VGB4* gene cassette (3.2 kb).

4.3 Construction of a precursor phagemid encoding VGB4-displaying HPV VLPs with NLS deletion

To delete the sequence encoding the NLS at the C-terminal end of the L1 protein, the precursor phagemid pOri2-L1-VGB4-ΔNLS was constructed using PCR amplification, phosphorylation, ligation, and transformed into competent JM109 cells. The deletion of *NLS* was confirmed through RE digestion, PCR amplification, and Sanger sequencing. Figure 4 shows the location of *NLS* in the *L1* sequence.

4.3.1 PCR amplification and phosphorylation

To delete the DNA sequence encoding the last 34 AA at the C-terminal end of L1 protein, primers were designed to amplify plasmid pOri2-L1-VGB4 excluding the NLS region while keeping the stop codon at the end of the sequence. L1-NLS-F and L1-NLS-R primers were used for PCR amplification shown in Table 3. The reaction setup was the same as outlined in Section 4.1.1. The PCR run conditions were shown in Table 4. The amplified product was then run on an agarose gel to confirm the DNA fragment length at 5.6 kb. The bands observed for pOri2-L1-VGB4 backbone was gel extracted using Monarch DNA Gel Extraction Kit (NEB, Ipswich, USA). The concentration and purity of gel-extracted DNA was then measured using the Thermo Fisher Scientific (Waltham, USA) NanoDrop 2000.

Phosphorylation of the PCR amplified product provides a phosphate group at the 5’ end to allow for successful ligation to produce the desired plasmid. The gel-extracted bands of pOri2-L1-VGB4 with NLS deletion was phosphorylated with NEB T4 Polynucleotide Kinase (PNK) in a 50 µL final reaction volume. Each reaction contained ~ 250 ng of DNA, 1 µL of T4 PNK, 5 µL

of 10X T4 PNK Buffer, 5 µL of 10 µM ATP and remaining nuclease-free water. The reaction was set on ice, then incubated at 37°C for 30 min, followed by heat inactivation at 60°C for 20 min. To remove any buffer retention and enzymatic reactions from PCR, the phosphorylated product was purified with Monarch PCR & DNA Cleanup kit (NEB, Ipswich, USA). The final product was then ligated and transformed into competent JM109 cells in the same manner as outlined in Section 4.2.2.

4.3.2 Confirming the deletion of NLS

To confirm the proper deletion of 34 AA at the C-terminal end of the L1 protein sequence, the precursor phagemid pOri2-L1-VGB4-ΔNLS was PCR amplified, and then sent for sequencing. Table 3 outlines the primers used for PCR amplification and sequencing. L1-3-F and L1-3-R (Table 2) were designed to amplify a region of the *L1* sequence including *NLS*. To compare the difference in band sizes, both pOri2-L1-VGB4 and pOri2-L1-VGB4-ΔNLS was PCR amplified. The PCR reaction setup was the same as outlined in Section 4.1.1. The PCR run conditions are shown in Table 4. The amplified product was then run a 3% gel to confirm the DNA fragment length corresponded to 589 bp for pOri2-L1-VGB4 and 487 bp for pOri2-L1-VGB4-ΔNLS.

To confirm the presence of the stop codon at the end of the *L1* sequence with truncation of *NLS*, pOri2-L1-VGB4-ΔNLS was then sent for Sanger sequencing at Sick Kids Centre for Applied Genomic TCAG facility (Toronto, Canada). Three sets of primers were designed for sequencing, shown in Table 3.

4.4 Miniphagemid production and purification

JM109 competent cells were used to produce miniphagemids. The bacterial cells were co-transformed with 100 ng of the helper phage plasmid and 100 ng of the precursor phagemid in the same manner as outlined in Section 4.1.3. The next day, a fresh colony of JM109 strain carrying both the helper plasmids and precursor phagemids was inoculated into 50 mL LB broth supplemented with 70 μg/mL Kan, 100 μg/mL Amp, and 5 mM $MgSO_4$. The culture was incubated in a shaking incubator at 37°C, 250 rpm until the broth reaches $OD_{600} \leq 0.5$. The culture was then centrifuged at 8,000 x g for 10 min at 4°C to separate the bacterial pellet from the supernatant. The supernatant containing the miniphagemids was purified through a 0.22 μM filter to remove residual bacterial debris and obtain unconcentrated miniphagemid lysate. The lysate can be stored at 4°C indefinitely. The filtered lysate was further concentrated through precipitation by adding $1/5^{th}$ the volume of PEG/NaCl solution and incubated at 4°C overnight. The next day, the lysate was centrifuged at 12,000 × g for 15 min at 4°C to separate the PEGylated miniphagemids (pellet) from the media (supernatant). The pellet was suspended in a small volume of ice-cold TN buffer (1 mL TN buffer per 25 mL lysate), and another PEG precipitation was carried to further concentrate the miniphagemids by adding $1/5^{th}$ the volume of PEG/NaCl solution, incubated at 4°C overnight, followed by another round of centrifugation. The pellet was then re-suspended in 200 μL ice-cold TN buffer. The PEG-precipitated lysate was treated with DNase I (Promega, Madison, USA) to remove any extraneous phage or bacterial DNA in the sample. The concentrated lysate can be stored at 4°C indefinitely. In total, 6 samples were produced as shown in Table 5.

Table 5: Miniphagemids produced in this study.

	Encodes for	**Names***
EGF-displaying miniphagemids	1. Green fluorescent protein (GFP) 2. VGB4-displaying HPV VLP 3. VGB4-displaying HPV VLP with NLS deletion	1. EGF-*gfp* 2. EGF-*L1-VGB4* 3. EGF-*L1-VGB4-ΔNLS*
Non-displaying miniphagemids	4. GFP 5. VGB4-displaying HPV VLP 6. VGB4-displaying HPV VLP with NLS deletion	4. *gfp* 5. *L1-VGB4* 6. *L1-VGB4-ΔNLS*

*The genes encapsulated by miniphagemids are italicized.

4.5 Dot blot of EGF-displaying miniphagemid

To confirm the EGF display on miniphagemids, a dot blot was performed with all the PEG-precipitated miniphagemid lysates shown in Table 5, and human EGF recombinant protein as a positive control (Catalog # PHG0311, Thermo Fisher Scientifics, USA). Serial dilutions of recombinant EGF, miniphagemids, and PBS were spotted onto nitrocellulose membrane and left to dry. The membrane was then blocked with 4% bovine serum albumin (BSA) buffer. Anti-EGF monoclonal mouse antibody (Catalog # M805, Thermo Fisher Scientific, Waltham, USA) was applied, followed by a secondary horseradish peroxidase (HRP)-conjugated anti-mouse antibody (Catalog # 31430, Thermo Fisher Scientific, Waltham, USA). The membrane was incubated with TMB-blotting solution (Thermo Fisher Scientific, Waltham, USA) for 15 min to visualize the presence of dotted samples.

4.6 Extraction of ssDNA from miniphagemids

ssDNA was extracted from the PEG-precipitated miniphagemids through phenol-chloroform extraction. Phenol was added to PEG-concentrated phage lysate at a ratio of 1:1, v/v and mixed by vortexing. After centrifugation for 5 min at 4°C the top aqueous layer was extracted. This layer was then extracted again with an equivalent volume of phenol:chloroform twice, and chloroform once. Finally, the DNA was precipitated overnight with 100% ethanol at −80 °C. The precipitated DNA was washed with 70% ethanol, dried, and re-suspended in RNase and DNase-free water. The concentration and purity of extracted ssDNA was measured using the Thermo Fisher Scientific (Waltham, USA) NanoDrop 2000.

4.7 Quantification of miniphagemids

The concentration of each PEG-precipitated miniphagemid lysate was quantified through SYBR Green quantitative PCR (qPCR). Calibration curves for quantify phages were performed using external standards: pOri2-L1-VGB4 and pOri2-cmv-gfp. Primers specific to a region of the L1 sequence were used to amplify miniphagemids encapsulating *L1* gene, and primers specific to a region of GFP sequence were used to amplify miniphagemids encapsulating the *gfp* gene. The sequences of the qPCR primers are shown in Table 3. To generate the calibration curve, a 10-fold serial dilution of each external control were prepared (10^{-1} to 10^{-8}) as template for the qPCR reaction.

The lysates were heated at 100°C for 15 min to isolate the encapsulated DNA. Since the concentration of miniphagemids in the lysates were unknown, a serial of ten-fold dilutions in the range of 10^{-3} – 10^{-5} were prepared as templates. The qPCR reaction contained 5 µL of PowerTrack SYBR Green Master Mix (Catalog # A46109, Thermo Fisher Scientific, Waltham,

USA), 1 µL each of 500 nM primers, 2 µL template and 1 µL nuclease-free water. The qPCR conditions were PCR cycling conditions were as follows: 50°C for 2 min, 95°C for 2 min, followed by 40 cycles at 95°C for 15 and 60°C for *gfp* gene or 70°C for *L1* gene for 1 min. The melt curve was set as for 1 cycle at 95°C for 15 s, 60°C for 1 min, and 95°C for 15 s. The reactions were run in triplicate on the StepOne Plus Real-Time PCR system (Applied Biosystems, Waltham, USA). The threshold cycle number (Cq) for each reaction was recorded and used in subsequent analysis. The conversion from the mass of DNA to the number of genome copies (gc) was calculated using

$$\text{mass of plasmid DNA needed} = \text{copy \# of interest x plasmid size x } (1.096 \text{ x } 10^{-21})$$

where mass of plasmid DNA needed is in g, plasmid size is in bp. The following table presents the calculated plasmid mass to achieve the starting copy number of interest ($1 \text{ x } 10^7$ gc). As 2 µL of plasmid DNA was pipetted into the qPCR reaction, the final concentration of plasmid DNA was calculated in g/µL. The amount of plasmid DNA added was determined using the dilution equation, $C_1V_1 = C_2V_2$, where gc is the concentration of miniphagemid genome copies/µL, mass is the mass of the external standard in g/µL, and size is the length of the external standard in bp. Miniphagemid concentrations were calculated based on their respective calibration curve. The Cq values of the standard plasmids were plotted against to log of known concentration for each dilution of the standard plasmid. By using the linear regression mode, the plot produces an equation of

$$Cq = mx + b$$

where Cq is the threshold cycle number, m is the slope, x is the base-10 log of the concentration in gc/mL, and b is the x-intercept. Subsequently, miniphagemid concentration (V) can be estimated by

$$V = 10^{(Cq-b)/m} \times 2$$

where multiplication by 2 adjusts for the estimation of single-stranded products (gc/µL) from dsDNA standards.

Miniphagemid concentrations were further quantified using multi-angle dynamic light scattering (MADLS) (Zetasizer, Malvern Panalytical, Worcestershire, UK). Lysates were diluted by 100-fold in nuclease-free water and transferred to a 12 mm sq cuvette (Catalog # FSTP9775594, Thermo Fisher Scientifics, Waltham, USA) to be measured in the MADLS. The same lysate samples used for qPCR as shown in Table 5 were measured three times for particle counts/mL. Values were recorded and used for subsequent analysis.

Lastly, colony assay was conducted to quantify full-size phagemid and helper phage titre based on the ability of lysate to confer antibiotic resistance to susceptible cells. 200µL of early log-phase *E. coli* JM 109 cells was mixed with 3 mL LB top agar supplemented with 5 mM $MgSO_4$, then poured on a pre-warmed LB agar plate. Separately, miniphagemid lysates were serially diluted in TN buffer, then 10 µL of each lysate dilution were spotted onto the top agar. Dried plates were incubated overnight at 37 °C and analyzed the next day. The contamination efficiency was calculated based on the colony forming units (CFU) observed on LB + Amp plate for the concentration of full-size phagemids, and CFU observed on LB+Kan plate for the concentration of helper phages. The contamination efficiencies of full-size phagemids and helper phages were reported as percentages using

$$\text{Contamination efficieincy (\%)} = \frac{\text{CFU/mL}}{\text{gc/mL}} \times 100$$

4.8 Transfection of human cells

HEK 293T and HeLa cells were seeded onto 24-well plates at a density of ~ 1 x 10^5 cells/mL. After 24 h, 0.5 µg of precursor phagemid, 1.0 µg of ssDNA extracted from miniphagemids, and 1 x 10^{10} gc/mL of miniphagemids (MOI = 100,000) are diluted in DMEM media respectively, and mixed with 2 µL TurboFect transfection reagent (Catalog # R0531, Thermo Fisher Scientifics, Waltham, USA). The samples were incubated at room temperature for 20 min and added to the cells. The ratio of transfection reagent:plasmid DNA was 3:1 for all wells, as suggested by the manufacturer of the reagent. Non-transfected cells were used as negative controls.

4.8.1 Assessing transfection efficiency of human cells

To assess the transfection efficiency at 96 h post transfection, cells were imaged using fluorescence microscopy on the EVOS FL Auto Imaging System (Thermo Fisher Scientific, Waltham, USA) to observe the presence of GFP fluorescent cells. Cells were then harvested to quantify total precent of fluorescent cells through flow cytometry. To harvest the cells, they were first washed once with sterile D-PBS. Next, 200 µL of Trypsin-EDTA (Catalog # 25200056, Gibco, Waltham, USA) was added to the cells and they were incubated at 37°C + 5% CO_2 for 5 min. 800 µL of prewarmed DMEM + 10% FBS was then added to inactivate the TripleE. 50 µL of each sample was aliquoted and stained in trypan blue to check for cell viability (%) and cell count (cells/mL). The remaining cells were centrifuged at 500 x g at room temperature for 5 min. The supernatant was discarded, and the pellet was washed once by re-suspending in 1 mL D-PBS. The cells were then centrifuged at 500 x g at room temperature for 5 min. The supernatant was discarded, and the pellet was fixed on ice for 30 min in 1 mL of 2% paraformaldehyde diluted in D-PBS. The fixed cells were then run through the BD Biosciences (San Jose, CA, USA) FACSCalibur flow cytometer. Green fluorescence emitted by the GFP protein was

detected using the FL1 detector. Non-transfected cells were also run through the flow cytometer as a control to detect for background signals. The flow cytometer settings were inputted to detect a maximum of 10,000 events (detectable cells) at a slow fluidic rate. The threshold value was set at 50,000. Analysis of the number of events (cells), mean fluorescence intensity, and presence of fluorescent cells was carried out using the FlowJo Software (Ashland, USA) to assess transfection efficiency. Transfection efficiency was calculated as a percent of the number of cells emitting fluorescence divided by the total number of cells detected.

4.8.2 Cell harvesting and lysis

At 96 h post transfection, cells were harvested for lysis. They were first washed once with sterile D-PBS. Next, 200 µL of Trypsin-EDTA was added to the cells and they were incubated at 37°C + 5% CO_2 for 5 min. 800 µL of prewarmed DMEM + 10% FBS was then added to inactivate the Trypsin. 50 µL of each sample was aliquoted and stained in trypan blue to check for cell viability (%) and cell count (cells/mL). The remaining cells were centrifuged at 500 x g at room temperature for 5 min. The supernatant was discarded, and the pellet was washed once by re-suspending in 1 mL D-PBS.

RIPA Lysis and Extraction Buffer (Catalog # 89900, Thermo Fisher Scientific, Waltham, USA) were used to lyse the cells. For every 1 x 10^6 cells, 1 mL of RIPA buffer was added to the cell pellet. The buffer was gently mixed with the cells and left on ice with occasional gentle mixing for 15 min. The mixture was then centrifuged at 14,000 x g for 15 min to pellet the cell debris. The supernatant (cell lysate) was then transferred to a new tube and stored at -20°C for subsequent assessment.

4.9 ELISA

The following section outlines the ELISA experiments used to detect HPV16 L1 proteins, VLPs, and the binding capacity of VGB4-displaying HPV VLPs to VEGFR-2.

4.9.1 Indirect ELISA

Indirect ELISA was used to detect the L1 protein and HPV VLPs. Both the cell supernatant and lysate were plated onto a 96-well Immulon 4HBX flat bottom plate at 100 µL per well (Thermo Fisher Scientific, Waltham, USA). The plates were then left overnight at 4°C to allow for binding of the protein samples to the bottom of each well. The next day, the samples were removed and washed three times with 1X wash buffer (1X phosphate buffered saline/Tween 20 (PBS-T)) using the Biotek 450 TS microplate washer (Winooski, USA). The plate was then blocked with 300 µL of blocking buffer (3% skim milk) for 1 h. The blocking buffer was removed and washed once with 1X wash buffer.

The plate was then incubated with 100 µL of primary Ab (Camvir-1 or H16:U4) at a concentration of 1 µg/mL (diluted in blocking buffer) and kept at room temperature for 2 h. Camvir-1 Abs detects L1 proteins, and H16:U4 Abs detects HPV VLPs. After this, the primary Ab was removed and washed three times with 1X wash buffer. Then, 100 µL of secondary anti-mouse IgG HRP Ab (Catalog # SLCG4695, Sigma Aldrich, St. Louis, USA) was added at a 1:10,000 dilution ratio and incubated for 1 h at room temperature. The secondary Ab was then removed and washed three times with 1X wash buffer. 100 µL/well of TMB ELISA solution (Thermo Fisher Scientifics, USA) was then added to the plate and covered with aluminum foil and left at room temperature for 30 min. To stop the reaction, 100 µL/well of stop solution (2M H_2SO_4) was added to each well, inducing a colour change that was visually detected if binding of the L1 protein and/or L1 VLPs

towards the primary Abs occurred. Absorbance values of the colour changes were measured at 450 nm using a plate reader (Molecular Devices, SpectraMax ABS, San Jose, USA).

4.9.2 Sandwich ELISA

Sandwich ELISA was conducted to determine the binding capacity of VGB4-displaying HPV VLPs to VEGFR-2. Recombinant human VEGFR-2 protein (Catalogue No. ab281825, Abcam, UK) was diluted in 1X PBS to a concentration of 5 µg/mL, coated a 96-well Immulon 4HBX flat bottom plate at 100 µL per well (Thermo Fisher Scientific, Waltham, USA) at 50 µL/well, and incubated at 4°C overnight. The next day, the plate was washed with 1X wash buffer (1X PBS-T) and subsequently blocked with 300 uL of blocking buffer (5% skim milk) in each well for 1 h at room temperature. Cell lysates were added to the plate and incubated at room temperature for 2 h. The plate was then washed three times with 1X wash buffer and incubated with 100 uL of the Camvir-1 Ab at a concentration of 1 µg/mL diluted in blocking buffer for 2 h at room temperature. The plate was then washed three times with 1X wash buffer and incubated with 100 uL of secondary anti-mouse IgG HRP Ab (Catalog # SLCG4695, Sigma Aldrich, St. Louis, USA) diluted in blocking buffer for 1 h at room temperature. The secondary Ab was then removed and washed three times with 1X wash buffer. 100 µL/well of TMB ELISA solution (Thermo Fisher Scientifics, Waltham, USA) was then added to the plate, covered with aluminum foil, and left at room temperature for 30 min. To stop the reaction, 100 µL/well of stop solution (2M H_2SO_4) was added to each well, inducing a colour change that was visually detected if binding of VGB4 to VEGFR-2 occurred. Absorbance values of the colour changes were measured at 450 nm using a plate reader (Molecular Devices, SpectraMax ABS, San Jose, USA).

Chapter 5 Results

5.1 Construction of an EGF-displaying helper phage plasmid

The targeting ligand EGF was inserted on the pIII of M13 coat protein, and the ability of this EGF-displaying helper phage will assemble miniphagemids. Construction of SW8-EGF was confirmed by gel electrophoresis, showing a PCR amplification of the *gIII::egf* gene fragment at the expected band size at ~1,400 bp (Figure 6). Additionally, the sequencing results confirmed the insertion of the *egf* gene is in-frame with *gIII*, and the sequencing data is attached in Appendix A. These results confirm the successful construction of the SW8-EGF helper phage plasmid, enabling further development of the miniphagemid system.

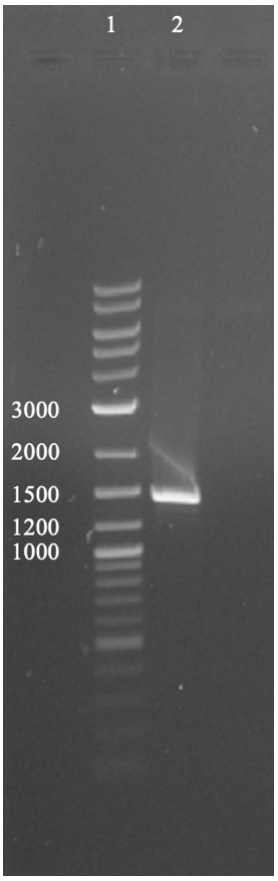

Figure 6: Agarose gel of SW8-EGF PCR amplification. Lane 1: 1 kb FroggaBio (Concord, CA) DNA ladder (Catalog # DM010-R500), labelled in bp. Lane 2: PCR amplification of the *gIII::egf* gene fragment on SW8-EGF helper phage plasmid.

5.2.1 Construction of a precursor phagemid encoding a VGB4-displaying HPV VLP

To produced miniphagemids encapsulating a VGB4-displaying HPV VLP (*L1-VGB4*) gene cassette, a precursor phagemid pOri2-L1-VGB4 was generated which contains the *L1-VGB4* gene cassette inserted between the split f1 *ori*. After transformation, a colony PCR testing confirmed the presence of L1 sequence, and lane 7, 8, 9, 11 showed the correct band size at ~ 688 bp (Figure 7). To further validate the construction of pOri2-L1-VGB4, RE digestion confirmed the presence of the *L1-VGB4* gene cassette (3.2 kb) and pOri2 backbone (2.5 kb) in their correct sizes (Figure 8, Lane 5, 6, 7).

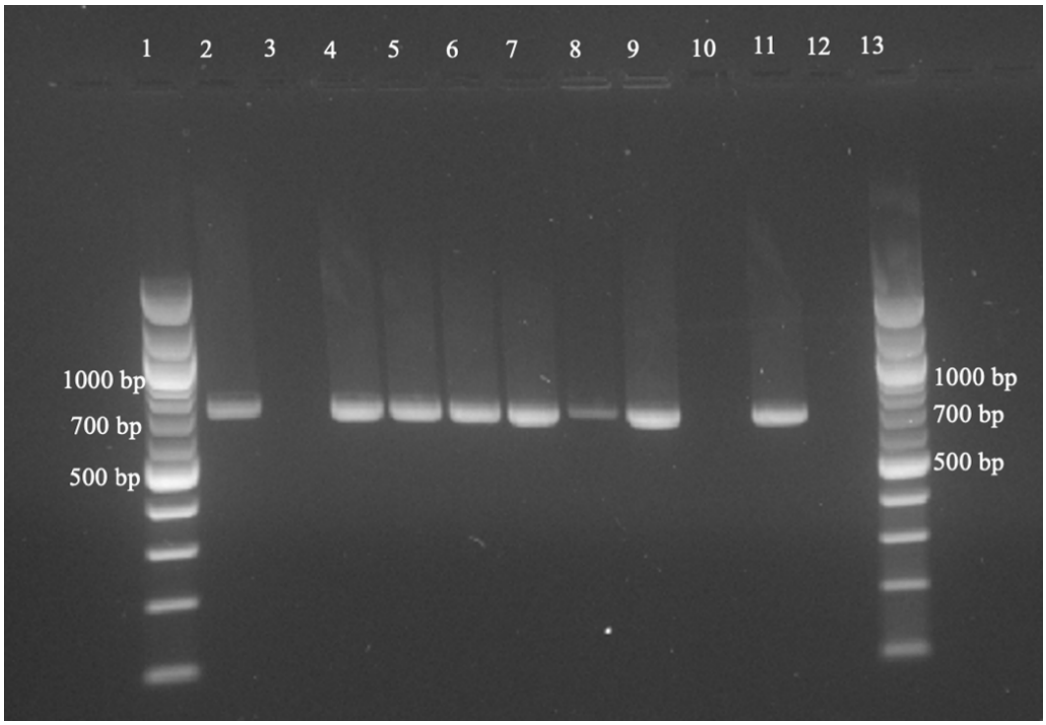

Figure 7: Agarose gel of colony PCR amplification of the precursor phagemid pOri2-L1-VGB4. Lane 1&13: 1 kb DNA ladder (Catalog # N3232, NEB, Ipswich, USA), labelled in bp. Lane 2-11: PCR amplification on *L1* gene of 10 selected colonies transformed with the ligation reactions. Lane 12: negative control for PCR reaction with no template DNA added.

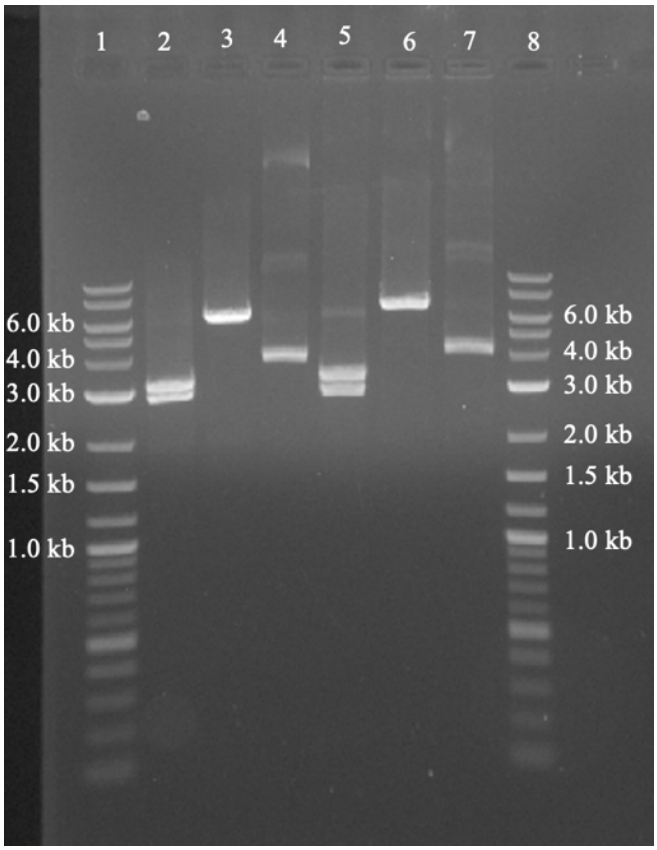

Figure 8: Agarose gel of RE digested pOri2-L1-VGB4 and pOri2-L1-VGB4-ΔNLS. Lane 1&8: 1 kb plus DNA ladder (Catalog # N0469S, NEB, Ipswich, USA), labelled in kb. Lane 2: pOri2-L1-VGB4-ΔNLS digested with BamHI and KpnI. Lane 3: pOri2-L1-VGB4-ΔNLS digested with BamHI. Lane 4: undigested pOri2-L1-VGB4-ΔNLS. Lane 5: pOri2-L1-VGB4 digested with BamHI and KpnI. Lane 6: pOri2-L1-VGB4 digested with BamHI. Lane 7: undigested pOri2-L1-VGB4.

5.2.2 Construction of a precursor phagemid encoding a VGB4-displaying HPV VLP with nuclear localization signal (NLS) deletion

The deletion of the DNA sequence (102 bp) encoding the NLS of L1 protein was confirmed by RE digestion the newly synthesized precursor phagemids of pOri2-L1-VGB4- ΔNLS. Lower molecular weight band patterns of the *L1-VGB4-ΔNLS* gene cassette (3.1 kb) and the pOri2 backbone (2.5 kb) were observed (Figure 8, Lane 2). To further confirm the size difference between the two precursor phagemids, a PCR was conducted to amplify a *L1* region including

the *NLS*. Figure 9 shows the expected band sizes for pOri2-L1-VGB4 (589 bp) and pOri2-L1-VGB4- ΔNLS (487 bp), which was approximately 100 bp less corresponding to the size of *NLS*. In general, these combined methods (RE digestion analysis and PCR amplification) cannot completely substantiate the deletion of *NLS* in the *L1* gene, while retaining the last stop codon with no frameshift, therefore, pOri2-L1-VGB4-ΔNLS was sent for Sanger sequencing. The sequencing data validated the intended outcome, and the result is attached in Appendix A.

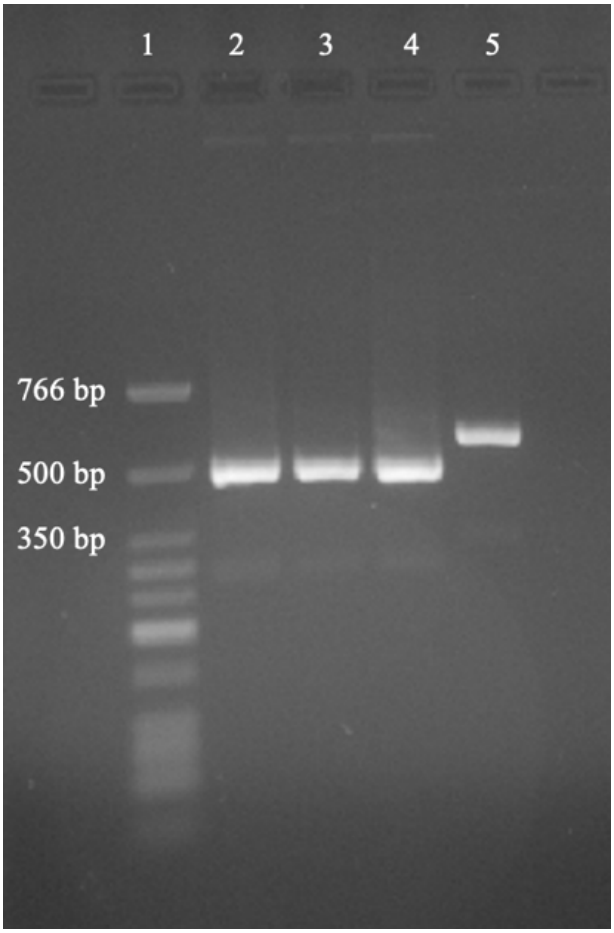

Figure 9. Agarose gel of PCR amplified pOri2-L1-VGB4 and pOri2-L1-VGB4-ΔNLS. Lane 1: Low Molecular Weight DNA Ladder (Catalog # N3233, NEB, Ipswich, USA), labelled in bp. Lanes 2, 3 & 4: PCR amplified fragments of pOri2-L1-VGB4-ΔNLS. Lane 5: PCR amplified fragments of pOri2-L1-VGB4.

5.3 Characterization and quantification of miniphagemids

To confirm the presence of EGF peptides on the miniphagemid samples, a dot blot assay was conducted. As shown in Figure 10, positive signals were detected for all EGF-displaying miniphagemids, while no signals were observed for non-displaying miniphagemids, as expected. This confirms the successful display of EGF peptides on miniphagemids. A serial dilution of recombinant human EGF was also dotted as a standard, which was used to visually estimate the concentration of EGF displayed on miniphagemids. Based on the intensity of the dots, EGF-*gfp* miniphagemids showed a relatively lower concentration than EGF-*L1-VGB4* miniphagemids and EGF-*L1-VGB4-ΔNLS* miniphagemid. As 2 µL of each sample was dotted onto the membrane, we could approximate the EGF concentration displayed on the miniphagemids. Based on the colour intensity, EGF-*gfp* miniphagemids dot was around 125 ng/µL, while EGF-*L1-VGB4* miniphagemids and EGF-*L1-VGB4-ΔNLS* miniphagemids appeared to be in the range of 250 ng/µL to 500 ng/µL or above. Overall, EGF peptides were displayed at above 125 ng/µL on the dotted miniphagemids.

qPCR and MADLS were conducted to quantify miniphagemids with the targeted genes. The DNA quantification method of qPCR is a highly accurate approach to calculate genomic copies, which is equivalent to counting the number of phage particles since every virion encapsulates one phage genome. A standard curve was generated from a dilution series of external plasmid control: pOri2-cmv-gfp (*gfp*) and pOri2-L1-VGB4 (*L1*). The lines of best fit were generated with R^2 values above 0.99 (Figure 11), which were used to calculate miniphagemid concentrations. The concentration of miniphagemid samples were further assessed through MADLS and compared against through qPCR. MADLS measures particle concentration by analyzing the

scattering intensity of light by particles in suspension, which correlates with the number of particles present. This process involves using dynamic light scattering at various angles to determine particle size and relating the scattering intensity to particle concentration. The qPCR and MADLS results are shown in Figure 12 and Table 6. In general, the MADLS-estimated virion concentrations were higher than the qPCR-estimated miniphagemid concentrations. Paired-t test was conducted to compare the difference between phagemid concentrations measured using qPCR and MADLS. EGF-*gfp* miniphagemids, *gfp* miniphagemids, EGF-*L1-VGB4* miniphagemids, EGF-*L1-VGB4-ΔNLS* miniphagemids suggested no statistically significant difference between the qPCR and MADLS measurements. *L1* miniphagemids and *L1-VGB4-ΔNLS* miniphagemids indicated a statistically significant difference between the qPCR-estimated and MADLS-estimated concentrations ($p < 0.05$). In general, MADLS over-estimated miniphagemid concentrations compared to qPCR, and the results were more variable. Therefore, we proceeded using qPCR to quantify and analyse miniphagemid concentrations for this study. Based on the qPCR results, the overall miniphagemid concentrations were around 10^{12} gc/mL. Of note, the concentration of miniphagemids encapsulating *cmv-gfp* gene cassette was slightly lower than miniphagemids encapsulating either *L1-VGB4* or *L1-VGB4-ΔNLS* gene cassette. This was consistent with the dot blot result, in which the colour intensity of EGF-*gfp* miniphagemids was less than the other EGF-displaying miniphagemids.

Next, the ssDNA extracted from miniphagemids were confirmed in their expected sizes (Figure 13), including *cmv-gfp* (1.3 kb), *L1-VGB4* (2.0 kb), and *L1-VGB4-ΔNLS* (1.9 kb). Only one clear band was observed from all the loaded samples, indicating no helper phage genome contamination and the absence of full-size phagemid DNA in the miniphagemid samples. Lastly,

colony assays confirmed the composition of EGF-displaying miniphagemids on LB + Amp agar plates. Amp resistance arose by cell uptake of full-size phagemid. No Amp^R colonies were observed on LB + Amp plates for EGF-*gfp* miniphagemids, while no Amp^R colonies were visible past the 10^8 dilution for the EGF-*L1-VGB4* miniphagemids and EGF-*L1-VGB4-ΔNLS* miniphagemids (Figure 14). The contamination efficiency of full-size phagemids and helper phages based on CFU and qPCR-estimated total concentration are given in Table 7.

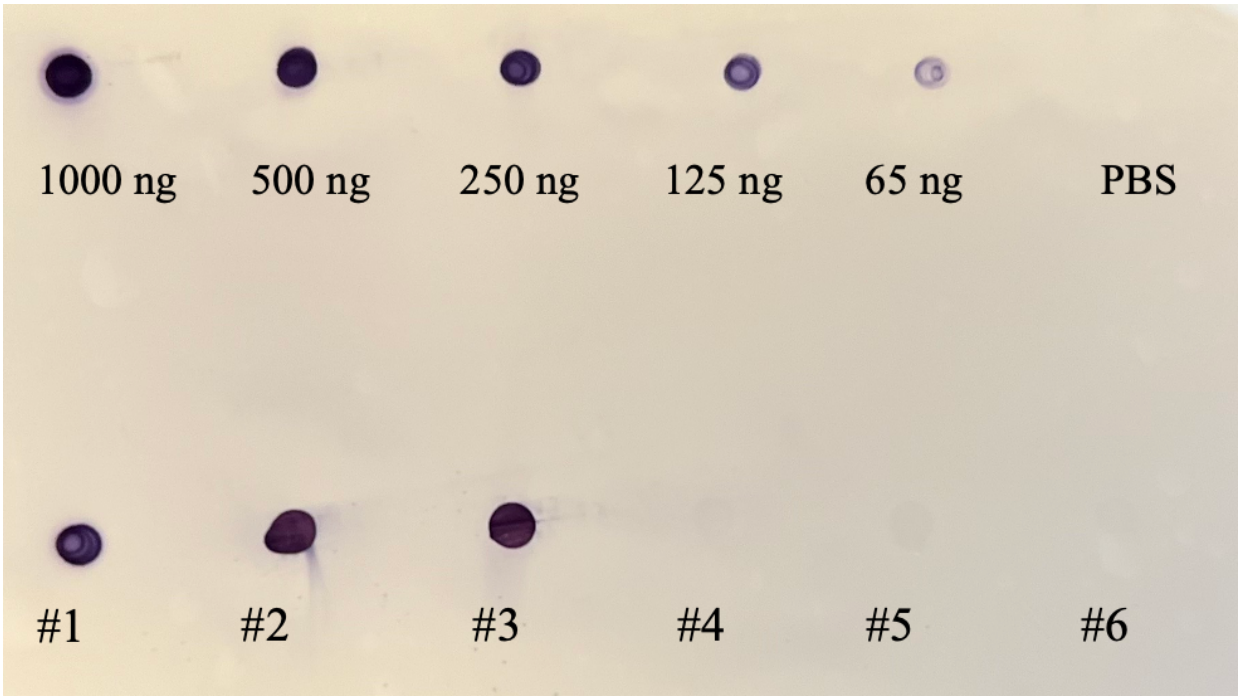

Figure 10. Dot blot of miniphagemids confirming the display of EGF peptides. The top 5 dots are dilutions of recombinant human EGF at various concentrations from 1000 ng to 65 ng. The bottom dots are 2 μL of miniphagemid samples, #1: EGF-*gfp* miniphagemid; #2: EGF-*L1-VGB4* miniphagemid; #3: EGF-*L1-VGB4-ΔNLS* miniphagemid; #4: *gfp* miniphagemid; #5: *L1-VGB4* miniphagemid;; #6: *L1-VGB4-ΔNLS* miniphagemid. PBS is a negative control spotted directly on the membrane.

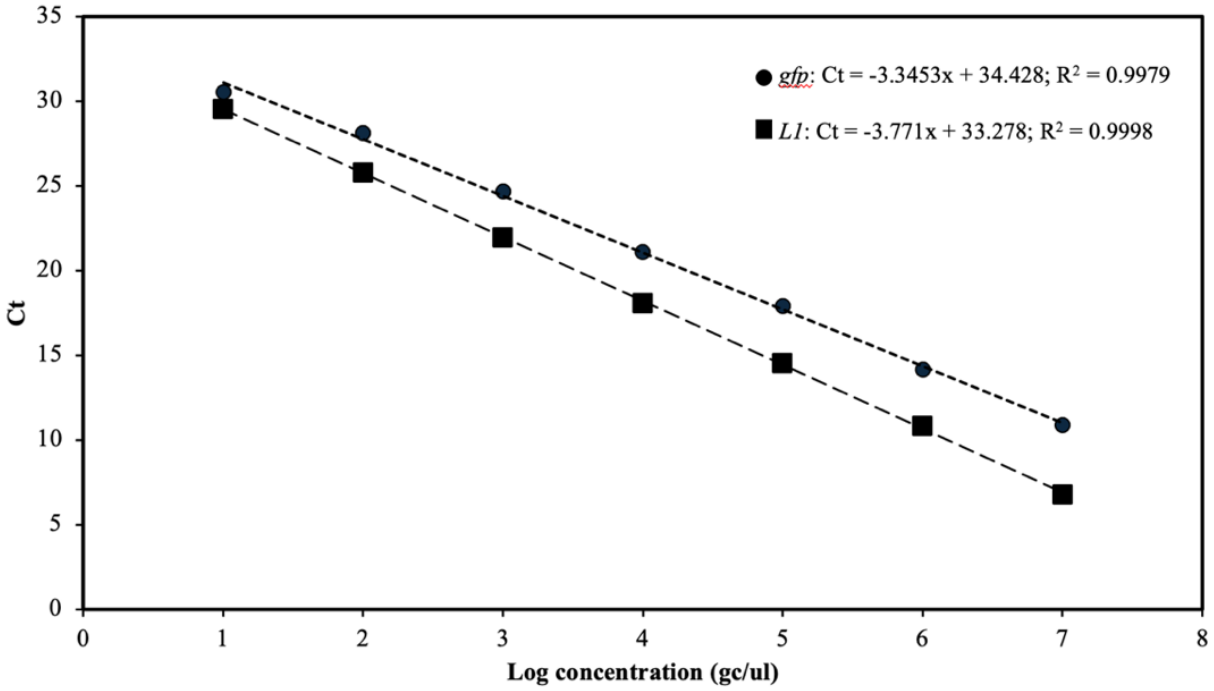

Figure 11: Standard curves to estimate phagemid concentration. Representative calibration curves are shown for each amplicon, as measured from qPCR of exogenous dsDNA controls: pOri2-cmv-gfp (*gfp*) and pOri2-L1-VGB4 (*L1*). The equation for each line of best fit and the R^2 value are reported. Data points represent the mean of 3 technical replicates.

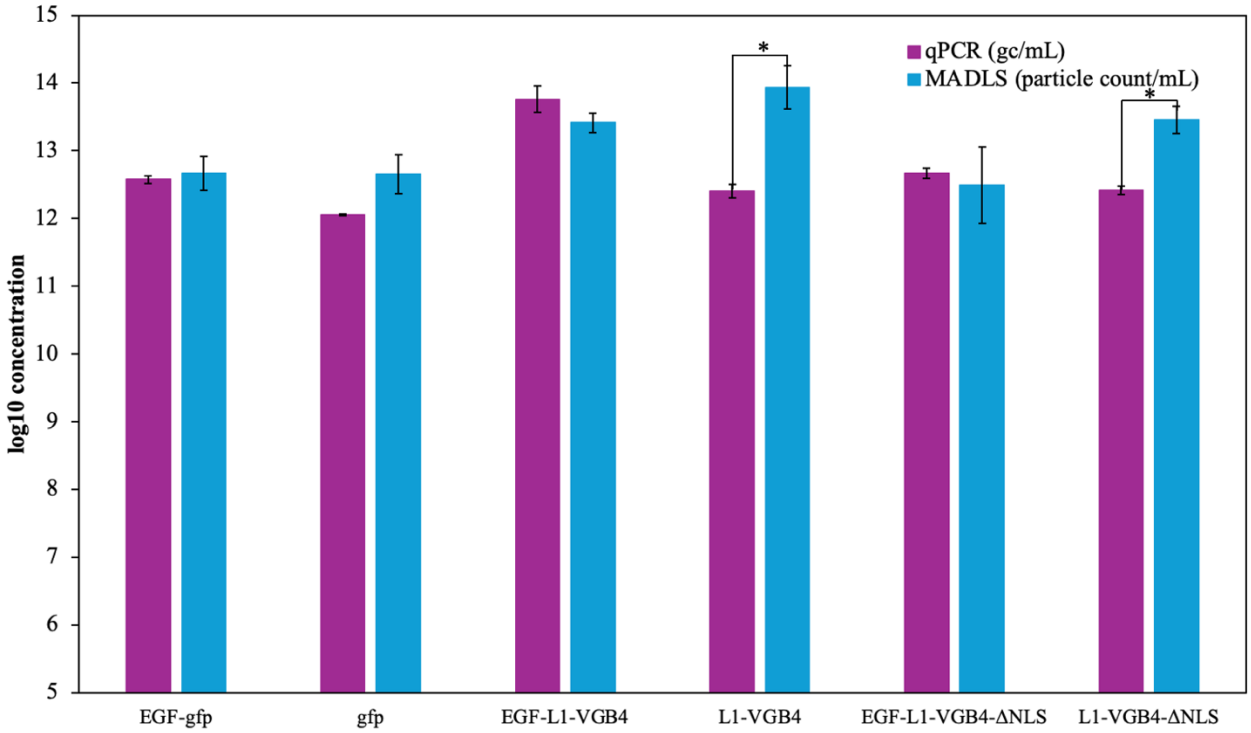

Figure 12: Miniphagemid concentrations estimated by qPCR compared to MADLS. The concentration of each miniphagemid sample is presented in gc/mL for qPCR, and particle count/mL for MADLS. Error bars represent ± SEM, n=3. The * above the bars indicates a statistically significant difference at $p < 0.005$ determined by paired-t test.

Table 6: Summary of miniphagemid concentrations measured through qPCR and MADLS.

Sample	Total phagemid concentration		
	qPCR (log gc/mL)	MADLS (log particle count/mL)	*p*
EGF-*gfp* miniphagemid	12.57 ± 0.06	12.67 ± 0.25	0.565
gfp miniphagemid	12.06 ± 0.08	12.65 ± 0.30	0.071
EGF-*L1-VGB4* miniphagemid	13.75 ± 0.20	13.41 ± 0.15	0.155
L1-VGB4 miniphagemid	12.40 ± 0.10	13.94 ± 0.32	0.010
EGF-*L1-VGB4-ΔNLS* miniphagemid	12.76 ± 0.07	12.50 ± 0.56	0.649
L1-VGB4-ΔNLS miniphagemid	12.42 ± 0.07	13.46 ± 0.20	0.006

Values are expressed as a mean of three independent assay ± SEM, n = 3.
Statistical differences in miniphagemid concentrations using the two quantification methods were determined by paired-t test, $p < 0.05$ indicates statistically significant difference.

A) B) C)

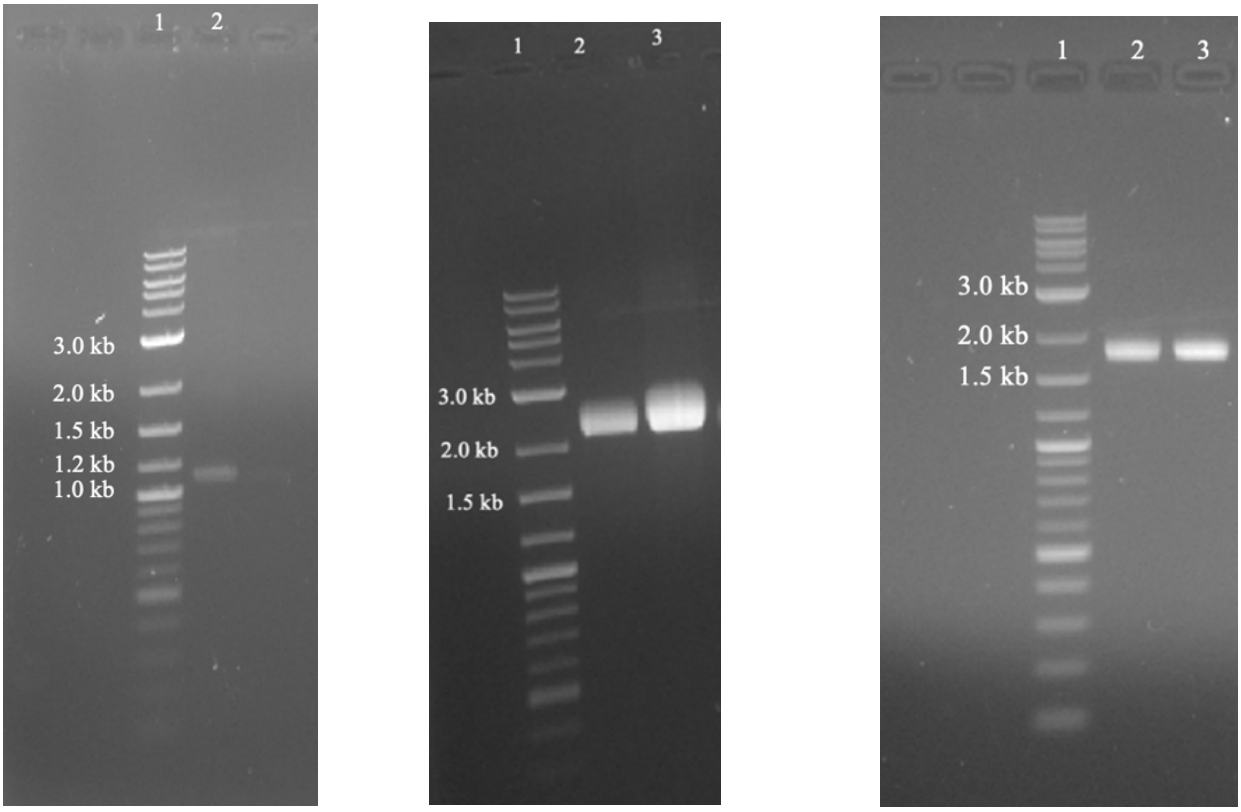

Figure 13. Agarose gels of ssDNA extracted from miniphagemids. A) ssDNA encoding the *cmv-gfp* gene cassettes. Lane 1: 1 kb plus DNA ladder (Catalog # N3200, NEB, Ipswich, USA), labelled in kb. Lane 2: ssDNA encoding *cmv-gfp* gene cassette. B) ssDNA encoding the *L1-VGB4* gene cassettes. Lane 1: 1 kb plus DNA ladder (Catalog # N3200, NEB, Ipswich, USA). Lane 2&3: ssDNA encoding L1 gene expression cassette. C) ssDNA encoding the *L1-VGB4-ΔNLS* gene cassettes. Lane 1: 1 kb plus DNA ladder (Catalog # N3200, NEB, Ipswich, USA). Lane 2&3: ssDNA encoding L1-ΔNLS gene expression cassette.

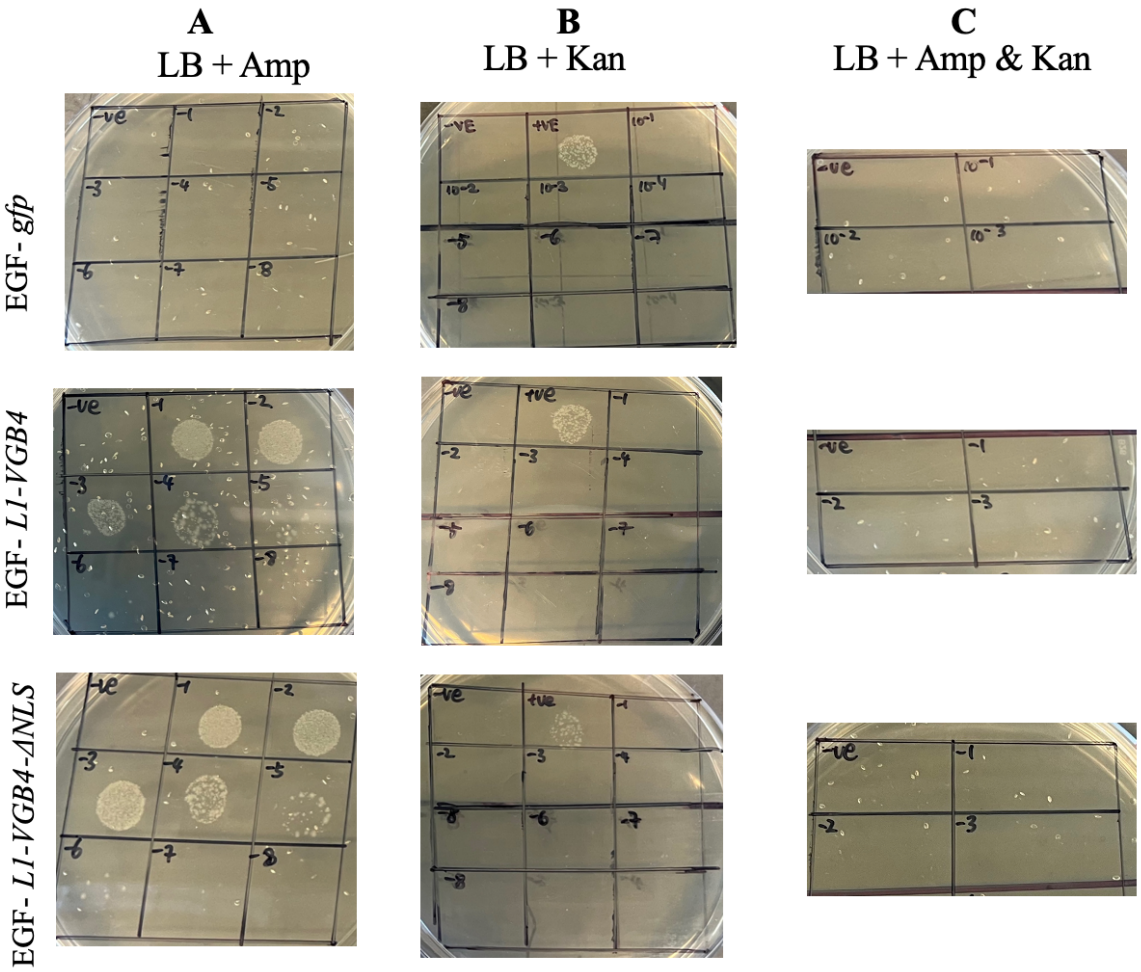

Figure 14. Colony assay of EGF-displaying miniphagemids. 10 µL of each lysate dilution were spotted onto a lawn of susceptible *E. coli* JM 109 cells. TN buffer was spotted as a negative control, and M13KO7 with kanamycin resistance was spotted as a position control. A) Diluted lysates were spotted onto LB agar supplemented with ampicillin (LB + Amp). B) Diluted lysates were spotted onto LB agar supplemented with kanamycin (LB + Kan). C) Diluted lysates were spotted onto LB agar supplemented with kanamycin and ampicillin (LB + Amp & Kan).

Table 7: Composition of EGF-displaying miniphagemids.

Miniphagemid lysate samples	**Titer**	**Full-Size Phagemid Contamination Efficiency (%)**	**Helper Phage Contamination Efficiency (%)**
EGF-*gfp*	3.72×10^{12}	2.69×10^{-11}	2.69×10^{-11}
EGF-*L1-VGB4*	5.62×10^{13}	3.56×10^{-4}	1.78×10^{-12}
EGF-*L1-VGB4-ΔNLS*	5.75×10^{12}	6.95×10^{-3}	1.74×10^{-11}

The full-size phagemid and helper phage contamination efficiencies of miniphagemid lysate samples are shown as a percentage of the total population based on qPCR-estimated concentration.

5.4 Assessment of the transfection efficiency of miniphagemids in HEK 293T and HeLa cells

HEK 293T and HeLa cells were transfected with precursor phagemids, ssDNA and miniphagemids to assess for their respective transfection efficiency. At 96 h post-transfection, GFP expression was detected in both cell lines transfected with the precursor phagemid pOri2-cmv-gfp and ssDNA encoding the *cmv-gfp* gene cassette (Figure 16 & 17). The mean percentage of fluorescent cells for pOri2-cmv-gfp was 25 % in HEK 293T and 34 % in HeLa cells. ssDNA encoding *cmv-gfp* exhibited 2.7 % expression in HEK 293T and 1.2 % in HeLa cells. GFP-fluorescent cells transfected with the precursor phagemid, ssDNA, and miniphagemids with TurboFect were observed and imaged at 96 h post transfection (Figure 18). GFP florescence was observed in HEK 293T and HeLa cells transfected with EGF-displaying miniphagemids, whereas no fluorescence was observed with non-displaying miniphagemids. Lower GFP fluorescence was observed in both cell lines transfected with EGF-displaying miniphagemids without the addition of TurboFect (Figure 19). The percentage of GFP expression in cells transfected with miniphagemids was assessed using flow cytometry, however, the level of expression was not detectable.

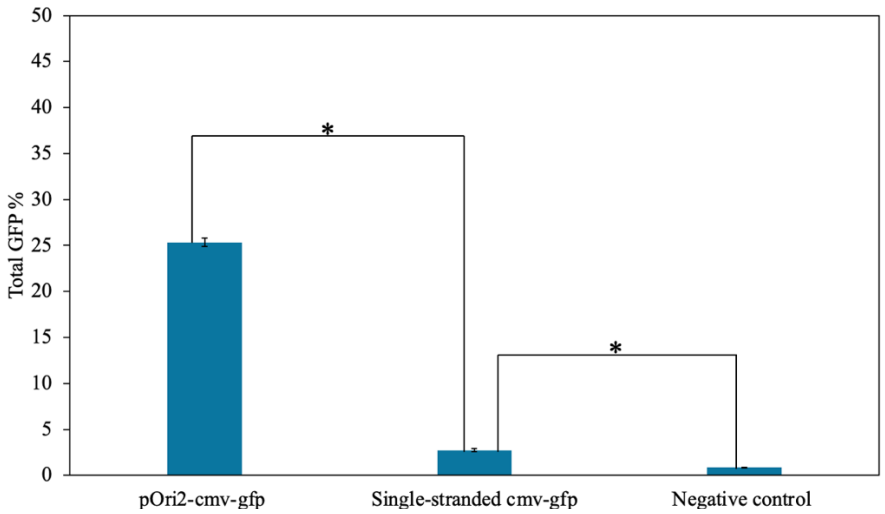

Figure 16. Precent of GFP fluorescent HEK 293T cells transfected with pOri2-cmv-gfp and ssDNA encoding *cmv-gfp* with TurboFect. Total percent (%) of GFP fluorescent HEK 293T cells was calculated for 10,000 events (cells) for each replicate (two) at 96h for HEK 293T cells transfected with pOri2-cmv-gfp, ssDNA encoding *cmv-gfp* gene cassettes extracted from miniphagemids with TurboFect. Non-transfected cells were used as a negative control. Data are presented as mean ± SEM for duplicate samples. The * above the bars indicates a statistically significant difference at $p < 0.005$ determined by paired-t test.

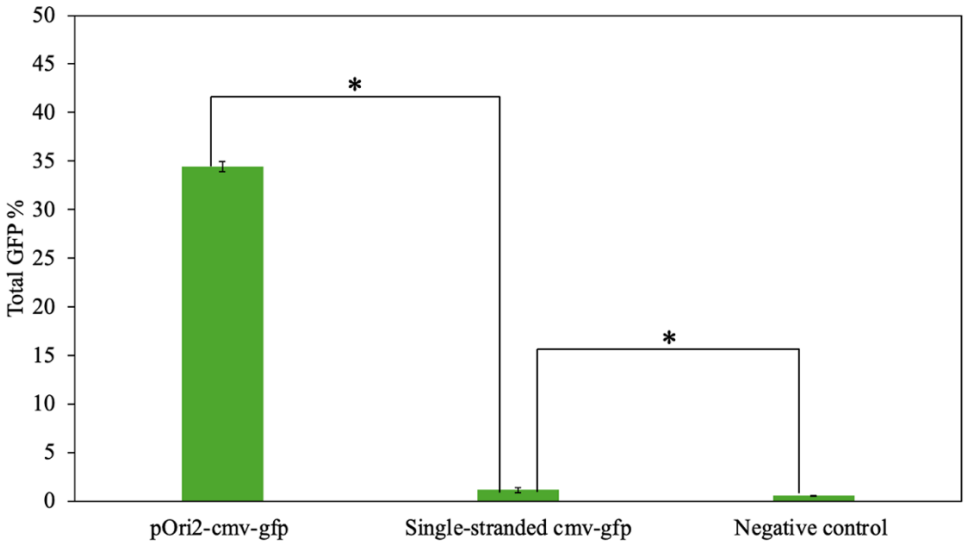

Figure 17. Precent of GFP fluorescent HeLa cells transfected with pOri2-cmv-gfp and ssDNA encoding *cmv-gfp* with TurboFect. Total percent (%) of GFP fluorescent HeLa cells was calculated for 10,000 events (cells) for each replicate (two) at 96h for HeLa cells transfected with pOri2-cmv-gfp, ssDNA encoding *cmv-gfp* gene cassettes extracted from miniphagemids with TurboFect. Non-transfected cells were used as a negative control. Data are presented as mean ± SEM for duplicate samples. The * above the bars indicates a statistically significant difference at $p < 0.005$ determined by paired-t test.

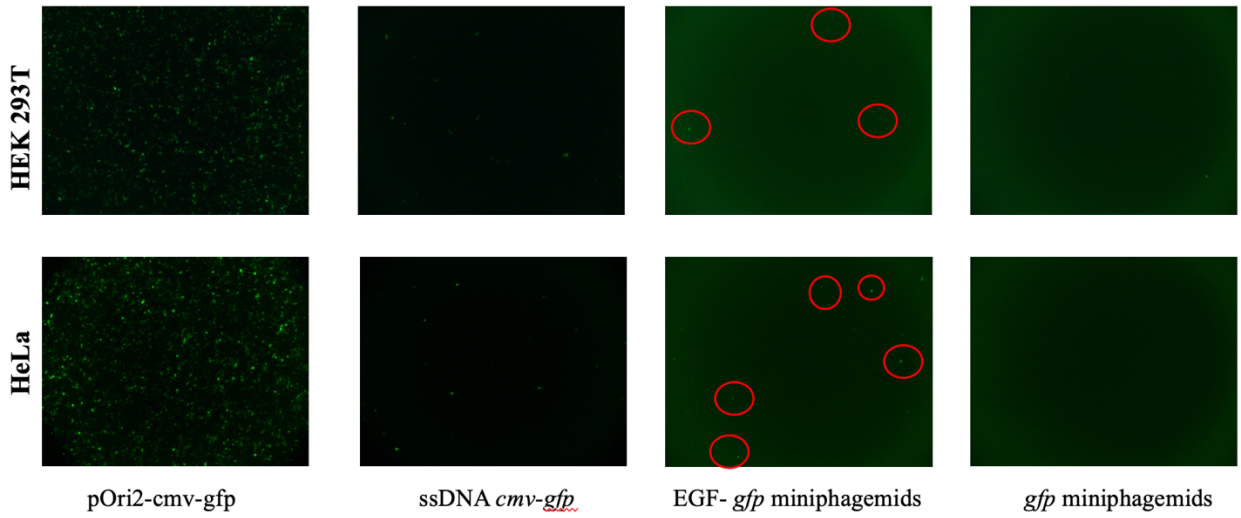

Figure 18. GFP gene expression in cells transfected with precursor phagemids, ssDNA and miniphagemids complexed with TurboFect. HEK 293T and HeLa cells were treated with precursor phagemid pOri2-cmv-gfp, ssDNA encoding *cmv-gfp* gene cassettes, EGF-*gfp* miniphagemids and *gfp* miniphagemids at MOI = 100,000. GFP expressions as encoded by EGF-*gfp* miniphagemids are circled in red. A transfection reagent, TurboFect was added to each sample. Images were taken at 96 h post transfection.

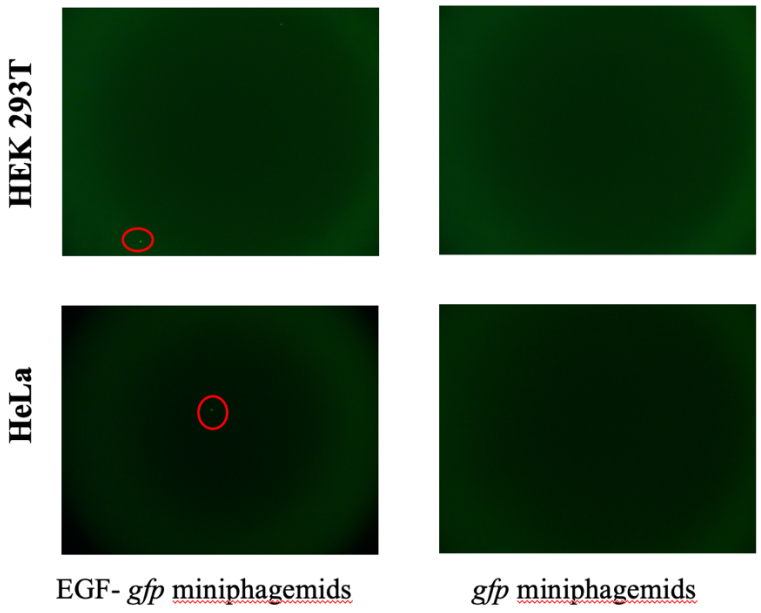

Figure 19. GFP gene expression in cells transfected with EGF-displaying and non-displaying *gfp* miniphagemids without TurboFect. HEK 293T and HeLa cells were treated EGF-*gfp* miniphagemids and *gfp* miniphagemids at MOI = 100,000 without the transfection reagent TurboFect. GFP expressions as encoded by EGF-*gfp* miniphagemids are circled in red. Images were taken at 96 h post transfection.

5.5.1 Characterization of HPV16 L1 protein production, VLP assembly and VLP escape from targeted tumour cells.

HEK 293T cells were transfected with precursor phagemid pOri2-L1-VGB4, pOri2-L1-VGB4-ΔNLS, ssDNA encoding *L1-VGB4* gene cassettes, and ssDNA encoding *L1-VGB4-ΔNLS* gene cassettes. At 96 h post transfection, the cell lysates and supernatants were harvested. Indirect ELISA confirmed the presence of HPV16 L1 proteins and VLPs in the cell lysates transfected with pOri2-L1-VGB4 and ssDNA encoding *L1-VGB4* (Figure 20 & Table 8). The presence of L1 proteins and VLPs within these samples were successfully detected by binding towards Camvir-1 and H16:U4 Abs, respectively, indicated by increased absorbance readings. The wells coated the negative controls (pOri2-cmv-gfp, ssDNA encoding *cmv-gfp*), and blank (non-transfected cell lysate) demonstrated low absorbance values in comparison to wells coated with the pOri2-L1-VGB4 and ssDNA encoding *L1-VGB4* transfected cell lysates, as expected. However, the absorbance values for cell lysates transfected with pOri2-L1-VGB4-ΔNLS and ssDNA encoding *L1-VGB4-ΔNLS* were much lower for Camvir-1 Ab, and not detected with H16:U4 Abs. This indicates L1 proteins were not produced at a sufficient amount to form VLPs in HEK 293T cells transfected with the *L1-VGB4-ΔNLS* gene cassette. The presence of L1 proteins and VLPs were not detected in all the cell supernatants.

Next, HeLa cells were transfected with the same precursor phagemids and ssDNA samples in addition to EGF-displaying miniphagemids. At 96 h post transfection, the cell lysates and supernatants were harvested. Indirect ELISA confirmed the presence of HPV16 L1 in the cell lysates transfected with pOri2-L1-VGB4 and ssDNA encoding *L1-VGB4* (Figure 21 & Table 9). However, the absorbance values were significantly lower than the values for the transfected

HEK293T cell lysates. Minimal amount of L1 proteins were detected in the transfected cell lysates with pOri2-L1-VGB4-ΔNLS and the ssDNA encoding *L1-VGB4-ΔNLS*, indicating slightly higher absorbance values than the blank and negative controls. However, L1 proteins were not detected in the transfected cell lysates with miniphagemids. There was no binding towards H16:U4 Ab in all the cell lysates, indicating no self-assembly of HPV VLPs in HeLa cells. Similar to the HEK 293T cells, the presence of L1 proteins and VLPs were not detected in all the HeLa cell supernatants.

Table 8: Summary of indirect ELISA detection of HPV16 L1 protein and VLP assembly in HEK 293T cells.

Transfected sample	Camvir-1 Ab (Absorbance at 450 nm)		H16:U4 Ab (Absorbance at 450 nm)	
	Cell lysate	Supernatant	Cell lysate	Supernatant
pOri2-cmv-gfp	0.001 ± 0.011	-0.014 ±0.007	0.000 ±0.003	-0.001 ±0.002
ssDNA-*cmv-gfp*	-0.002 ±0.005	-0.011 ±0.005	-0.006 ±0.002	-0.002 ±0.002
pOri2-L1-VGB4	2.302 ±0.014	0.027 ±0.152	2.197 ±0.002	0.004 ±0.042
ssDNA-*L1-VGB4*	0.172 ±0.033	0.025 ±0.003	0.038 ±0.001	-0.002 ±0.001
pOri2-L1-ΔNLS-VGB4	0.160 ±0.030	0.035 ±0.005	-0.002 ±0.001	-0.002 ±0.001
ssDNA-*L1-ΔNLS-VGB4*	0.013 ±0.018	0.025 ±0.007	-0.002 ±0.000	-0.002 ±0.002

Values are subtracted by the average blank value and expressed as a mean of three independent assays ± SEM, n = 3. Transfected HEK 293T cell lysates and supernatants are tested separately with two different primary Abs, Camvir-1 to detect the presence of L1 protein and H16:U4 to detect the formation of HPV VLPs. The raw absorbance values are attached in Appendix D.

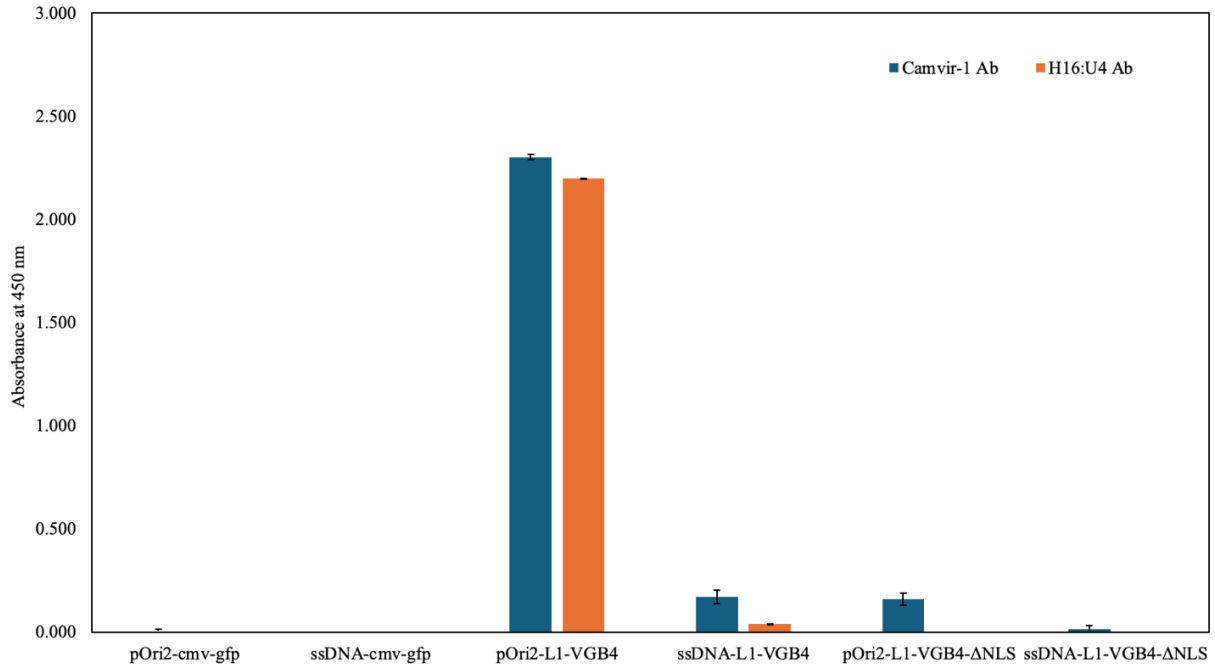

Figure 20. Indirect ELISA detection of HPV16 L1 protein and VLP assembly in cell lysates harvested from HEK 293T cells. The average absorbance values for HEK 293T cell lysate samples are subtracted by the average blank value. The error bars represent mean absorbance values of triplicate samples ± SEM @ 450 nm detected with either Camvir-1 or H16:U4 Ab, as labelled in the graph.

Table 9: Summary of indirect ELISA detection of HPV16 L1 protein and VLP assembly in HeLa cells.

Transfected sample	Camvir-1 Ab (Absorbance at 450 nm)		H16:U4 Ab (Absorbance at 450 nm)	
	Cell lysate	Supernatant	Cell lysate	Supernatant
pOri2-cmv-gfp	0.022 ±0.007	-0.002 ±0.007	-0.004 ±0.000	-0.002 ±0.005
ssDNA-*cmv-gfp*	0.069 ±0.020	-0.033 ±0.004	0.000 ±0.000	0.009 ±0.016
pOri2-L1-VGB4	0.460 ±0.012	-0.013 ±0.001	0.006 ±0.000	0.003 ±0.013
ssDNA-*L1-VGB4*	0.178 ±0.081	-0.013 ±0.005	-0.001 ±0.001	0.001 ±0.007
EGF-*L1-VGB4* miniphagemids	0.071 ±0.039	-0.024 ±0.016	0.000 ±0.000	-0.005 ±0.001
pOri2-L1-VGB4-ΔNLS	0.144 ±0.036	-0.017 ±0.006	-0.002 ±0.001	-0.005 ±0.000
ssDNA-*L1-VGB4-ΔNLS*	0.091 ±0.030	-0.005 ±0.009	-0.002 ±0.000	-0.004 ±0.001
EGF-*L1-VGB4-ΔNLS* miniphagemids	0.067 ±0.029	-0.012 ±0.000	0.003 ±0.004	0.018 ±0.031

Values are subtracted by the average blank value and expressed as a mean of three independent assays ± SEM, n = 3. Transfected HeLa cell lysates and supernatants are tested separately with two different primary Abs, Camvir-1 to detect the presence of L1 protein and H16:U4 to detect the formation of HPV VLPs. The raw absorbance values are attached in Appendix D.

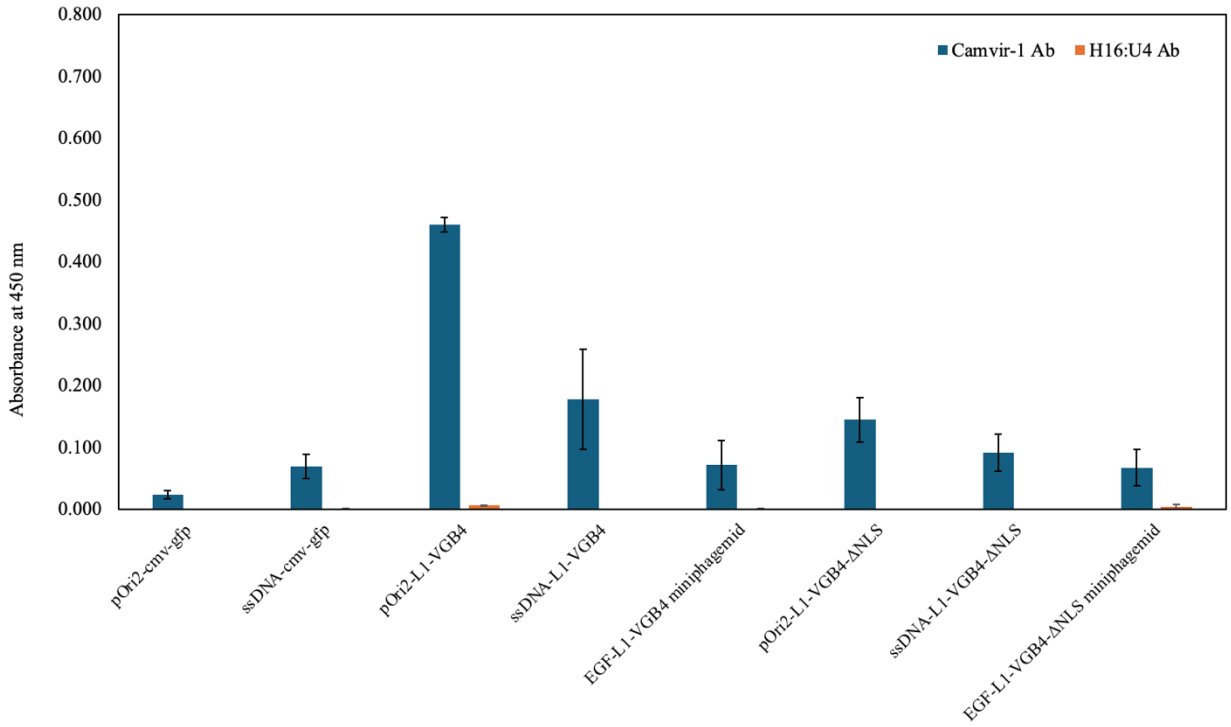

Figure 21. Indirect ELISA detection of HPV16 L1 proteins in cell lysates harvested from HeLa cells. The average absorbance values for HeLa cell lysate samples are subtracted by the average blank value. The error bars represent mean absorbance values of triplicate samples ± SEM @ 450 nm detected with either Camvir-1 or H16:U4 Abs.

5.5.2 Characterization of the binding capacity of VGB4-displaying HPV VLPs to VEGFR

Based on the previous ELISA results, HPV VLPs were only detected in the HEK 293T cells transfected with pOri2-L1-VGB4 and ssDNA encoding *L1-VGB4* within the cell lysates. Sandwich ELISA confirmed that in transfected cell lysate with pOri2-L1-VGB4, there was a slight increase in absorbance values (Figure 22 & Table 10), indicating a preferential binding towards VEGFR-2. The binding towards VEGFR-2 was not detected in the transfected cell lysates with ssDNA encoding *L1-VGB4*. The blank (non-transfected cell lysates) and negative control (pOri2-cmv-gfp cell lysates) demonstrated low absorbance values, suggesting the lack of specificity of these samples towards VEGFR-2, as expected.

Table 10: Summary of Sandwich ELISA detecting the binding of VGB4-displaying HPV VLPs to VEGFR-2.

Transfected sample	Camvir-1 Ab (Absorbance at 450 nm)
	Cell lysate
pOri2-cmv-gfp	0.000 ± 0.031
pOri2-L1-VGB4	0.064 ± 0.001
ssDNA-*L1-VGB4*	0.001 ± 0.007

Values are subtracted by the average blank value and expressed as a mean of three independent assays ± SEM, n = 3. Transfected HEK 293T cell lysate samples are tested with primary Abs Camvir-1 to detect the binding capacity of VGB4-displaying HPV VLPs to VEGFR-2. The raw absorbance values are attached in Appendix D.

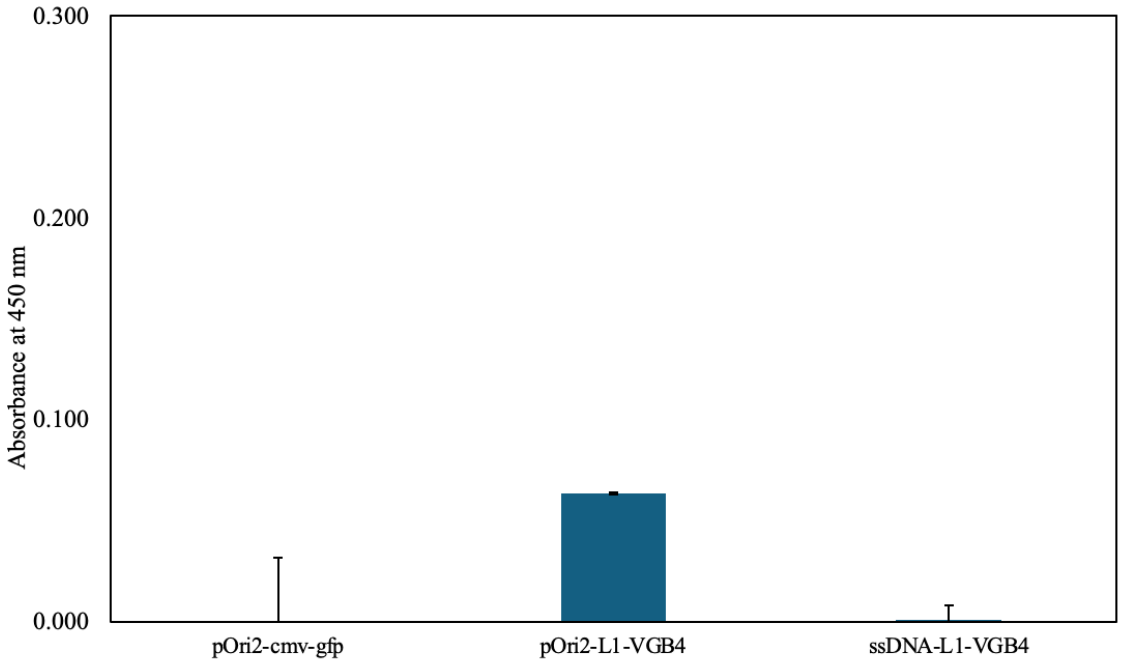

Figure 22. Sandwich ELISA detecting the binding of VGB4-displaying HPV VLPs to VEGFR-2. The average absorbance values for HEK 293T cell lysate samples are subtracted by the average blank value. The error bars represent mean absorbance values of triplicate samples ± SEM @ 450 nm detected with Camvir-1 Abs.

Chapter 6 Discussion

M13 phages have emerged as a novel and targeted delivery vector in gene therapy, specifically with the usage of phage display technology (Petrov et al., 2022). By displaying specific ligands on the phage capsid proteins, this technology has opened new avenues for cancer gene therapy with the potential to deliver therapeutic genes to tumour cells. Additionally, the genetic flexibility of M13 phages allows for easy modification to target specific cells and tissues, thus making them an attractive candidate platform for gene therapy. VLPs are also a promising tool in cancer immunotherapy, harnessing their structural similarity to viruses without the associated pathogenicity (Zepeda-Cervantes et al., 2020), and can effectively induce immune responses, making them suitable candidates for developing therapeutic strategies against cancer. Several successful gene-based vaccine studies have promoted the study of DNA-encoded VLPs, harvesting the benefits of both gene therapy and immunotherapy (Lamprecht et al., 2016; Leder et al., 2001). With the feasibility and cancer-therapeutic directed clinical applications in mind for this study, HPV VLPs were chosen as the VLP of study for several reasons including its ease of characterization, potent immunogenicity, and peptide fusion tolerance.

This was an exploratory study with the purpose to examine the ability of delivering a DNA encoded HPV VLP displaying an anti-angiogenic peptide known as VGB4 through a M13 phage-derived miniphagemid. The miniphagemid was engineered to display a cell specific ligand, EGF, and used HEK293T cells to assess the transfection efficiency of the precursor phagemid and ssDNA extracted from miniphagemids. Additionally, the study used HeLa cells to assess the specificity of gene transfer through EGF-displaying miniphagemids since these cells express significantly higher levels of EGFR in comparison to other tumour cell lines. EGF was

the peptide of choice for display as it retains its function when displayed on phage and has been well-documented in targeting for other types of vectors in gene therapy applications (Bortot et al., 2022; Halder et al., 2023; Huh et al., 2022). In this study, we demonstrated the display of EGF on miniphagemids enables targeted interaction with EGFR positive cell lines and the gene cassette encoding a VGB4-displayng HPV VLP with a specific binding towards VEGFR-2 can be produced in mammalian cells.

6.1 EGF ligands are successfully displayed on the miniphagemids but the production efficiency is potentially sequence-dependent

EGF has been successfully displayed on pIII of the M13 coat protein, in both N-terminal and C-terminal fusions (Larocca et al., 2001; Z. Li et al., 2006). A dot blot was performed and confirmed the presence of EGF on the miniphagemids produced in this study. As shown in Figure 10, EGF was successfully and specifically detected in all the displaying miniphagemids, indicating the successful translational fusion of EGF to pIII. A serial dilution of human recombination EGF was used as a reference for estimating the concentration of EGF displayed miniphagemids. All the EGF-displaying miniphagemids showed a high level of EGF expression, showing coloured dots with an intensity around 125 ng/μL or above. It was visually noted that the colour of the dotted EGF-*gfp* miniphagemids was less intense than the dotted EGF-*L1-VGB4* miniphagemid and EGF-*L1-VGB4-ΔNLS* miniphagemid, suggesting the concentration of EGF-*gfp* miniphagemids might be lower than the other two miniphagemids.

Next, the concentrations of miniphagemids were quantified using qPCR and MADLS. In this study, we sought to use two difference methods to quantify the concentrations, however, in our previous studies, we demonstrated that the qPCR method for phage quantification is highly

sensitive, reproducible and faster than the standard infectivity assays such as plaque and colony assays. Although infectivity-based assays can serve as a reference to develop novel quantification methods, high variability has been documented in these assays, which arises from the inherent differences in bacterial growth parameters and variability between plate pouring and spreading techniques, among other factors (Ács et al., 2020). Therefore, a more precise and reproducible method to quantify phagemid production is represented by qPCR (Ács et al., 2020). This method requires the generation of a calibration curve by creating a serial dilution of an external control plasmid encoding the gene of interest. The miniphagemid samples encapsulating the gene of interest can be amplified through qPCR, and the genomic copies of the targeted gene in a sample is calculated based on the calibration curve. qPCR is extremely sensitive, and is capable of detecting and quantifying very low amounts of nucleic acids. It also has a high specificity due to the use of sequence-specific primers and probes. We have previously demonstrated qPCR as a more superior and sensitive quantification method than the standard infectivity assay (Wong, 2022). Nevertheless, this experimental process is time-consuming, and requires a significant amount of work to optimize primers and run conditions. To further simplify phage quantification, we explored the usage of MADLS to count particle concentration. Preparing samples for MADLS is much simpler than qPCR and less time-consuming for analysis, thus making it an attractive method for phage quantification. It also provides additional information on particle size distribution, surface charge, and their stability through zeta potential measurements. Comparing the qPCR and MADLS-estimated concentrations of each sample, MADLS in general produced a higher value. It is possible that empty phagemid containing no DNA can be packaged by the helper phage, which may account for this discrepancy. MADLS is not a targeted method to determine concentration of the gene of interest as it only measures the

presence of phage particles, therefore, empty phagemids could be detected through this method. Based on the qPCR results, all the miniphagemid samples have concentrations above 10^{12} gc/mL. The MADLS results are more variable, giving miniphagemid concentrations in the range of $10^{12} – 10^{13}$ particle counts/mL. While most samples had no statistically significant difference between the qPCR-estimated and MADLS-estimated concentrations, the *L1-VGB4* miniphagemids and *L1-VGB4-ΔNLS* miniphagemids had a significant difference ($p < 0.05$), in which the MADLS over-estimated the concentration. As a result, further optimization is needed to quantify miniphagemids through MADLS.

Consistent with our previous work, we observed no impact from pIII display of EGF on phagemid production. Our previous work showed the yield by SW8 helper phage packaging a *gfp* miniphagemid was around 5 x 10^{11} gc/mL (Wong et al., 2023). Based on the qPCR data generated in this study, the concentration of all the miniphagemid samples were around 10^{12} gc/mL. This indicates that using our package-deficient helper phage (SW8) does not impact the packaging efficiency of phagemid. Furthermore, there is no significant difference between the concentrations of EGF-displaying phagemid and non-displaying phagemid (Table 6), suggesting the display of an EGF ligand at the N-terminal of M13 coat protein pIII does not affect its packaging ability. Interestingly, we noticed that the concentration of miniphagemids encapsulating the *cmv-gfp* cassette was lower than the two other miniphagemids encapsulating either *L1-VGB4* or *L1-VGB4-ΔNLS* gene cassettes. The relatively low concentrations of EGF-*gfp* miniphagemid can also be visualized in the dot blot result. There is no significant difference in the overall length of the three transgene cassettes, and they all share the same *cmv* promoter. The coding sequence encapsulated in these miniphagemids is the main difference among these

samples. We have previously postulated that the production efficiency of miniphagemids may be affected by the sequences of the transgene cassettes (Wong, 2022). Miniphagemids encapsulate ssDNA, which is subjected to the formation of secondary structure. A high number of secondary structures within a phagemid sequence can potentially hinder the efficiency of converting from double-stranded RF to a single-stranded form during packaging, thus leading to lower production of phage particles.

In summary, the display of EGF does not affect miniphagemid production. EGF can be displayed on miniphagemids at a relatively high concentration. qPCR is still by far the most accurate and robust method for quantifying phagemid concentrations. While MADLS is much easier to operate and less time-consuming, it produces more variable results. Thus, further validation and optimization are needed. Based on the qPCR results, the concentration of the EGF-displaying and non-displaying miniphagemids encapsulating different gene expression cassette are around 10^{12} gc/mL. Lastly, the secondary structure formed within the transgene cassette may adversely affect the production efficiency of miniphagemids.

6.2 EGF-displaying miniphagemids contain no helper phage and minimal full-size phagemid contamination

The miniphagemids are produced upon a split f1 *ori* present on the precursor phagemids (Wong et al., 2023). We used the miniphagemid as a gene delivery vector to eliminate any bacterial element such as antibiotic resistance markers, the bacterial *ori*, and CpG motifs. The elimination of these elements has been proven to have an improved safety profile and prevents immunostimulatory transgene silencing (Häcker et al., 2002; Krieg, 2002). However, an intact *PS* is also present on the precursor phagemid outside the region of the split f1 *ori*, therefore, we

expected some full-size phagemids could be transcribed and packaged in the final lysates. To examine the presence of any full-size phagemid in the lysates, the ssDNA encapsulated by the miniphagemids were extracted from their capsids. The subsequent visualization of ssDNA showed only one distinct band, corresponding to the size of the split f1 *ori* with the inserted transgene cassette (Figure 13). Full-size phagemid DNA was not visualized in the ssDNA extracted in this study. Furthermore, colony assay confirmed the packaging of full-size phagemid and helper phage is significantly low in proportion to the total miniphagemid titre (Table 7). The contamination efficiency of full-size phagemid for EGF-*gfp* miniphagemids is lower than the other two miniphagemids encapsulating the VGB4-displaying HPV VLP gene cassette. This also suggests that the production efficiency of miniphagemids is potentially sequence dependent. Nevertheless, full-size phagemid contaminations are low across all samples, indicating the production of miniphagemids from a split f1 *ori* was an effective way of eliminating any bacterial backbone present in the precursor phagemids. The helper phage contaminations of all EGF-displaying miniphagemids are low, as no CFU were observed on LB+Kan plates. This confirms that the removal of *PS* in the helper phage plasmid is an effective way of reducing helper phage self-packing during the production of

In this study we have successfully produced miniphagemids encoding a transgene expression cassette from a precursor phagemids with a split f1 *ori* and a package-deficient helper phage. The visualizations of ssDNA extracted from the phagemid lysates produced in this study suggest miniphagemids are preferentially produced over full-size phagemids, and the presence of full-size phagemids is very minimal and is not detectable at a molecular level. To further assess the presence of full-size phagemids in the final lysates, qPCR can be used to amplify the *amp*

resistance gene in the backbone of the precursor phagemid. This can be a more sensitive and quantitative approach to detect any full-size phagemids contaminations.

6.3 EGF-displaying miniphagemids improve gene transfer

To assess the transfection efficiency of our precursor phagemid construct and ssDNA extracted from miniphagemid lysates and miniphagemids, HEK 293T and HeLa cells were used to express and produce GFP. The precursor phagemid pOri2-cmv-gfp contains a GFP gene expression cassette cloned in-between the split f1 *ori*. The expression of GFP is under controlled by a *cmv* promoter, which is the same promoter used for the expression of the L1 VLPs investigated in this study. Therefore, this would give a general ideal of the transfection efficiency of the L1 VLPs gene expression cassette. HEK 293T cells are derived from the HEK 293 cell line but have been transformed with the large T antigen from SV40, which allows for high-efficiency transfection (Tan et al., 2021). This makes them particularly suitable for experiments requiring the introduction of foreign DNA. HEK 293T cells are also easy to maintain, grow at accelerated rates compared to other mammalian cells, highly transfectable, and demonstrate increased levels of genome stability over time (Stepanenko & Dmitrenko, 2015). These combined factors promote HEK 293T as a good candidate for assessing transfection efficiency and producing VLPs for this study. However, they express EGFR at a relatively low level at ~ 20,000 molecules per cell (Yavas et al., 2016). Therefore, these cells are not representative of EGF-specific transfection via EGF-displaying miniphagemids. HeLa cells were also used in the study. They are also known to express EGFR at significant levels at ~300,000 molecules per cell, providing a relevant model for studying EGFR-related therapeutic testing (Capuani et al., 2015). HeLa cells originate from a human cervical carcinoma. Their genetic and phenotypic characteristics are

representative of many cancer cell behaviors, making them directly relevant for studying the biology of human cancer (Masters, 2002).

The precursor phagemid pOri2-cmv-gfp and ssDNA encoding *cmv-gfp* gene cassettes extracted from miniphagemids were transfected in HEK 293T and HeLa cells complexed with a transfection reagent TurboFect as a positive control to assess the maximal level of GFP expression with our construct. TurboFect is a cationic polymer-based transfection reagent used for delivering nucleic acids (DNA or RNA) into eukaryotic cells. It binds to nucleic acids through electrostatic interactions, forming compact and stable nucleic acid-polymer complexes (Jamour et al., 2024). These complexes protect the nucleic acids from degradation and facilitate their entry into cells. The composition of the reagent promotes endosomal disruption, preventing nucleic acids from being degraded within the endosomes and allowing them to reach their target sites within the cells (Jamour et al., 2024). We have shown that TurboFect improves miniphagemid-mediated gene transfer (Wong, 2022). The addition of TurboFect also does not affect cell viability as a very minimal amount was used in our previous study. In this study, transfected cells were harvested at 96 h post transfection, and quantified for total GFP expression through flow cytometry. We showed that the GFP expression level of cells transfected with pOri2-cmv-gfp was 25 % in HEK 293T and 34 % in HeLa cells (Figure 14 and 15). ssDNA encoding *cmv-gfp* exhibited 2.7 % expression in HEK 293T and 1.2 % in HeLa cells. Although HeLa cells exhibited good transfection efficiency, its transfection efficiency for ssDNA was slightly lower than HEK293T cells. Nevertheless, the utility of HeLa cells lies in their specific relevance to human cancer biology and EGFR-related studies.

Next, we assessed the effectiveness of miniphagemid-mediated gene transfer by transfecting EGF-displaying and non-displaying miniphagemids encapsulating the *cmv-gfp* gene cassette (EGF-*gfp* miniphagemids and *gfp* miniphagemids) in HEK 293T and HeLa cells at 96 h post transfection. The transfections were conducted with and without TurboFect. In HeLa cells, GFP fluorescence was visualized in cells transfected with EGF-*gfp* miniphagemids with TurboFect, but at a significant reduction in cells transfected with the same miniphagemids without TurboFect (Figure 16 and 17). This is consistent with our previous observations that the addition of TurboFect enhances gene transfer (Wong, 2022). GFP fluorescence was not observed in HeLa cells transfected with *gfp* miniphagemids with no EGF display. This suggests the display of EGF improves the internalization of miniphagemids through the process of EGF:EGFR endocytosis, enabling the bypass of the plasma membrane and subsequent gene transfer. This emphasizes the necessity of constructing a cell-targeted gene delivery vector. Furthermore, we showed the addition of cationic polymers such as TurboFect improves transfection efficiency by aiding endosomal escape. Despite the enhancement of gene expression efficiency using miniphagemids, cell-targeting ligands, and chemical reagents, the overall gene expression achieved through phagemid-mediated gene delivery remains low compared to that of plasmids and ssDNA. We postulate that the internalized miniphagemids may become trapped within the endosomal compartment, where they are subsequently trafficked to lysosomes and subjected to DNA degradation. Studies have shown through intracellular imaging in HeLa cells that M13 phages enter primarily through clathrin-mediated endocytosis, accumulate in the endosomes which subsequently mature into lysosomes (Tian et al., 2015). Endosomal escape is a critical step in the development of an effective gene delivery system (Cupic et al., 2019). It remains a significant challenge, but also a promising area of research in gene therapy. Therefore, the underlying

causes of the low gene expression levels associated with the miniphagemid-mediated delivery approach need to be further investigated.

Overall, we employed multiple approaches in this study to enhance the efficiency of miniphagemid-mediated gene transfer. This includes eliminating bacterial elements in the delivery vector by constructing miniphagemids, displaying cell-specific ligand (EGF) on the miniphagemids, and using cationic polymers to aid endosomal escape. While GFP fluorescence was detected with EGF-displaying miniphagemids, the expression level did not match that achieved with plasmid or ssDNA-mediated delivery. This highlights the necessity of researching and optimizing an effective strategy to facilitate the escape of miniphagemids from the endosomal compartment.

6.4 VGB4-displaying HPV VLPs can be delivered as a DNA-encoded sequence in a precursor phagemid for production in human cells

In our previous study, VGB4-displaying HPV16 VLPs were successfully produced in HEK 293T cells by transfecting them with a DNA-encoded sequence within the eukaryotic expression plasmid pGL2-cmv-L1-de (Figure 5). In the current study, we produced miniphagemids encapsulating the same DNA sequence encoding VGB4-displaying HPV16 VLP by cloning this gene expression cassette between the split f1 *ori* of the precursor phagemid pOri2. HEK 293T cells were transfected with the precursor phagemid pOri2-L1-VGB4 and ssDNA encoding *L1-VGB4* gene cassettes extracted from miniphagemids. Indirect ELISA confirmed the presence of L1 proteins and HPV VLPs in the transfected HEK 293T cell lysates with precursor phagemid pOri2-L1-VGB4 (Figure 18). The Camvir-1 Ab bound more significantly to the transfected cell lysate samples compared to the H16:U4 Ab, which is consistent with our previous findings

(Pushparajah, 2022), and could be attributed to the fact that not all the L1 proteins present would be anticipated to assemble into VLPs. Studies have also shown that the formation of intermolecular disulfide bonds between the L1 proteins is essential for the self-assembly and stabilization of HPV VLPs (Palucha et al., 2005; Sapp et al., 1998). The L1 trimer formation is a critical step in the assembly of viral capsids (Florin et al., 2002; Sapp et al., 1998). This process is only mediated by two cysteine residues at AA position 176 and 427, forming intermolecular disulfide bonds. In this study, VGB4 peptide is inserted within the DE loop between AA 136 and 137, which does not significantly impact the formation of VLPs. The presence of L1 proteins was also detected in cell lysate samples transfected with ssDNA encoding *L1-VGB4*, but at a significantly lower level compared to cell lysates transfected with the precursor phagemid. This is consistent with our previous transfection efficiency data, indicating that ssDNA generally expresses genes at a significantly lower level than dsDNA. Nevertheless, a low level of HPV VLPs was detected in transfected cell lysates with ssDNA encoding *L1-VGB4* using H16:U4 Ab. In the lysates harvested from HeLa cells, the presence of HPV16 L1 proteins can be produced in cells transfected with the precursor phagemid pOri2-L1-VGB4, and at a low amount in cells transfected with ssDNA encoding the *L1-VGB4* gene cassette. However, HPV VLPs cannot be detected in the cell lysates. This suggests that an insufficient amount of L1 proteins is produced in HeLa cells to self-assemble into VLPs, or the level of VLPs in the cell lysates is low which cannot be detected using ELISA. In general, indirect ELISA may not accurately estimate the relative levels of HPV VLP formation. Therefore, a more sensitive method may be required to confirm the assembly of VLPs with ssDNA-based gene delivery.

The specificity of VGB4-displaying HPV VLPs for VEGFR-2 was evaluated using sandwich ELISA. Since HPV VLPs were detectable only in the lysates of transfected HEK 293T cells, the ELISA was conducted on these lysates. Results indicated that lysates from cells transfected with pOri2-L1-VGB4 exhibited a slightly higher affinity for VEGFR-2 compared to the negative controls (blank and pOri2-cmv-gfp), suggesting specific binding of the VGB4-displaying HPV VLPs to VEGFR-2. However, the absorbance values were relatively low. This is consistent with the low absorbance values obtained from our previous study (Pushparajah, 2022). Consequently, to definitively verify the VEGFR-2-targeted binding of the VLPs and confirm the validity of this assay, a positive control sample is necessary. Ideally, this positive control should be either a commercially available VGB4 peptide or a standard VEGF ligand, both of which specifically bind to VEGFR-2. Additionally, VLPs can be concentrated by ultracentrifugation through a density gradient (e.g., sucrose or cesium chloride). The VLPs band at a specific density, which can then be collected and further concentrated if needed.

In summary, we successfully demonstrated the production and partial assembly of VGB4-displaying HPV VLPs in HEK 293T cells, confirming the presence of L1 proteins and the specificity of the VLPs for VEGFR-2. However, the results highlighted limitations in the detection sensitivity and VLP assembly efficiency, particularly in HeLa cells. The study underscores the need for further optimization of the methods used to assess VLP formation and binding, including the incorporation of positive controls and concentration techniques like ultracentrifugation to enhance VLP detection and validation.

6.5 The modified *L1-VGB4-ΔNLS* gene cassette does not appear to assemble into VLPs nor induce cell lysis

HPV VLPs are non-enveloped; the most common mechanism for non-enveloped viruses to escape is through cell lysis (Bird & Kirkegaard, 2015). The accumulation of viral particles can lead to increased pressure and the production of viral proteins that disrupt cellular membranes, eventually causing the host cell to rupture and release the virions into the extracellular environment. Given that our previous study demonstrated that the production of HPV VLPs in HEK 293T cells does not result in cell lysis, we aimed to increase the amounts of HPV VLPs accumulating in the cell cytoplasm in this study in order to determine if we can induce cell lysis (Pushparajah, 2022). The production of HPV VLPs vaccines can be optimized by deleting the 34 AA expressing NLS at the C-terminal end of the L1 protein (between AA 472 and 505), which promotes cytoplasmic assembly of VLPs, improving yield and simplifying purification processes in vaccine production systems (Hallek & Burger, 2009). Based on this patent, we postulated that deleting the NLS in the precursor phagemid pOri2-L1-VGB4 can prevent the L1 protein from localizing to the nucleus, causing it to remain in the cytoplasm. Cytoplasmic accumulation of HPV VLPs can potentially induce cell lysis to release them in the extracellular environment where the VGB4 displayed on their surfaces can bind to VEGFR.

Using indirect ELISA, we detected minimal amounts of L1 proteins in the transfected HEK 293T and HeLa cell lysates with pOri2-L1-VGB4-ΔNLS and ssDNA encoding *L1-VGB4-ΔNLS* gene cassette, but not in the transfected cell lysates with miniphagemids (Table 7 & 8). HPV VLPs were not detected in all the cell lysates. L1 proteins and HPV VLPs were also not detected in all the cell supernatant samples. This suggests that *L1-VGB4-ΔNLS* gene cassette does not promote

VLP assembly in the cytoplasm nor induce cell lysis. It is worth noting that the L1 protein used in this study was modified with a VGB4 peptide insertion at the DE loop. This is different from the reference patent, in which the original L1 sequence was used and modified with a NLS deletion (Hallek & Burger, 2009). Although the intramolecular disulfide bond between the two cysteines at AA position 176 and 427 in the L1 protein is indispensable for VLP formation, the deletion of NLS is between AA position 472 and 505. We also sequenced the *L1-VGB4-ΔNLS* gene cassette and verified the presence of cysteines. The significant reduction in L1 protein expression might be caused by other factors which have not been investigated in this study. Although in our previous study the production of L1 proteins and VLP self-assembly are not affected when VGB4 is inserted at the DE loop, the addition of NLS truncation somehow limited the expression of L1 protein. We postulate that NLS might play a role in stabilizing the VGB4 peptide within the L1 protein structure, thus, L1 protein folding and subsequent VLP assembly are hindered when the L1 protein sequence is modified with the insertion of VGB4 and the deletion of NLS.

Chapter 7 Conclusions and Future Research

The number of applications for a phage-based drug delivery system is growing at a unprecedent speed (Petrov et al., 2022). This approach is particularly advantageous due to its low immunogenicity, ease of engineering, and capacity for high specificity (Bakhshinejad & Sadeghizadeh, 2014; Chongchai et al., 2024). In our previous work, we constructed a novel M13 phage-based gene delivery platform by producing highly concentrated miniphagemids from a packaging-deficient helper phage and a precursor phagemid with a split f1 *ori*. However, its application as a targeted gene therapy has not been investigated to date. The intent of this work was to construct an EGF-displaying miniphagemid encapsulating a DNA-encoded HPV VLP displaying VGB4 peptide, and to characterize its specificity and efficiency as a gene delivery vector within mammalian cells. In this study, we successfully produced and quantified EGF-displaying and non-displaying miniphagemids utilizing the production platform we previously constructed. Two quantification techniques were used to measure the concentration of miniphagemids. While MADLS is simple and fast, qPCR is still by far the most accurate and robust quantification method. Overall, we demonstrated that the display of EGF does not affect the rescue of miniphagemids. Miniphagemids can be produced at a high concentration, encapsulating the gene of interest at around 10^{12} gc/mL. To assess the transfection efficiency, we encapsulated the *cmv-gfp* gene expression cassettes in EGF-displaying and non-displaying miniphagemids. Increased GFP fluorescence have been observed with EGF-displaying miniphagemids compared to non-displaying miniphagemids at 96 h post transfection in both HEK 293T and HeLa cells. The significance of using miniphagemid is its ability to be engineered as a targeted gene delivery vector by displaying a cell-specific ligand such as EGF. Furthermore, miniphagemids only encapsulate a transgene expression cassette, which offers a

strong safety profile by eliminating any bacterial elements present in plasmid-based gene transfer. However, one of the obstacles of phage-mediated gene transfer is nuclear localization, as phages are more likely routed for lysosomal degradation upon internalization. The combination of a cationic polymer improves phage-mediated gene transfer, but appears insufficient to ensure highly efficient gene transfer.

Another main objective of this work is to produce EGF-displaying miniphagemids and non-displaying miniphagemids encapsulating a *L1-VGB4* gene cassette. This gene cassette was successfully cloned into a precursor phagemid with a split f1 *ori*. HPV16 L1 proteins are formed in both HEK 293T and HeLa cells transfected with the cloned precursor phagemid and ssDNA encoding *L1-VGB4* gene cassettes extracted from miniphagemids. However, the assembly of VGB4-displaying HPV VLPs are only formed in HEK 293T cells. Consistent with our previous work, HPV VLPs accumulate within cells and do not induce cell lysis (Pushparajah, 2022). However, these VLPs need to be released to the extracellular environment, which would allow VGB4 to bind VGFRs and inhibit angiogenesis (Farzaneh Behelgardi et al., 2018). We sought to promote cytoplasmic accumulation of HPV VLPs by deletion of the nuclear localization signal (NLS) in the L1 protein. We successfully produced a *L1-VGB4-ΔNLS* gene cassette, cloned into the precursor phagemid with a split f1 *ori*, and produced miniphagemids. However, low amounts of L1 proteins were detected only in the cell lysates transfected with the precursor phagemids. This suggests the deletion of NLS does not promote cytoplasmic accumulation of VGB4-displaying HPV VLPs, thus VLPs cannot cause cell lysis to be released in the cell supernatant. We postulate that NLS might interact with the VGB4 insertion in the L1 protein, thus the

deletion of it significantly hinders the proper folding of L1 and subsequently the self-assembly of VGB4-displaying HPV VLPs.

In conclusion, this study demonstrates the potential of EGF-displaying miniphagemids as targeted gene delivery vectors, highlighting their increased transfection efficiency compared to non-displaying miniphagemids. However, the challenges remain in terms of achieving the same level of gene expression as conventional plasmids, promoting an effective cytoplasmic accumulation, and subsequent release of VGB4-displaying HPV VLPs. This leads to the need for further characterization and optimization of miniphagemids and the DNA sequence expressing the VGB4-diplaying HPV VLPs as an effective cancer immunotherapy.

The future of this work should focus on characterizing the efficiency of miniphagemid-mediated gene transfer, assessing the immunogenicity of VGB4-displaying HPV VLPs, and inducing the release of VGB4-displaying HPV VLPs to the extracellular environment. Future research and experiments are recommended as outlined below:

1) To better understand the intracellular localization of miniphagemids over time, fluorescent labelling of miniphagemids and visualizing through confocal microscopy should be performed. Miniphagemids can be conjugated with a fluorescent dye such as Alexa Fluor, followed by transfecting in the targeted cells. This experiment can precisely show the intracellular localization of miniphagemids in real-time, and help to determine if they are subjected to lysosomal degradation.
2) Assessing the transfection efficiency of miniphagemids with luciferase assay should also be done to further investigate their transfection efficiency at increased sensitivity. In this

study, we only produced miniphagemids expressing GFP to assess for transfection efficiency. Although GFP expression allows for direct observation and visualization of transfected cells using fluorescence microscopy, it has limitations in sensitivity. An alternative method is to use luciferase assay, which is superior in terms of sensitivity. This would be suitable to detect low transfection efficiency or low levels of gene expression. EGF-displaying miniphagemids encapsulating a luciferase gene cassette needs to be generated to conduct this luciferase assay.

3) As briefly outlined in the discussion, further testing needs to be conducted to confirm the specificity of VGB4-displaying HPV VLPs toward VEGFR. This can be done by inserting a scrambled peptide sequence within the DE loop region of the L1 protein to eliminate the possibility of non-specific binding towards VEGFR. Additional positive control samples can be employed to the ELISA experiments, such as a commercially available VGB4 peptide or a standard VEGF ligand which binds specifically to VEGFR.
4) Conduction of a cytokine release assay to assess the immunogenicity of VGB4-displaying HPV VLPs should also be performed. This assay can measure cytokine production in response to VLPs. To conduct this experiment, purified VGB4-displaying HPV VLPs need to be collected from cell lysates, and then co-cultured with immune cells such as human peripheral blood mononuclear cells (PBMC). Cell supernatants will be collected, and the cytokine levels can be analyzed using ELISA or multiplex cytokine assays. This will allow for a comparison between the cytokine profiles of immune cells treated with the VLPs and untreated cells.
5) Prediction of the folding and stability of L1 protein with VGB4 insertion and NLS deletion would help to determine the stability of the proteins. Computational approaches

can be used to determine if the deletion of NLS affects the production of L1 proteins with VGB4 insertion. Utilizing specialized software, the tertiary structure of the protein can be predicted based on its amino acid sequence. This may help to identify any disordered regions which may affect protein function and analyze the stability of the protein.

6) Insertion of a signal peptide in the L1 protein to promote endoplasmic reticulum (ER) secretion. Signal peptides are short amino acids sequences at the N-terminal end of a protein that direct the transport of protein to the ER. Engineering signal peptides onto the L1 proteins can potentially facilitate the secretion of HPV VLPs to the extracellular environment. More thorough investigations and considerations are needed to determine the feasibility of this approach in terms of the compatibility, cleavage efficiency and protein stability with an insertion of signal peptide.

References

Ács, N., Gambino, M., & Brøndsted, L. (2020). Bacteriophage Enumeration and Detection Methods. *Frontiers in Microbiology*, *11*. https://doi.org/10.3389/fmicb.2020.594868

Adams, G. P., & Weiner, L. M. (2005). Monoclonal antibody therapy of cancer. *Nature Biotechnology*, *23*(9), Article 9. https://doi.org/10.1038/nbt1137

Alberts, B., Johnson, A., Lewis, J., Raff, M., Roberts, K., & Walter, P. (2002). Helper T Cells and Lymphocyte Activation. *Molecular Biology of the Cell. 4th Edition*. https://www.ncbi.nlm.nih.gov/books/NBK26827/

Aloisio, A., Nisticò, N., Mimmi, S., Maisano, D., Vecchio, E., Fiume, G., Iaccino, E., & Quinto, I. (2021). Phage-Displayed Peptides for Targeting Tyrosine Kinase Membrane Receptors in Cancer Therapy. *Viruses*, *13*(4), Article 4. https://doi.org/10.3390/v13040649

Amjad, M. T., Chidharla, A., & Kasi, A. (2022). Cancer Chemotherapy. In *StatPearls*. StatPearls Publishing. http://www.ncbi.nlm.nih.gov/books/NBK564367/

Baghban, R., Roshangar, L., Jahanban-Esfahlan, R., Seidi, K., Ebrahimi-Kalan, A., Jaymand, M., Kolahian, S., Javaheri, T., & Zare, P. (2020). Tumor microenvironment complexity and therapeutic implications at a glance. *Cell Communication and Signaling*, *18*(1), 59. https://doi.org/10.1186/s12964-020-0530-4

Bakhshinejad, B., & Sadeghizadeh, M. (2014). Bacteriophages as vehicles for gene delivery into mammalian cells: Prospects and problems. *Expert Opinion on Drug Delivery*, *11*(10), 1561–1574. https://doi.org/10.1517/17425247.2014.927437

Bazan, J., Całkosiński, I., & Gamian, A. (2012). Phage display—A powerful technique for immunotherapy. *Human Vaccines & Immunotherapeutics*, *8*(12), 1817–1828. https://doi.org/10.4161/hv.21703

Bellone, S., El-Sahwi, K., Cocco, E., Casagrande, F., Cargnelutti, M., Palmieri, M., Bignotti, E., Romani, C., Silasi, D.-A., Azodi, M., Schwartz, P. E., Rutherford, T. J., Pecorelli, S., & Santin, A. D. (2009). Human Papillomavirus Type 16 (HPV-16) Virus-Like Particle L1-Specific CD8+ Cytotoxic T Lymphocytes (CTLs) Are Equally Effective as E7-Specific CD8+ CTLs in Killing Autologous HPV-16-Positive Tumor Cells in Cervical Cancer Patients: Implications for L1 Dendritic Cell-Based Therapeutic Vaccines. *Journal of Virology*, *83*(13), 6779–6789. https://doi.org/10.1128/JVI.02443-08

Berger, C., Madshus, I. H., & Stang, E. (2012). Cetuximab in combination with anti-human IgG antibodies efficiently down-regulates the EGF receptor by macropinocytosis. *Experimental Cell Research*, *318*(20), 2578–2591. https://doi.org/10.1016/j.yexcr.2012.09.001

Bird, S. W., & Kirkegaard, K. (2015). Escape of non-enveloped virus from intact cells. *Virology*, *0*, 444–449. https://doi.org/10.1016/j.virol.2015.03.044

Bortot, B., Apollonio, M., Baj, G., Andolfi, L., Zupin, L., Crovella, S., di Giosia, M., Cantelli, A., Saporetti, R., Ulfo, L., Petrosino, A., Di Lorenzo, G., Romano, F., Ricci, G., Mongiat, M., Danielli, A., Calvaresi, M., & Biffi, S. (2022). Advanced photodynamic therapy with an engineered M13 phage targeting EGFR: Mitochondrial localization and autophagy induction in ovarian cancer cell lines. *Free Radical Biology and Medicine*, *179*, 242–251. https://doi.org/10.1016/j.freeradbiomed.2021.11.019

Brennan, P. J., Kumogai, T., Berezov, A., Murali, R., & Greene, M. I. (2000). HER2/Neu: Mechanisms of dimerization/oligomerization. *Oncogene*, *19*(53), 6093–6101. https://doi.org/10.1038/sj.onc.1203967

Buck, C. B., Day, P. M., & Trus, B. L. (2013). The papillomavirus major capsid protein L1. *Virology*, *445*(1), 169–174. https://doi.org/10.1016/j.virol.2013.05.038

Buonaguro, L., Tagliamonte, M., Tornesello, M. L., & Buonaguro, F. M. (2011). Developments in virus-like particle-based vaccines for infectious diseases and cancer. *Expert Review of Vaccines*, *10*(11), 1569–1584. https://doi.org/10.1586/erv.11.135

Burd, E. M., & Dean, C. L. (2016). Human Papillomavirus. *Microbiology Spectrum*, *4*(4), 4.4.18. https://doi.org/10.1128/microbiolspec.DMIH2-0001-2015

Burger, A., & Hallek, M. (2003). *Papilloma virus capsomere vaccine formulations and methods of use* (Canada Patent CA2229955C). https://patents.google.com/patent/CA2229955C/en?oq=hpv+l1+nuclear+localization+signal

Caldeira, J. C., Perrine, M., Pericle, F., & Cavallo, F. (2020). Virus-Like Particles as an Immunogenic Platform for Cancer Vaccines. *Viruses*, *12*(5), 488. https://doi.org/10.3390/v12050488

Capuani, F., Conte, A., Argenzio, E., Marchetti, L., Priami, C., Polo, S., Di Fiore, P. P., Sigismund, S., & Ciliberto, A. (2015). Quantitative analysis reveals how EGFR activation and downregulation are coupled in normal but not in cancer cells. *Nature Communications*, *6*(1), 7999. https://doi.org/10.1038/ncomms8999

Carter, J. J., Wipf, G. C., Benki, S. F., Christensen, N. D., & Galloway, D. A. (2003). Identification of a Human Papillomavirus Type 16-Specific Epitope on the C-Terminal Arm of the Major Capsid Protein L1. *Journal of Virology*, *77*(21), 11625–11632. https://doi.org/10.1128/JVI.77.21.11625-11632.2003

Cascales, E., Buchanan, S. K., Duché, D., Kleanthous, C., Lloubès, R., Postle, K., Riley, M., Slatin, S., & Cavard, D. (2007). Colicin Biology. *Microbiology and Molecular Biology Reviews*, *71*(1), 158–229. https://doi.org/10.1128/MMBR.00036-06

Cavazzana, M., Six, E., Lagresle-Peyrou, C., André-Schmutz, I., & Hacein-Bey-Abina, S. (2016). Gene Therapy for X-Linked Severe Combined Immunodeficiency: Where Do We Stand? *Human Gene Therapy*, *27*(2), 108–116. https://doi.org/10.1089/hum.2015.137

Chabeda, A., van Zyl, A. R., Rybicki, E. P., & Hitzeroth, I. I. (2019). Substitution of Human Papillomavirus Type 16 L2 Neutralizing Epitopes Into L1 Surface Loops: The Effect on Virus-Like Particle Assembly and Immunogenicity. *Frontiers in Plant Science*, *10*. https://www.frontiersin.org/articles/10.3389/fpls.2019.00779

Chasteen, L., Ayriss, J., Pavlik, P., & Bradbury, A. R. M. (2006). Eliminating helper phage from phage display. *Nucleic Acids Research*, *34*(21), e145. https://doi.org/10.1093/nar/gkl772

Chen, Q., Sun, L., & Chen, Z. J. (2016). Regulation and function of the cGAS–STING pathway of cytosolic DNA sensing. *Nature Immunology*, *17*(10), 1142–1149. https://doi.org/10.1038/ni.3558

Chen, W., Yuan, Y., & Jiang, X. (2020). Antibody and antibody fragments for cancer immunotherapy. *Journal of Controlled Release*, *328*, 395–406. https://doi.org/10.1016/j.jconrel.2020.08.021

Chen, X. S., Garcea, R. L., Goldberg, I., Casini, G., & Harrison, S. C. (2000). Structure of Small Virus-like Particles Assembled from the L1 Protein of Human Papillomavirus 16. *Molecular Cell*, *5*(3), 557–567. https://doi.org/10.1016/S1097-2765(00)80449-9

Chongchai, A., Bentayebi, K., Chu, G., Yan, W., Waramit, S., Phitak, T., Kongtawelert, P., Pothacharoen, P., Suwan, K., & Hajitou, A. (2024). Targeted treatment of

chondrosarcoma with a bacteriophage-based particle delivering a secreted tumor necrosis factor-related apoptosis-inducing ligand. *Molecular Therapy Oncology*, *32*(2). https://doi.org/10.1016/j.omton.2024.200805

Cleary, J. M., & Ray, D. S. (1980). Replication of the plasmid pBR322 under the control of a cloned replication origin from the single-stranded DNA phage M13. *Proceedings of the National Academy of Sciences of the United States of America*, *77*(8), 4638–4642. https://www.ncbi.nlm.nih.gov/pmc/articles/PMC349900/

Click, E. M., & Webster, R. E. (1998). The TolQRA Proteins Are Required for Membrane Insertion of the Major Capsid Protein of the Filamentous Phage f1 during Infection. *Journal of Bacteriology*, *180*(7), 1723–1728. https://www.ncbi.nlm.nih.gov/pmc/articles/PMC107083/

Clokie, M. R., Millard, A. D., Letarov, A. V., & Heaphy, S. (2011). Phages in nature. *Bacteriophage*, *1*(1), 31–45. https://doi.org/10.4161/bact.1.1.14942

Costache, M. I., Ioana, M., Iordache, S., Ene, D., Costache, C. A., & Săftoiu, A. (2015). VEGF Expression in Pancreatic Cancer and Other Malignancies: A Review of the Literature. *Romanian Journal of Internal Medicine = Revue Roumaine De Medecine Interne*, *53*(3), 199–208. https://doi.org/10.1515/rjim-2015-0027

Cross, D., & Burmester, J. K. (2006). Gene Therapy for Cancer Treatment: Past, Present and Future. *Clinical Medicine and Research*, *4*(3), 218–227. https://www.ncbi.nlm.nih.gov/pmc/articles/PMC1570487/

Cupic, K. I., Rennick, J. J., Johnston, A. P., & Such, G. K. (2019). Controlling Endosomal Escape Using Nanoparticle Composition: Current Progress and Future Perspectives. *Nanomedicine*, *14*(2), 215–223. https://doi.org/10.2217/nnm-2018-0326

Degors, I. M. S., Wang, C., Rehman, Z. U., & Zuhorn, I. S. (2019). Carriers Break Barriers in Drug Delivery: Endocytosis and Endosomal Escape of Gene Delivery Vectors. *Accounts of Chemical Research*, *52*(7), 1750–1760. https://doi.org/10.1021/acs.accounts.9b00177

Du, Z., & Lovly, C. M. (2018). Mechanisms of receptor tyrosine kinase activation in cancer. *Molecular Cancer*, *17*(1), 58. https://doi.org/10.1186/s12943-018-0782-4

Dunbar, C. E., High, K. A., Joung, J. K., Kohn, D. B., Ozawa, K., & Sadelain, M. (2018). Gene therapy comes of age. *Science*, *359*(6372), eaan4672. https://doi.org/10.1126/science.aan4672

Esensten, J. H., Bluestone, J. A., & Lim, W. A. (2017). Engineering Therapeutic T Cells: From Synthetic Biology to Clinical Trials. *Annual Review of Pathology*, *12*, 305–330. https://doi.org/10.1146/annurev-pathol-052016-100304

Farzaneh Behelgardi, M., Gholami Shahvir, Z., & Asghari, S. M. (2022). Apoptosis induction in human lung and colon cancer cells via impeding VEGF signaling pathways. *Molecular Biology Reports*, *49*(5), 3637–3647. https://doi.org/10.1007/s11033-022-07203-9

Farzaneh Behelgardi, M., Zahri, S., Gholami Shahvir, Z., Mashayekhi, F., Mirzanejad, L., & Asghari, S. M. (2020). Targeting signaling pathways of VEGFR1 and VEGFR2 as a potential target in the treatment of breast cancer. *Molecular Biology Reports*, *47*(3), 2061–2071. https://doi.org/10.1007/s11033-020-05306-9

Farzaneh Behelgardi, M., Zahri, S., Mashayekhi, F., Mansouri, K., & Asghari, S. M. (2018). A peptide mimicking the binding sites of VEGF-A and VEGF-B inhibits VEGFR-1/-2 driven angiogenesis, tumor growth and metastasis. *Scientific Reports*, *8*(1), Article 1. https://doi.org/10.1038/s41598-018-36394-0

Ferrara, N., Hillan, K. J., Gerber, H.-P., & Novotny, W. (2004). Discovery and development of bevacizumab, an anti-VEGF antibody for treating cancer. *Nature Reviews Drug Discovery*, *3*(5), Article 5. https://doi.org/10.1038/nrd1381

Florin, L., Sapp, C., Streeck, R. E., & Sapp, M. (2002). Assembly and Translocation of Papillomavirus Capsid Proteins. *Journal of Virology*, *76*(19), 10009–10014. https://doi.org/10.1128/JVI.76.19.10009-10014.2002

Frey, M. R., & Brent Polk, D. (2014). ErbB receptors and their growth factor ligands in pediatric intestinal inflammation. *Pediatric Research*, *75*(1), 127–132. https://doi.org/10.1038/pr.2013.210

Fuenmayor, J., Gòdia, F., & Cervera, L. (2017). Production of virus-like particles for vaccines. *New Biotechnology*, *39*, 174–180. https://doi.org/10.1016/j.nbt.2017.07.010

Gavas, S., Quazi, S., & Karpiński, T. M. (2021). Nanoparticles for Cancer Therapy: Current Progress and Challenges. *Nanoscale Research Letters*, *16*, 173. https://doi.org/10.1186/s11671-021-03628-6

Gissmann, L., Zhou, J., Muller, M., & Painstil, J. (2000). *Carboxyl terminal of papilloma virus L1 region is not required for formation of virus-like particles* (United States Patent US6066324A). https://patents.google.com/patent/US6066324/en?oq=hpv+l1+nuclear+localization+signal

Glaviano, A., Foo, A. S. C., Lam, H. Y., Yap, K. C. H., Jacot, W., Jones, R. H., Eng, H., Nair, M. G., Makvandi, P., Geoerger, B., Kulke, M. H., Baird, R. D., Prabhu, J. S., Carbone, D., Pecoraro, C., Teh, D. B. L., Sethi, G., Cavalieri, V., Lin, K. H., … Kumar, A. P.

(2023). PI3K/AKT/mTOR signaling transduction pathway and targeted therapies in cancer. *Molecular Cancer*, *22*(1), 138. https://doi.org/10.1186/s12943-023-01827-6

Goel, H. L., & Mercurio, A. M. (2013). VEGF targets the tumour cell. *Nature Reviews. Cancer*, *13*(12), 871–882. https://doi.org/10.1038/nrc3627

Gruijs, M., Braster, R., Overdijk, M. B., Hellingman, T., Verploegen, S., Korthouwer, R., van der Wilk, B. J., Parren, P. W. H. I., van der Vliet, H. J., Bögels, M., & van Egmond, M. (2022). Epidermal Growth Factor Receptor as Target for Perioperative Elimination of Circulating Colorectal Cancer Cells. *Journal of Oncology*, *2022*, 3577928. https://doi.org/10.1155/2022/3577928

Guo, Y.-J., Pan, W.-W., Liu, S.-B., Shen, Z.-F., Xu, Y., & Hu, L.-L. (2020). ERK/MAPK signalling pathway and tumorigenesis. *Experimental and Therapeutic Medicine*, *19*(3), 1997–2007. https://doi.org/10.3892/etm.2020.8454

Hacein-Bey-Abina, S., Le Deist, F., Carlier, F., Bouneaud, C., Hue, C., De Villartay, J.-P., Thrasher, A. J., Wulffraat, N., Sorensen, R., Dupuis-Girod, S., Fischer, A., Davies, E. G., Kuis, W., Leiva, L., & Cavazzana-Calvo, M. (2002). Sustained Correction of X-Linked Severe Combined Immunodeficiency by ex Vivo Gene Therapy. *New England Journal of Medicine*, *346*(16), 1185–1193. https://doi.org/10.1056/NEJMoa012616

Häcker, G., Redecke, V., & Häcker, H. (2002). Activation of the immune system by bacterial CpG-DNA. *Immunology*, *105*(3), 245–251. https://doi.org/10.1046/j.0019-2805.2001.01350.x

Haigh, N. G., & Webster, R. E. (1999). The pI and pXI assembly proteins serve separate and essential roles in filamentous phage assembly. *Journal of Molecular Biology*, *293*(5), 1017–1027. https://doi.org/10.1006/jmbi.1999.3227

Halder, S., Basu, S., Lall, S. P., Ganti, A. K., Batra, S. K., & Seshacharyulu, P. (2023). Targeting the EGFR signaling pathway in cancer therapy: What's new in 2023? *Expert Opinion on Therapeutic Targets*, *27*(4–5), 305–324. https://doi.org/10.1080/14728222.2023.2218613

Hallek, M., & Burger, A. (2009). *Papilloma virus truncated L1 protein and fusion protein constructs* (United States Patent US7494658B2). https://patents.google.com/patent/US7494658/en?oq=PAPILLOMAVIRUS+TRUNCATED+L1+PROTEIN+AND+FUSION+PROTEIN+CONSTRUCTS

Harding, M. C., Sloan, C. D., Merrill, R. M., Harding, T. M., Thacker, B. J., & Thacker, E. L. (2018). Transitions From Heart Disease to Cancer as the Leading Cause of Death in US States, 1999–2016. *Preventing Chronic Disease*, *15*, 180151. https://doi.org/10.5888/pcd15.180151

Hatfull, G. F., Dedrick, R. M., & Schooley, R. T. (2022). Phage Therapy for Antibiotic-Resistant Bacterial Infections. *Annual Review of Medicine*, *73*(1), 197–211. https://doi.org/10.1146/annurev-med-080219-122208

Huang, S., Armstrong, E. A., Benavente, S., Chinnaiyan, P., & Harari, P. M. (2004). Dual-Agent Molecular Targeting of the Epidermal Growth Factor Receptor (EGFR): Combining Anti-EGFR Antibody with Tyrosine Kinase Inhibitor. *Cancer Research*, *64*(15), 5355–5362. https://doi.org/10.1158/0008-5472.CAN-04-0562

Huber, B., Schellenbacher, C., Shafti-Keramat, S., Jindra, C., Christensen, N., & Kirnbauer, R. (2017). Chimeric L2-Based Virus-Like Particle (VLP) Vaccines Targeting Cutaneous Human Papillomaviruses (HPV). *PLoS ONE*, *12*(1), e0169533. https://doi.org/10.1371/journal.pone.0169533

Huh, H., Chen, D.-W., Foldvari, M., Slavcev, R., & Blay, J. (2022a). EGFR-targeted bacteriophage lambda penetrates model stromal and colorectal carcinoma tissues, is taken up into carcinoma cells, and interferes with 3-dimensional tumor formation. *Frontiers in Immunology*, *13*, 957233. https://doi.org/10.3389/fimmu.2022.957233

Huh, H., Chen, D.-W., Foldvari, M., Slavcev, R., & Blay, J. (2022b). EGFR-targeted bacteriophage lambda penetrates model stromal and colorectal carcinoma tissues, is taken up into carcinoma cells, and interferes with 3-dimensional tumor formation. *Frontiers in Immunology*, *13*. https://www.frontiersin.org/articles/10.3389/fimmu.2022.957233

Huh, H., Wong, S., St. Jean, J., & Slavcev, R. (2019). Bacteriophage interactions with mammalian tissue: Therapeutic applications. *Advanced Drug Delivery Reviews*, *145*, 4–17. https://doi.org/10.1016/j.addr.2019.01.003

Jamour, P., Jamali, A., Langeroudi, A. G., Sharafabad, B. E., & Abdoli, A. (2024). Comparing chemical transfection, electroporation, and lentiviral vector transduction to achieve optimal transfection conditions in the Vero cell line. *BMC Molecular and Cell Biology*, *25*(1), 15. https://doi.org/10.1186/s12860-024-00511-x

Jang, H.-J., Suh, P.-G., Lee, Y. J., Shin, K. J., Cocco, L., & Chae, Y. C. (2018). PLCγ1: Potential arbitrator of cancer progression. *Advances in Biological Regulation*, *67*, 179–189. https://doi.org/10.1016/j.jbior.2017.11.003

Kajitani, N., Satsuka, A., Kawate, A., & Sakai, H. (2012). Productive Lifecycle of Human Papillomaviruses that Depends Upon Squamous Epithelial Differentiation. *Frontiers in Microbiology*, *3*, 152. https://doi.org/10.3389/fmicb.2012.00152

Karlsson, F., Borrebaeck, C. A. K., Nilsson, N., & Malmborg-Hager, A.-C. (2003). The Mechanism of Bacterial Infection by Filamentous Phages Involves Molecular

Interactions between TolA and Phage Protein 3 Domains. *Journal of Bacteriology*, *185*(8), 2628–2634. https://doi.org/10.1128/JB.185.8.2628-2634.2003

Kawasaki, T., & Kawai, T. (2014). Toll-Like Receptor Signaling Pathways. *Frontiers in Immunology*, *5*. https://www.frontiersin.org/articles/10.3389/fimmu.2014.00461

Keen, E. C. (2015). A century of phage research: Bacteriophages and the shaping of modern biology. *BioEssays : News and Reviews in Molecular, Cellular and Developmental Biology*, *37*(1), 6–9. https://doi.org/10.1002/bies.201400152

Kim, A., Shin, T.-H., Shin, S.-M., Pham, C. D., Choi, D.-K., Kwon, M.-H., & Kim, Y.-S. (2012). Cellular Internalization Mechanism and Intracellular Trafficking of Filamentous M13 Phages Displaying a Cell-Penetrating Transbody and TAT Peptide. *PLoS ONE*, *7*(12), e51813. https://doi.org/10.1371/journal.pone.0051813

Krieg, A. M. (2002). CpG Motifs in Bacterial DNA and Their Immune Effects. *Annual Review of Immunology*, *20*(1), 709–760. https://doi.org/10.1146/annurev.immunol.20.100301.064842

Lamprecht, R. L., Kennedy, P., Huddy, S. M., Bethke, S., Hendrikse, M., Hitzeroth, I. I., & Rybicki, E. P. (2016). Production of Human papillomavirus pseudovirions in plants and their use in pseudovirion-based neutralisation assays in mammalian cells. *Scientific Reports*, *6*(1), 20431. https://doi.org/10.1038/srep20431

Larocca, D., Jensen-Pergakes, K., Burg, M. A., & Baird, A. (2001). Receptor-Targeted Gene Delivery Using Multivalent Phagemid Particles. *Molecular Therapy*, *3*(4), 476–484. https://doi.org/10.1006/mthe.2001.0284

Leder, C., Kleinschmidt, J. A., Wiethe, C., & Müller, M. (2001). Enhancement of Capsid Gene Expression: Preparing the Human Papillomavirus Type 16 Major Structural Gene L1 for

DNA Vaccination Purposes. *Journal of Virology*, *75*(19), 9201–9209. https://doi.org/10.1128/JVI.75.19.9201-9209.2001

Ledsgaard, L., Kilstrup, M., Karatt-Vellatt, A., McCafferty, J., & Laustsen, A. H. (2018). Basics of Antibody Phage Display Technology. *Toxins*, *10*(6), 236. https://doi.org/10.3390/toxins10060236

Lee, Y. T., Tan, Y. J., & Oon, C. E. (2018). Molecular targeted therapy: Treating cancer with specificity. *European Journal of Pharmacology*, *834*, 188–196. https://doi.org/10.1016/j.ejphar.2018.07.034

Lemmon, M. A., & Schlessinger, J. (2010). Cell signaling by receptor-tyrosine kinases. *Cell*, *141*(7), 1117–1134. https://doi.org/10.1016/j.cell.2010.06.011

Lemmon, M. A., Schlessinger, J., & Ferguson, K. M. (2014). The EGFR Family: Not So Prototypical Receptor Tyrosine Kinases. *Cold Spring Harbor Perspectives in Biology*, *6*(4), a020768. https://doi.org/10.1101/cshperspect.a020768

Levinson, A., Silver, D., & Seed, B. (1984). Minimal size plasmids containing an M13 origin for production of single-strand transducing particles. *Journal of Molecular and Applied Genetics*, *2*(6), 507–517.

Li, T., Kang, G., Wang, T., & Huang, H. (2018). Tumor angiogenesis and anti-angiogenic gene therapy for cancer. *Oncology Letters*, *16*(1), 687–702. https://doi.org/10.3892/ol.2018.8733

Li, Z., Jiang, H., Zhang, J., & Gu, J. (2006). Cell-Targeted Phagemid Particles Preparation Using Escherichia Coli Bearing Ligand-pIII Encoding Helper Phage Genome. *BioTechniques*, *41*(6), 706–707. https://doi.org/10.2144/000112294

Liu, Y., Li, Y., Wang, Y., Lin, C., Zhang, D., Chen, J., Ouyang, L., Wu, F., Zhang, J., & Chen, L. (2022). Recent progress on vascular endothelial growth factor receptor inhibitors with dual targeting capabilities for tumor therapy. *Journal of Hematology & Oncology*, *15*(1), 89. https://doi.org/10.1186/s13045-022-01310-7

Liu, Z.-L., Chen, H.-H., Zheng, L.-L., Sun, L.-P., & Shi, L. (2023). Angiogenic signaling pathways and anti-angiogenic therapy for cancer. *Signal Transduction and Targeted Therapy*, *8*(1), 1–39. https://doi.org/10.1038/s41392-023-01460-1

Loh, B., Kuhn, A., & Leptihn, S. (2019). The fascinating biology behind phage display: Filamentous phage assembly. *Molecular Microbiology*, *111*(5), 1132–1138. https://doi.org/10.1111/mmi.14187

Lukacs, G. L., Haggie, P., Seksek, O., Lechardeur, D., Freedman, N., & Verkman, A. S. (2000). Size-dependent DNA Mobility in Cytoplasm and Nucleus *. *Journal of Biological Chemistry*, *275*(3), 1625–1629. https://doi.org/10.1074/jbc.275.3.1625

Luo, K., Li, N., Ye, W., Gao, H., Luo, X., & Cheng, B. (2022). Activation of Stimulation of Interferon Genes (STING) Signal and Cancer Immunotherapy. *Molecules*, *27*(14), Article 14. https://doi.org/10.3390/molecules27144638

Mandal, S., Bandyopadhyay, S., Tyagi, K., & Roy, A. (2021). Recent advances in understanding the molecular role of phosphoinositide-specific phospholipase C gamma 1 as an emerging onco-driver and novel therapeutic target in human carcinogenesis. *Biochimica et Biophysica Acta (BBA) - Reviews on Cancer*, *1876*(2), 188619. https://doi.org/10.1016/j.bbcan.2021.188619

Manivannan, A. C., Dhandapani, R., Velmurugan, P., Thangavelu, S., Paramasivam, R., Ragunathan, L., & Saravanan, M. (2022). Phage in cancer treatment—Biology of

therapeutic phage and screening of tumor targeting peptide. *Expert Opinion on Drug Delivery*, *19*(7), 873–882. https://doi.org/10.1080/17425247.2022.2094363

Marhelava, K., Pilch, Z., Bajor, M., Graczyk-Jarzynka, A., & Zagozdzon, R. (2019). Targeting Negative and Positive Immune Checkpoints with Monoclonal Antibodies in Therapy of Cancer. *Cancers*, *11*(11), 1756. https://doi.org/10.3390/cancers11111756

Masters, J. R. (2002). HeLa cells 50 years on: The good, the bad and the ugly. *Nature Reviews Cancer*, *2*(4), 315–319. https://doi.org/10.1038/nrc775

Mazur, B. J., & Model, P. (1973). Regulation of coliphage f1 single-stranded DNA synthesis by a DNA-binding protein. *Journal of Molecular Biology*, *78*(2), 285–300. https://doi.org/10.1016/0022-2836(73)90117-4

Michel, T., Hentges, F., & Zimmer, J. (2013). Consequences of the crosstalk between monocytes/macrophages and natural killer cells. *Frontiers in Immunology*, *3*, 403. https://doi.org/10.3389/fimmu.2012.00403

Min, H.-Y., & Lee, H.-Y. (2022). Molecular targeted therapy for anticancer treatment. *Experimental & Molecular Medicine*, *54*(10), Article 10. https://doi.org/10.1038/s12276-022-00864-3

Müller, T. G., Sakin, V., & Müller, B. (2019). A Spotlight on Viruses—Application of Click Chemistry to Visualize Virus-Cell Interactions. *Molecules*, *24*(3), Article 3. https://doi.org/10.3390/molecules24030481

Naskalska, A., & Pyrć, K. (2015). Virus Like Particles as Immunogens and Universal Nanocarriers. *Polish Journal of Microbiology*, *64*(1), 3–13. https://doi.org/10.33073/pjm-2015-001

Nayerossadat, N., Maedeh, T., & Ali, P. A. (2012). Viral and nonviral delivery systems for gene delivery. *Advanced Biomedical Research*, *1*, 27. https://doi.org/10.4103/2277-9175.98152

Nicoli, F., Mantelli, B., Gallerani, E., Telatin, V., Bonazzi, I., Marconi, P., Gavioli, R., Gabrielli, L., Lazzarotto, T., Barzon, L., Palù, G., & Caputo, A. (2020). HPV-Specific Systemic Antibody Responses and Memory B Cells are Independently Maintained up to 6 Years and in a Vaccine-Specific Manner Following Immunization with Cervarix and Gardasil in Adolescent and Young Adult Women in Vaccination Programs in Italy. *Vaccines*, *8*(1), 26. https://doi.org/10.3390/vaccines8010026

Nooraei, S., Bahrulolum, H., Hoseini, Z. S., Katalani, C., Hajizade, A., Easton, A. J., & Ahmadian, G. (2021). Virus-like particles: Preparation, immunogenicity and their roles as nanovaccines and drug nanocarriers. *Journal of Nanobiotechnology*, *19*, 59. https://doi.org/10.1186/s12951-021-00806-7

Normanno, N., De Luca, A., Bianco, C., Strizzi, L., Mancino, M., Maiello, M. R., Carotenuto, A., De Feo, G., Caponigro, F., & Salomon, D. S. (2006). Epidermal growth factor receptor (EGFR) signaling in cancer. *Gene*, *366*(1), 2–16. https://doi.org/10.1016/j.gene.2005.10.018

Oda, K., Matsuoka, Y., Funahashi, A., & Kitano, H. (2005). A comprehensive pathway map of epidermal growth factor receptor signaling. *Molecular Systems Biology*, *1*, 2005.0010. https://doi.org/10.1038/msb4100014

Oholendt, A. L., & Zadlo, J. L. (2015). Ramucirumab: A New Therapy for Advanced Gastric Cancer. *Journal of the Advanced Practitioner in Oncology*, *6*(1), 71–75. https://www.ncbi.nlm.nih.gov/pmc/articles/PMC4577036/

Olayioye, M. A., Neve, R. M., Lane, H. A., & Hynes, N. E. (2000). NEW EMBO MEMBERS' REVIEW. *The EMBO Journal*, *19*(13), 3159–3167. https://doi.org/10.1093/emboj/19.13.3159

Palucha, A., Loniewska, A., Satheshkumar, S., Boguszewska-Chachulska, A. M., Umashankar, M., Milner, M., Haenni, A., & Savithri, H. S. (2005). Virus-Like Particles: Models for Assembly Studies and Foreign Epitope Carriers. *Progress in Nucleic Acid Research and Molecular Biology*, *80*, 135–168. https://doi.org/10.1016/S0079-6603(05)80004-2

Peng, Y., Wang, Y., Zhou, C., Mei, W., & Zeng, C. (2022). PI3K/Akt/mTOR Pathway and Its Role in Cancer Therapeutics: Are We Making Headway? *Frontiers in Oncology*, *12*, 819128. https://doi.org/10.3389/fonc.2022.819128

Petrov, G., Dymova, M., & Richter, V. (2022). Bacteriophage-Mediated Cancer Gene Therapy. *International Journal of Molecular Sciences*, *23*(22), Article 22. https://doi.org/10.3390/ijms232214245

Pinilla-Macua, I., & Sorkin, A. (2015). Methods to study endocytic trafficking of the EGF receptor. *Methods in Cell Biology*, *130*, 347–367. https://doi.org/10.1016/bs.mcb.2015.05.008

Pushparajah, D. (2022). *Design of a DNA-Encoded Human Papilloma Virus-Like Particle Displaying a Vascular Endothelial Growth Factor Antagonistic Peptide for Characterization in Mammalian Cells* [Master Thesis, University of Waterloo]. https://uwspace.uwaterloo.ca/handle/10012/18982

Raymond, E., Faivre, S., & Armand, J. P. (2000). Epidermal Growth Factor Receptor Tyrosine Kinase as a Target for Anticancer Therapy. *Drugs*, *60*(1), 15–23. https://doi.org/10.2165/00003495-200060001-00002

Refolo, M. G., Lotesoriere, C., Lolli, I. R., Messa, C., & D'Alessandro, R. (2020). Molecular mechanisms of synergistic action of Ramucirumab and Paclitaxel in Gastric Cancers cell lines. *Scientific Reports*, *10*(1), Article 1. https://doi.org/10.1038/s41598-020-64195-x

Reis e Sousa, C. (2004). Activation of dendritic cells: Translating innate into adaptive immunity. *Current Opinion in Immunology*, *16*(1), 21–25. https://doi.org/10.1016/j.coi.2003.11.007

Rosca, E. V., Koskimaki, J. E., Rivera, C. G., Pandey, N. B., Tamiz, A. P., & Popel, A. S. (2011). Anti-angiogenic peptides for cancer therapeutics. *Current Pharmaceutical Biotechnology*, *12*(8), 1101–1116. https://www.ncbi.nlm.nih.gov/pmc/articles/PMC3114256/

Sadelain, M., Rivière, I., & Riddell, S. (2017). Therapeutic T cell engineering. *Nature*, *545*(7655), 423–431. https://doi.org/10.1038/nature22395

Sapp, M., Fligge, C., Petzak, I., Harris, J. R., & Streeck, R. E. (1998). Papillomavirus Assembly Requires Trimerization of the Major Capsid Protein by Disulfides between Two Highly Conserved Cysteines. *Journal of Virology*, *72*(7), 6186–6189. https://www.ncbi.nlm.nih.gov/pmc/articles/PMC110432/

Sasaki, T., Hiroki, K., & Yamashita, Y. (2013). The Role of Epidermal Growth Factor Receptor in Cancer Metastasis and Microenvironment. *BioMed Research International*, *2013*, 546318. https://doi.org/10.1155/2013/546318

Shi, F., Telesco, S. E., Liu, Y., Radhakrishnan, R., & Lemmon, M. A. (2010). ErbB3/HER3 intracellular domain is competent to bind ATP and catalyze autophosphorylation. *Proceedings of the National Academy of Sciences*, *107*(17), 7692–7697. https://doi.org/10.1073/pnas.1002753107

Shibuya, M. (2011). Vascular Endothelial Growth Factor (VEGF) and Its Receptor (VEGFR) Signaling in Angiogenesis. *Genes & Cancer*, *2*(12), 1097–1105. https://doi.org/10.1177/1947601911423031

Sidhu, S. S., Feld, B. K., & Weiss, G. A. (2007). M13 Bacteriophage Coat Proteins Engineered for Improved Phage Display. In K. M. Arndt & K. M. Müller (Eds.), *Protein Engineering Protocols* (pp. 205–219). Humana Press. https://doi.org/10.1385/1-59745-187-8:205

Siegel, R. L., Miller, K. D., Fuchs, H. E., & Jemal, A. (2022). Cancer statistics, 2022. *CA: A Cancer Journal for Clinicians*, *72*(1), 7–33. https://doi.org/10.3322/caac.21708

Sigismund, S., Woelk, T., Puri, C., Maspero, E., Tacchetti, C., Transidico, P., Di Fiore, P. P., & Polo, S. (2005). Clathrin-independent endocytosis of ubiquitinated cargos. *Proceedings of the National Academy of Sciences of the United States of America*, *102*(8), 2760–2765. https://doi.org/10.1073/pnas.0409817102

Sinclair, A., Islam, S., & Jones, S. (2016). Gene Therapy: An Overview of Approved and Pipeline Technologies. In *CADTH Issues in Emerging Health Technologies*. Canadian Agency for Drugs and Technologies in Health. http://www.ncbi.nlm.nih.gov/books/NBK538378/

Slupetzky, K., Gambhira, R., Culp, T. D., Shafti-Keramat, S., Schellenbacher, C., Christensen, N. D., Roden, R. B. S., & Kirnbauer, R. (2007). A papillomavirus-like particle (VLP) vaccine displaying HPV16 L2 epitopes induces cross-neutralizing antibodies to HPV11. *Vaccine*, *25*(11), 2001–2010. https://doi.org/10.1016/j.vaccine.2006.11.049

Smeal, S. W., Schmitt, M. A., Pereira, R. R., Prasad, A., & Fisk, J. D. (2017). Simulation of the M13 life cycle I: Assembly of a genetically-structured deterministic chemical kinetic simulation. *Virology*, *500*, 259–274. https://doi.org/10.1016/j.virol.2016.08.017

Sorkin, A., & Goh, L. K. (2008). Endocytosis and intracellular trafficking of ErbBs. *Experimental Cell Research*, *314*(17), 3093–3106. https://doi.org/10.1016/j.yexcr.2008.07.029

Sorkin, A., & von Zastrow, M. (2009). Endocytosis and signalling: Intertwining molecular networks. *Nature Reviews Molecular Cell Biology*, *10*(9), Article 9. https://doi.org/10.1038/nrm2748

Stebegg, M., Kumar, S. D., Silva-Cayetano, A., Fonseca, V. R., Linterman, M. A., & Graca, L. (2018). Regulation of the Germinal Center Response. *Frontiers in Immunology*, *9*. https://www.frontiersin.org/articles/10.3389/fimmu.2018.02469

Stepanenko, A. A., & Dmitrenko, V. V. (2015). HEK293 in cell biology and cancer research: Phenotype, karyotype, tumorigenicity, and stress-induced genome-phenotype evolution. *Gene*, *569*(2), 182–190. https://doi.org/10.1016/j.gene.2015.05.065

Sum, C., Wettig, S., & Slavcev, R. (2014). Impact of DNA Vector Topology on Non-Viral Gene Therapeutic Safety and Efficacy. *Current Gene Therapy*, *14*(4), 309–329. https://doi.org/10.2174/1566523214666140612154929

Sung, H., Ferlay, J., Siegel, R. L., Laversanne, M., Soerjomataram, I., Jemal, A., & Bray, F. (2021). Global Cancer Statistics 2020: GLOBOCAN Estimates of Incidence and Mortality Worldwide for 36 Cancers in 185 Countries. *CA: A Cancer Journal for Clinicians*, *71*(3), 209–249. https://doi.org/10.3322/caac.21660

Tan, E., Chin, C. S. H., Lim, Z. F. S., & Ng, S. K. (2021). HEK293 Cell Line as a Platform to Produce Recombinant Proteins and Viral Vectors. *Frontiers in Bioengineering and Biotechnology*, *9*, 796991. https://doi.org/10.3389/fbioe.2021.796991

Tao, M., Kruhlak, M., Xia, S., Androphy, E., & Zheng, Z.-M. (2003). SignalsThat Dictate Nuclear Localization of Human Papillomavirus Type 16Oncoprotein E6 in LivingCells. *Journal of Virology*, *77*(24), 13232–13247. https://doi.org/10.1128/JVI.77.24.13232-13247.2003

Tariq, H., Batool, S., Asif, S., Ali, M., & Abbasi, B. H. (2022). Virus-Like Particles: Revolutionary Platforms for Developing Vaccines Against Emerging Infectious Diseases. *Frontiers in Microbiology*, *12*, 790121. https://doi.org/10.3389/fmicb.2021.790121

Tian, Y., Wu, M., Liu, X., Liu, Z., Zhou, Q., Niu, Z., & Huang, Y. (2015). Probing the Endocytic Pathways of the Filamentous Bacteriophage in Live Cells Using Ratiometric pH Fluorescent Indicator. *Advanced Healthcare Materials*, *4*(3), 413–419. https://doi.org/10.1002/adhm.201400508

Tie, Y., Tang, F., Wei, Y., & Wei, X. (2022). Immunosuppressive cells in cancer: Mechanisms and potential therapeutic targets. *Journal of Hematology & Oncology*, *15*, 61. https://doi.org/10.1186/s13045-022-01282-8

Tormoen, G. W., Crittenden, M. R., & Gough, M. J. (2018). Role of the immunosuppressive microenvironment in immunotherapy. *Advances in Radiation Oncology*, *3*(4), 520–526. https://doi.org/10.1016/j.adro.2018.08.018

Uddin, M. N., Henry, B., Carter, K. D., Roni, M. A., & Kouzi, S. S. (2019). A Novel Formulation Strategy to Deliver Combined DNA and VLP Based HPV Vaccine. *Journal of Pharmacy & Pharmaceutical Sciences*, *22*, 536–547. https://doi.org/10.18433/jpps30768

Van den Bergh, J. M. J., Guerti, K., Willemen, Y., Lion, E., Cools, N., Goossens, H., Vorsters, A., Van Tendeloo, V. F. I., Anguille, S., Van Damme, P., & Smits, E. L. J. M. (2014).

HPV vaccine stimulates cytotoxic activity of killer dendritic cells and natural killer cells against HPV-positive tumour cells. *Journal of Cellular and Molecular Medicine*, *18*(7), 1372–1380. https://doi.org/10.1111/jcmm.12284

Varsani, A., Williamson, A.-L., de Villiers, D., Becker, I., Christensen, N. D., & Rybicki, E. P. (2003). Chimeric Human Papillomavirus Type 16 (HPV-16) L1 Particles Presenting the Common Neutralizing Epitope for the L2 Minor Capsid Protein of HPV-6 and HPV-16. *Journal of Virology*, *77*(15), 8386–8393. https://doi.org/10.1128/JVI.77.15.8386-8393.2003

Wang, Q., Chen, X., & Wang, Z. (2015). Dimerization drives EGFR endocytosis through two sets of compatible endocytic codes. *Journal of Cell Science*, *128*(5), 935–950. https://doi.org/10.1242/jcs.160374

Wee, P., & Wang, Z. (2017). Epidermal Growth Factor Receptor Cell Proliferation Signaling Pathways. *Cancers*, *9*(5), 52. https://doi.org/10.3390/cancers9050052

Wong, S. (2022). *Construction and characterization of a hybrid bacteriophage gene delivery platform* [Doctoral Thesis, University of Waterloo]. https://uwspace.uwaterloo.ca/handle/10012/18171

Wong, S., Jimenez, S., & Slavcev, R. A. (2023). Construction and characterization of a novel miniaturized filamentous phagemid for targeted mammalian gene transfer. *Microbial Cell Factories*, *22*(1), 124. https://doi.org/10.1186/s12934-023-02135-w

Wu, C.-H., Liu, I.-J., Lu, R.-M., & Wu, H.-C. (2016). Advancement and applications of peptide phage display technology in biomedical science. *Journal of Biomedical Science*, *23*(1), 8. https://doi.org/10.1186/s12929-016-0223-x

Yahya, E. B., & Alqadhi, A. M. (2021). Recent trends in cancer therapy: A review on the current state of gene delivery. *Life Sciences*, *269*, 119087. https://doi.org/10.1016/j.lfs.2021.119087

Yang, J., Wang, Y.-L., & Si, L.-S. (2006). Predicting the Nuclear Localization Signals of 107 Types of HPV L1 Proteins by Bioinformatic Analysis. *Genomics, Proteomics & Bioinformatics*, *4*(1), 34–41. https://doi.org/10.1016/S1672-0229(06)60014-4

Yavas, S., Macháň, R., & Wohland, T. (2016). The Epidermal Growth Factor Receptor Forms Location-Dependent Complexes in Resting Cells. *Biophysical Journal*, *111*(10), 2241–2254. https://doi.org/10.1016/j.bpj.2016.09.049

Zepeda-Cervantes, J., Ramírez-Jarquín, J. O., & Vaca, L. (2020). Interaction Between Virus-Like Particles (VLPs) and Pattern Recognition Receptors (PRRs) From Dendritic Cells (DCs): Toward Better Engineering of VLPs. *Frontiers in Immunology*, *11*. https://www.frontiersin.org/articles/10.3389/fimmu.2020.01100

Zhang, W., & Liu, H. T. (2002). MAPK signal pathways in the regulation of cell proliferation in mammalian cells. *Cell Research*, *12*(1), 9–18. https://doi.org/10.1038/sj.cr.7290105

Zhao, Q., Potter, C. S., Carragher, B., Lander, G., Sworen, J., Towne, V., Abraham, D., Duncan, P., Washabaugh, M. W., & Sitrin, R. D. (2014). Characterization of virus-like particles in GARDASIL® by cryo transmission electron microscopy. *Human Vaccines & Immunotherapeutics*, *10*(3), 734–739. https://doi.org/10.4161/hv.27316

Zhong, L., Li, Y., Xiong, L., Wang, W., Wu, M., Yuan, T., Yang, W., Tian, C., Miao, Z., Wang, T., & Yang, S. (2021). Small molecules in targeted cancer therapy: Advances, challenges, and future perspectives. *Signal Transduction and Targeted Therapy*, *6*(1), Article 1. https://doi.org/10.1038/s41392-021-00572-w

Zhou, J., Doorbar, J., Sun, X. Y., Crawford, L. V., McLean, C. S., & Frazer, I. H. (1991). Identification of the nuclear localization signal of human papillomavirus type 16 L1 protein. *Virology*, *185*(2), 625–632. https://doi.org/10.1016/0042-6822(91)90533-h

Zuppi, M., Hendrickson, H. L., O'Sullivan, J. M., & Vatanen, T. (2022). Phages in the Gut Ecosystem. *Frontiers in Cellular and Infection Microbiology*, *11*. https://www.frontiersin.org/articles/10.3389/fcimb.2021.822562

Appendix A: Sequencing data

gtgaaaaaattattattcgcaattcctttagttgttcctttctattctcactctaatagtgactctgaatgtcccctgtcccacgatgggtactgcctc
catgatggtgtgtgcatgtatattgaagcattggacaagtatgcatgcaactgtgttgttggctacatcggggagcgatgtcagtaccgagac
ctgaagtggtgggaactgcgcggtggtggttcttcggccgaaactgttgaaagttgtttagcaaaatcccatacagaaaattcatttactaacg
tctggaaagacgacaaaactttagatcgttacgctaactatgagggctgtctgtggaatgctacaggcgttgtagtttgtactggtgacgaaac
tcagtgttacggtacatgggttcctattgggcttgctatccctgaaaatgagggtggtggctctgagggtggcggttctgagggtggcggttct
gagggtggcggtactaaacctcctgagtacggtgatacacctattccgggctatacttatatcaaccctctcgacggcacttatccgcctggta
ctgagcaaaaccccgctaatcctaatccttctcttgaggagtctcagcctcttaatactttcatgtttcagaataataggttccgaaataggcagg
gggcattaactgtttatacgggcactgttactcaaggcactgaccccgttaaaacttattaccagtacactcctgtatcatcaaaagccatgtat
gacgcttactggaacggtaaattcagagactgcgctttccattctggctttaatgaggatttatttgtttgtgaatatcaaggccaatcgtctgacc
tgcctcaacctcctgtcaatgctggcggcggctctggtggtggttctggtggcggctctgagggtggtggctctgagggtggcggttctgag
gtggcggctctgagggaggcggttccggtggtggctctggttccggtgattttgattatgaaaagatggcaaacgctaataaggggggctat
gaccgaaaatgccgatgaaaacgcgctacagtctgacgctaaaggcaaacttgattctgtcgctactgattacggtgctgctatcgatggttt
cattggtgacgtttccggccttgctaatggtaatggtgctactggtgattttgctggctctaattcccaaatggctcaagtcggtgacggtgataa
ttcacctttaatgaataatttccgtcaatatttaccttccctccctcaatcggttgaatgtcgccctttgtctttggcgctggtaaaccatatgaatttt
ctattgattgtgacaaaataaacttattccgtggtgtctttgcgtttcttttatatgttgccacctttatgtatgtattttctacgtttgctaacatactgc
gtaataaggagtcttaa

Figure A.1: M13 *gIII* sequence with *egf* insertion. The yellow highlighted region indicated the inserted *egf* sequence. EGF was inserted in the N-terminus of pIII after the peptide leader sequence, via a GGGS (Gly-Gly-Gly-Ser) linker.

atgagcctgtggctgcccagcgaggccaccgtgtacctgccccccgtgcccgtgagcaaggtggtgagcaccgacgagtacgtggcca
gaaccaacatctactaccacgccggcaccagcagactgctggccgtgggccacccctacttccccatcaagaagcccaacaacaacaag
atcctggtgcccaaggtgagcggcctgcagtacagagtgttcagaatccacctgcccgaccccaacaagttcggcttccccgacaccagct
tctacaaccccgacacccagagactggtgtgggcctgcgtgggcgtggaggtgggcagaggccagcccctgggcgtgggcatcagcg
gccacccccctgctgaacaagctggacgacaccgagaacgccagcgcctacgccggctgcatcaagccccaccagggccagcacatctg
caacgacgagggcgccaacgccggcgtggacaacagagagtgcatcagcatggactacaagcagacccagctgtgcctgatcggctgc
aagccccccatcggcgagcactggggcaagggcagcccctgcaccaacgtggccgtgaaccccggcgactgccccccccctggagctg
atcaacaccgtgatccaggacggcgacatggtggacaccggcttcggcgccatggacttcaccaccctgcaggccaacaagagcgaggt
gcccctggacatctgcaccagcatctgcaagtaccccgactacatcaagatggtgagcgagccctacggcgacagcctgttcttctacctg
agaagagagcagatgttcgtgagacacctgttcaacagagccggcgccgtgggcgagaacgtgcccgacgacctgtacatcaagggca
gcggcagcaccgccaacctggccagcagcaactacttccccacccccagcggcagcatggtgaccagcgacgcccagatcttcaacaa
gccctactggctgcagagagcccagggccacaacaacggcatctgctggggcaaccagctgttcgtgaccgtggtggacaccaccaga
agcaccaacatgagcctgtgcgccgccatcagcaccagcgagaccacctacaagaacaccaacttcaaggagtacctgagacacggcg
aggagtacgacctgcagttcatcttccagctgtgcaagatcaccctgaccgccgacgtgatgacctacatccacagcatgaacagcaccat
cctggaggactggaacttcggcctgcagccccccccggcggcaccctggaggacacctacagattcgtgaccagccaggccatcgcct
gccagaagcacaccccccccgcccccaaggaggacccccctgaagaagtacaccttctgggaggtgaacctgaaggagaagttcagcgc
cgacctggaccagttccccctgggcagaaagttcctgctgcaggccggcctgaaggccaagcccaagttcaccctgggcaagagaaag
gccacccccaccaccagcagcaccagcaccaccgccaagagaaagaagagaaagctgtga

Figure A.2: HPV16 *L1* sequence with *VGB4* sequence insertion in the DE loop. The red highlighted region indicated the inserted *VGB4* sequence. GGC bases are linkers placed before and after the inserted *VGB4* sequence. The yellow highlighted region indicates the deleted *NLS* sequence.

Appendix B: Media and buffer compositions

Ampicillin Stock

This was used as a selective marker for the precursor phagemid in the *E. coli* hosts, and was added to the broth at 100 μg/ml from a stock prepared at a concentration of 50 mg/ml into sterile MilliQ water. This stock powder was stored at -20 °C.

Kanamycin Stock

This was used as a selective marker for the helper phage plasmids in the *E. coli* hosts and was added to the broth at 70 μg/ml from a stock prepared at a concentration of 50 mg/ml into filter-sterile water. This stock powder was stored at -20 °C.

Luria Bertani (LB) Broth

LB broth is a nutritionally rich medium used for the rapid propagation of bacteria in culture. It consists of 10 g tryptone, 5 g yeast abstract and 5 g NaCl dissolved in 1 L MilliQ water, autoclaved, and stored at room temperature.

LB Agar

LB agar was used as a solid support for the growth of bacterial cultures. It consists of 10 g tryptone, 5 g yeast abstract, 5 g NaCl and 13 g Grade A BactoTM agar dissolved in 1 L MilliQ water. It was sterilized, poured onto sterile plates and stored at 4 °C.

LB Top Agar

LB top agar was used as an overlay on top of regular nutrient agar plates. The semi-solid consistency permits progeny phages to diffuse through the media to infect the evenly-dispersed, "lawn" of bacterial culture. It consists of 10 g tryptone, 5 g yeast abstract, 5 g NaCl and 7 g Grade A BactoTM agar, dissolved in 1 L MilliQ H_2O, sterilized and stored in 52 °C water bath to maintain the molten state.

PEG (Polyethylene Glycol)/NaCl solution

PEG was used to precipitate phage particles and purification. It was prepared by dissolving 0.2 M PEG 8000, 0.15 M NaCl in 1 L MilliQ water (pH 7.8). The solution was stored at room temperature.

TN Buffer

Phages were stored in TN buffer at 4 °C. It was prepared by dissolving 0.1 M NaCl, 0.01 M Tris-HCl (pH 7.8) and autoclaving afterwards. The solution was stored at room temperature.

TBS-T Buffer

1X TBS-T buffer was used as a washing buffer for dot blot assay. 10X TBS buffer was prepared by dissolving 15.2 mM Tris-HCl, 4.62 mM Tris base and 150 mM NaCl (pH 7.6) and autoclaving afterwards. 1X TBS-T buffer was made by further diluting 10X TBS in MilliQ water in addition to 0.1% Tween 20.

PBS-T Buffer

1X TBS-T buffer was used as a washing buffer for ELISA. 10X PBS buffer was prepared by dissolving 1370 mM NaCl, 27mM KCl,100mM of Na2HPO4, 18mM of KH2PO4 in MilliQ H2O (pH 7.4) and was autoclaved. 1X PBS-T buffer was made by further diluting 10X PBS in MilliQ water in addition to 0.1% Tween 20.

Appendix C: Supplementary qPCR data

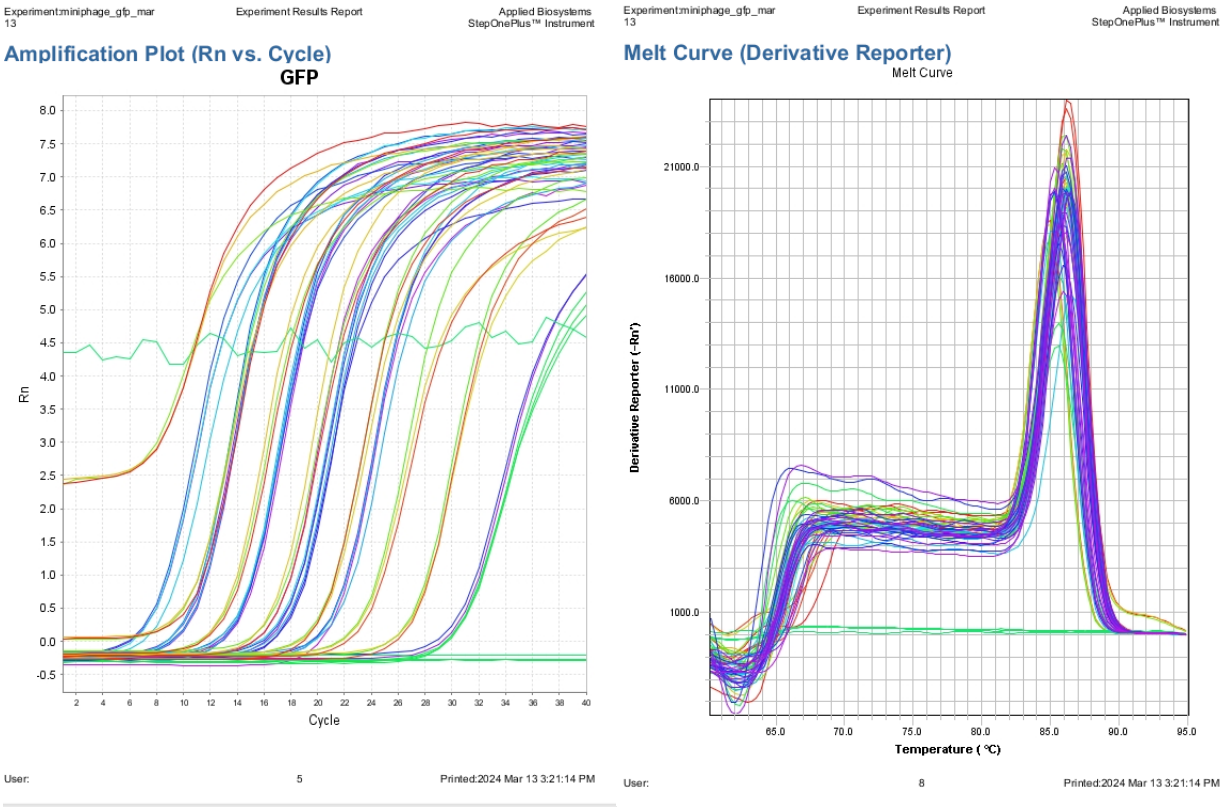

Figure C.1: Amplification plot and melt curve for the *gfp* amplicon.

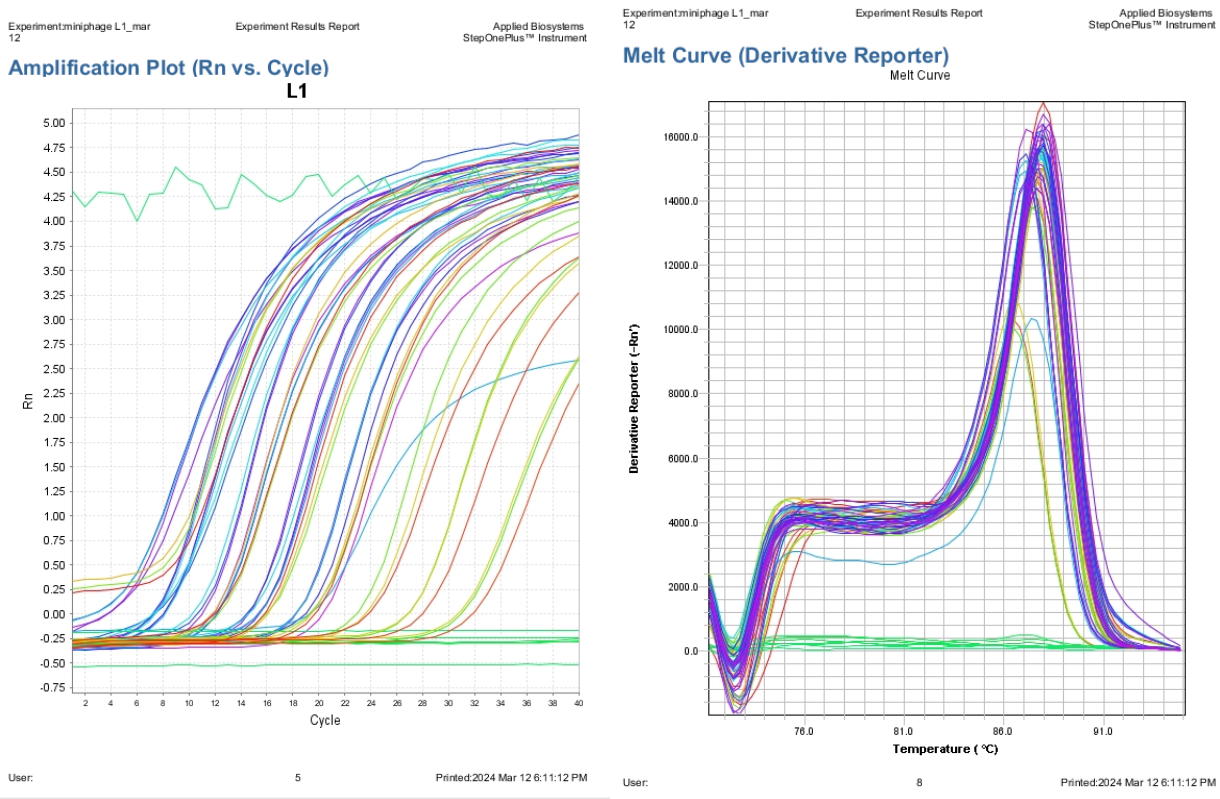

Figure C.2: Amplification plot and melt curve for the *L1* amplicon.

Appendix D: Supplementary ELISA data

Table D.1: Raw values of indirect ELISA detection of HPV16 L1 protein and VLP assembly in HEK 293T cells.

Transfected sample	Camvir-1 Ab (Absorbance at 450 nm)				H16:U4 Ab (Absorbance at 450 nm)			
	Cell lysate	- AVG blank	Supernatant	- AVG blank	Cell lysate	-AVG blank	Supernatant	-AVG blank
Blank	0.197 ± 0.021		0.330 ± 0.007		0.103 ± 0.002		0.093 ± 0.001	
pOri2-cmv-gfp	0.199 ± 0.011	0.001	0.316 ± 0.005	-0.014	0.103 ± 0.003	0.000	0.092 ± 0.002	-0.001
ssDNA-*cmv-gfp*	0.195 ± 0.005	-0.002	0.319 ± 0.004	-0.011	0.097 ± 0.002	-0.006	0.092 ± 0.002	-0.002
pOri2-L1-VGB4	2.499 ± 0.014	2.302	0.358 ± 0.152	0.027	2.299 ± 0.002	2.197	0.098 ± 0.042	0.004
ssDNA-*L1-VGB4*	0.369 ± 0.033	0.172	0.355 ± 0.003	0.025	0.140 ± 0.001	0.038	0.091 ± 0.001	-0.002
pOri2-L1-ΔNLS-VGB4	0.358 ± 0.030	0.160	0.366 ± 0.005	0.035	0.101 ± 0.001	-0.002	0.091 ± 0.001	-0.002
ssDNA-*L1-ΔNLS-VGB4*	0.210 ± 0.018	0.013	0.355 ± 0.007	0.025	0.101 ± 0.000	-0.002	0.092 ± 0.002	-0.002

The raw absorbance values were expressed as a mean of three independent assays ± SEM, n = 3. The final values were reported as the raw absorbance values subtracted by the average blank absorbance value. Transfected HEK 293T cell lysates and supernatants are tested separately with two different primary Abs, Camvir-1 to detect the presence of L1 protein and H16:U4 to detect the formation of HPV VLPs.

Table D.2: Raw values of indirect ELISA detection of HPV16 L1 protein and VLP assembly in HeLa cells.

Transfected sample	Camvir-1 Ab (Absorbance at 450 nm)				H16:U4 Ab (Absorbance at 450 nm)			
	Cell lysate	-AVG blank	Supernatant	-AVG blank	Cell lysate	-AVG blank	Supernatant	-AVG blank
Blank	0.124		0.300 ±0.008		0.101 ±0.000		0.098 ±0.008	
pOri2-cmv-gfp	0.147 ±0.007	0.022	0.298 ±0.007	-0.002	0.097 ±0.000	-0.004	0.096 ±0.005	-0.002
ssDNA-*cmv-gfp*	0.193 ±0.020	0.069	0.267 ±0.004	-0.033	0.101 ±0.000	0.000	0.107 ±0.016	0.009
pOri2-L1-VGB4	0.584 ±0.012	0.460	0.287 ±0.001	-0.013	0.107 ±0.000	0.006	0.101 ±0.013	0.003
ssDNA-*L1-VGB4*	0.302 ±0.081	0.178	0.288 ±0.005	-0.013	0.100 ±0.001	-0.001	0.099 ±0.007	0.001
EGF-*L1-VGB4* miniphagemids	0.195 ±0.039	0.071	0.276 ±0.016	-0.024	0.101 ±0.000	0.000	0.093 ±0.001	-0.005
pOri2-L1-VGB4-ΔNLS	0.268 ±0.036	0.144	0.283 ±0.006	-0.017	0.099 ±0.001	-0.002	0.092 ±0.000	-0.005
ssDNA-*L1-VGB4-ΔNLS*	0.215 ±0.030	0.091	0.295 ±0.009	-0.005	0.099 ±0.000	-0.002	0.094 ±0.001	-0.004
EGF-*L1-VGB4-ΔNLS* miniphagemids	0.211 ±0.029	0.067	0.288 ±0.000	-0.012	0.104 ±0.004	0.003	0.116 ±0.031	0.018

The raw absorbance values were expressed as a mean of three independent assays ± SEM, n = 3. The final values were reported as the raw absorbance values subtracted by the average blank absorbance value. Transfected HeLa cell lysates and supernatants are tested separately with two different primary Abs, Camvir-1 to detect the presence of L1 protein and H16:U4 to detect the formation of HPV VLPs.

Table D.3: Raw values of sandwich ELISA detecting the binding of VGB4-displaying HPV VLPs to VEGFR-2.

Transfected sample	Camvir-1 Ab (Absorbance at 450 nm)	
	Cell lysate	-AVG Blank
Blank	0.096 ± 0.001	
pOri2-cmv-gfp	0.091 ± 0.031	0.000
pOri2-L1-VGB4	0.161 ± 0.001	0.064
ssDNA-*L1-VGB4*	0.097 ± 0.007	0.001

The raw absorbance values were expressed as a mean of three independent assays ± SEM, n = 3. The final values were reported as the raw absorbance values subtracted by the average blank absorbance value. Transfected HEK 293T cell lysate samples are tested with primary Abs Camvir-1 to detect the binding capacity of VGB4-displaying HPV VLPs to VEGFR-2.